Annual Report
Jahresbericht

2002

WALTHER–MEISSNER–INSTITUT
für Tieftemperaturforschung
Bayerische Akademie der Wissenschaften

Contact:

Prof. Dr. Rudolf Gross
Walther–Meissner–Institut für Tieftemperaturforschung
Bayerische Akademie der Wissenschaften
and
Lehrstuhl für Technische Physik – E23
Technische Universität München

Address:

Walther–Meissner–Str. 8	Phone:	+49 – (0)89 289 14201
D - 85748 Garching	Fax:	+49 – (0)89 289 14206
GERMANY	e–mail:	Rudolf.Gross@wmi.badw.de
	WWW–address:	http://www.wmi.badw.de

Secretary's Office:

Jutta Laaser	Phone:	+49 – (0)89 289 14202
	Fax:	+49 – (0)89 289 14206
	e–mail:	Jutta.Laaser@wmi.badw.de
Emel Dönertas	Phone:	+49 – (0)89 289 14205
	Fax:	+49 – (0)89 289 14206
	e–mail:	Emel.Doenertas@wmi.badw.de

Preface

The Walther–Meissner–Institute for Low Temperature Research (WMI) is operated by the Commission for Low Temperature Physics of the Bavarian Academy of Science. At the same time the WMI is the host institute of the chair for Technical Physics (E 23) of the Technical University of Munich with the director of the WMI being ordinarius at the Faculty of Physics of the Technical University of Munich. The WMI carries out research projects at low and ultra–low temperatures and supplies liquid helium to both universities in Munich. It also provides the technological basis for low and ultra–low temperature techniques and methods. The research program of the WMI is devoted to both **fundamental** and **applied research** in the field of **low temperature solid state physics**.

With respect to **basic research** the main focus of the WMI is on

- superconductivity and superfluidity,
- magnetism and spin transport,
- mesoscopic systems and quantum phenomena in nanostructures,
- and the general properties of metallic systems at low and very low temperatures.

The WMI also conducts **applied research** in the fields of

- superconducting and spintronic devices,
- oxide electronics,
- solid state based quantum information processing systems,
- and the development of low and ultra low temperature systems and techniques.

With respect to **materials science** the research program is focused on

- the synthesis of superconducting and magnetic materials,
- the single crystals growth of oxide materials,
- and the epitaxial growth of complex oxide heterostructures.

Despite many technical problems with part of the new infrastructure and considerable delays in the reconstruction activities going on at the WMI, in the year 2002 most research facilities could be operated again and used for the ongoing research projects. In particular, the new clean room (about 50 m^2) with the electron beam and the optical lithography and the new thin film laboratory (about 80 m^2) with all the thin film equipment (Laser Molecular Beam Epitaxy (L-MBE) system, magnetron sputtering system, ion beam sputtering system, ion beam etching system, e–beam evaporation system) could be routinely operated. The same is true for the new x–ray laboratory with both a two–circle and high resolution four–circle diffractometer, the high field laboratory with a 8/10 and 15/17 Tesla magnet unit and the SQUID magnetometer for the measurement of magnetic sample properties between 1.5 and 700 K. The equipment of the new laboratory for the synthesis of bulk materials and single crystal growth has been completed in 2002 by the installation of a four-mirror image furnace allowing the growth of various oxide materials using the traveling solvent floating zone technique. That is, despite considerable problems with the building projects, already most of the experimental basis installed at the WMI could be successfully used during for the ongoing research projects this year.

The research at the WMI has been very successful in 2002 as demonstrated by more than 40 scientific papers and a large number of invited presentations at national and international conferences as well as seminar talks and colloquia. The ongoing research projects have been successfully continued and new projects have been started. In particular, the WMI took the leadership in setting up a coordinated long term research program (Sonderforschungsbereich) on Solid State Based Quantum Information Processing Systems bringing together different research groups from the Technical University of Munich, the Ludwig-Maximilians-University, the Max-Planck-Institute for Quantum Optics as well as groups from the Universities of Augsburg and Regensburg. The goal of this long-term research effort is to develop the physical concepts and materials aspects for scalable quantum information processing systems by bringing together research groups with competence in the fields of experimental and theoretical solid state physics, materials and nanotechnology, quantum information theory, low temperature techniques and quantum optics.

Throughout 2002, an average of 15 scientific staff members, 18 members of the administrative and technical staff, 10 doctorate candidates, 7 diploma candidates and more than 20 short and long–term guests belonged to the institute. Of course, the scientific productivity of the WMI would not be possible without the collaborative atmosphere, the high motivation of our research groups and the support of various funding agencies. In particular, we acknowledge the financial support from the Bavarian Academy of Science, the German Science Foundation, the Bavarian Ministry for Science and Arts, the BMBF and the EU.

This Annual Report gives an overview on the scientific results of the WMI which in many cases have been obtained within joint national and international research projects and in close collaboration with international guests. Our 2002 Annual Report is intended to provide an overview of our work to our friends and partners in research and industry and thereby to intensify our numerous collaborations. I would be particularly pleased if the report would stimulate new collaborations. In order to be useful also for our numerous international partners, especially within EU projects, the report is written in English.

I finally would like to thank all the colleagues, guests, students, post–docs and cooperating partners, who contributed to the success of our work within the last year, and last but not least all our friends and sponsors for their interest, trust and continuous support.

Rudolf Gross

Garching, December 2002

Contents

The Walther–Meissner–Institute

The Walther–Meissner–Institute for Low Temperature Research (WMI) is operated by the Commission for Low Temperature Physics of the Bavarian Academy of Science (BAdW). The Commissions (Research Groups) of the Bavarian Academy are set up in order to carry out long–term projects which are too ambitious for the lifetime or capacity of any single researcher, or which require the collaboration of specialists in various disciplines. At present, the Bavarian Academy of Science consists of 36 Commissions with more than 300 employees. The WMI also is the host institute of the chair for Technical Physics (E 23) of the Technical University of Munich. The director of the WMI at the same time is ordinarius at the Faculty of Physics of the Technical University of Munich.

The research at the Walther–Meissner–Institute is focused on low temperature physics (see reports below). The WMI also develops systems and techniques for low and ultra–low temperature experiments. As typical examples we mention a dry mK-system that can be operated without liquid helium by using a pulse-tube refrigerator for precooling, a nuclear demagnetization cryostat for temperature down to below 100 μK, or very flexible dilution refrigerator inserts for temperatures down to about 20 mK fitting into a 2 inch bore. These systems have been engineered and fabricated at the WMI. Within the last years, several dilution refrigerators have been provided to other research groups for various low temperature experiments. The WMI also developed a pumping system for liquid helium that is commercialized in collaboration with a company.

The individual research groups of the WMI offer attractive research opportunities for diploma (graduate) students, PhD students and postdoctoral fellows. The WMI ist equipped with state of the art facilities for the preparation and characterization of superconducting and magnetic materials as well as for various low and ultra–low temperature experiments. The main experimental and technological resources of the WMI are listed in the following.

Materials Preparation and Fabrication of Nanostructures

- Laser Molecular Beam Epitaxy system for oxide heterostructures (equipped with in–situ RHEED, AFM/STM system, atomic oxygen source, laser heating system, metallization)
- magnetron sputtering system for oxide heteroepitaxy (equipped with four sputtering guns and an oxygen ion gun)
- ion beam sputtering system
- metallization system (equipped with e–gun and thermal evaporators)
- ion beam etching system equipped with a LN_2 cooled sample holder
- polishing machine for substrate preparation
- ultrasonic bonding machine
- 50 m^2 class 1000 clean room facility
- optical lithography (Süss maskaligner MJB 3, projection lithography)
- electron beam lithography (based on Philips XL 30 SFEG scanning electron microscope and Raith Elphy Plus lithography system including a laser stage)
- four-mirror image furnace for crystal growth

Characterization

- 2–circle x–ray diffractometer (Bruker D8 Advance, sample temperature up to 1 600°C)
- high resolution 4–circle x–ray diffractometer (Bruker D8 Discover)

- scanning electron microscope with EDX analysis
- AFM/STM system
- two Raman spectroscopy systems (1.5 to 300 K, in-situ sample preparation)
- SQUID magnetometer (1.5 to 700 K, up to 7 Tesla)
- several high field magnet systems (up to 17 Tesla)
- experimental set–ups for the measurement of noise including low noise SQUID amplifiers and signal analyzers
- high frequency network analyzer (up to 40 GHz) for the determination of high frequency parameters

Low temperature systems and techniques

- several ^{3}He/^{4}He dilution refrigerators inserts for temperatures down to 10 mK
- "dry" mK-cooler based on a dilution refrigerator with pulse-tube precooling
- ultra–low temperature facility for temperatures down to below 100 μK based on a nuclear demagnetization cryostat
- experimental set–ups for the measurement of specific heat, magnetization, thermal expansion as well as electrical and thermal transport properties as a function of temperature, magnetic field and pressure

Coexistence of Superconductivity and Charge Density Wave in the Organic Metal α-(BEDT-TTF)$_2$KHg(SCN)$_4$

D. Andres, M. Kartsovnik, W. Biberacher, K. Neumaier

The layered organic metal α-(BEDT-TTF)$_2$KHg(SCN)$_4$ has a strongly anisotropic electron system with coexisting quasi-one-dimensional (Q1D) and quasi-two-dimensional (Q2D) conducting bands. Numerous experiments point to a nesting instability of the Q1D parts of the electronic bands causing the formation of a charge density wave (CDW) at $\approx$ 8.5 K (for a review see, e.g., [1, 2] and references therein). The Q2D band remains metallic resulting in a decreasing resistance with cooling down to lowest temperatures. As reported last year hydrostatic pressure suppresses the CDW state in α-(BEDT-TTF)$_2$KHg(SCN)$_4$, re-establishing the normal metallic (NM) state above $P_0 \approx 2.5$ kbar [2]. Moreover, the title compound also has been found to become superconducting (SC) under hydrostatic pressure. Superconductivity was proposed to already exist at ambient pressure by Ito et al. [3], who found an accelerated decrease of the resistance below 300 mK, which depends on the applied current and magnetic field. The incomplete SC transition (non-zero resistance) was interpreted [3] in terms of the proximity of the in-plane sheet resistance to the critical value $h/4e^2$ of a superconductor-insulator transition in disordered two-dimensional superconductors [4]. By contrast, the isomorphous salt α-(BEDT-TTF)$_2$NH$_4$Hg(SCN)$_4$ does not undergo the CDW transition but instead becomes superconducting at $T_c \approx 1$ K [5]. The rather sharp bulk SC transition in that compound was thus explained [3] by the sheet resistance far below $h/4e^2$. In the above discussion of incomplete superconductivity it is assumed that the density wave increases the sheet resistance. Thus, one might expect that the suppression of the CDW by pressure would lead to an enhancement of superconductivity. In this report, we show how the CDW acts on the SC transition and that the above suggested scenario of incomplete superconductivity is hardly realized in this system.

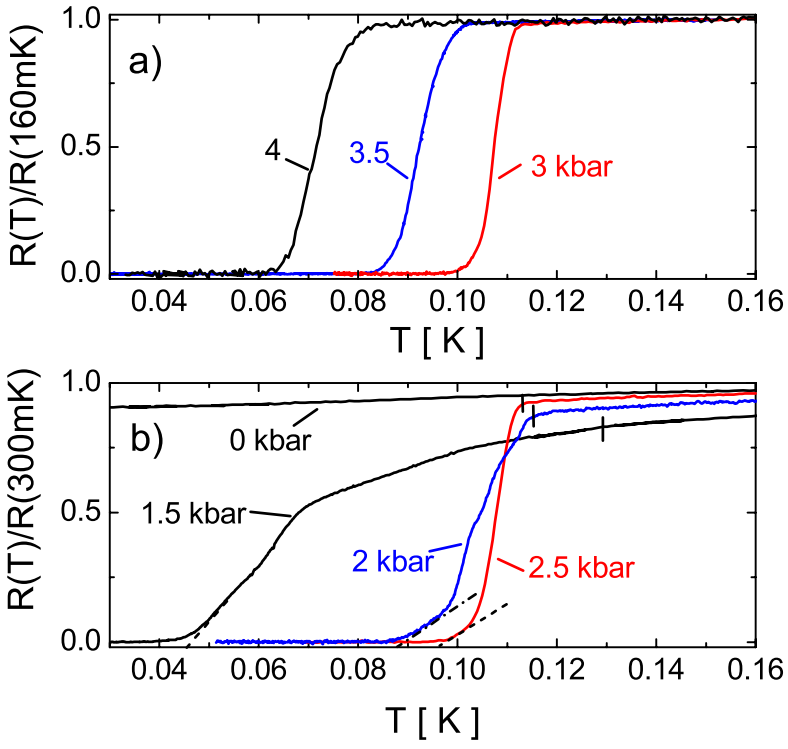

Figure 1: SC transitions in the temperature dependence of the interplane resistance at (a) $P > 2.5$ kbar and (b) $P \leq 2.5$ kbar. In (b) an onset of the transition is determined by a step-like change of the slope (vertical dashes) and an offset by linear extrapolations to zero-resistance (dotted lines).

The data presented here were taken from interlayer resistance measurements on two different samples. Pressure was applied using the conventional clamp cell technique. The cell was mounted on a dilution refrigerator allowing the sample to be cooled down to $\approx$ 20 mK. To avoid heating the sample current was kept below 100 nA. Thus, the temperature increase was estimated to $<$ 5 mK at T = 20 mK.

Fig.1 shows temperature dependencies of the resistance of sample #1 at various pressures. As can be seen in the NM region (Fig.1a), i.e. at $P > P_0$, relatively sharp SC transitions are observed.

The transition temperatures T_c, extracted from the inflection point of the resistive transition, are presented as filled circles in Fig. 2. T_c clearly decreases with increasing pressure, a scenario commonly observed in the NM states of organic metals [5]. On lowering the pressure below P_0 (Fig.1b), the SC transition becomes strongly influenced by the presence of the density wave. This can be described as follows: (i) The transition itself changes, becoming the broader the better the nesting of the density wave is. Due to the broadening an exact determination of T_c is not possible at $P < P_0$. We therefore determine the on- and offset transition temperatures as shown in Figs. 1b and 2. (ii) Within the transition several distinct steps emerge. (iii) Already at temperatures far above the step features the resistance starts to decrease in a SC-like manner. The starting temperature (not shown) is found to be slightly pressure dependent: 250 mK at 2.5 kbar and 300 mK at 2 kbar and 0 kbar. This decrease is easily suppressed by a small magnetic field and depends on current as already reported for $P = 0$ kbar [3]. This suggests the presence of small SC regions or filaments.

Obviously the sharp transitions at $P \geq 2.5$ kbar are far below the proposed T_c value at ambient pressure, i.e. 300 mK. The incomplete superconductivity within the CDW state therefore can hardly be attributed to the proximity to an metal to insulator transition, since in the latter model T_c is expected to increase with decreasing sheet resistance. Furthermore, in the NM state of the title compound dT_c/dP is found to be $\approx$ 30 mK/kbar, that is, nearly an order of magnitude smaller than observed in α-(BEDT-TTF)$_2$NH$_4$Hg(SCN)$_4$ [5]. This might be due to different parts of the Fermi surface contributing to superconductivity in both compounds. Therefore, a direct comparison of the SC properties most likely is inappropriate.

The observed sample dependence of the transition temperatures (Fig.2) gives evidence for a possibly non-pure *s*-wave nature of the SC order parameter, as it already has been suggested in some other BEDT-TTF based superconductors [5]. We expect crystal defects or impurities to have a large effect on T_c, since in both samples the crystal quality, which can be determined from the residual resistance ratios or from the Shubnikov-de Haas oscillations of the Q2D band, appeared to be similarly high. Remarkably, within the CDW state of our compound the sample dependence of the transition points is found to become even stronger (see 1.5 kbar in Fig.2). Thus, the additional influence of the CDW on superconductivity also most likely depends on impurities or defects. Indeed, such a dependence is proposed for a CDW and superconductivity coexisting on an imperfectly nested Fermi surface [6]. In this model, T_c is proposed to decrease with increasing nesting conditions. If this is the case here, there would still remain the question why such a strong broadening of the transition in the CDW state occurs. To clarify the situation it would be in particularly helpful to perform measurements of the inplane resistance.

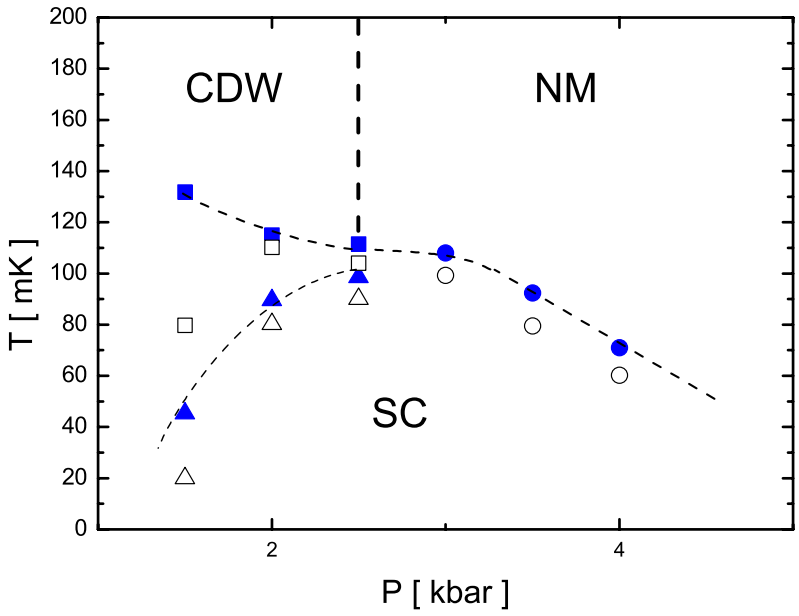

Figure 2: Low-temperature part of the T-P phase diagram: circles show inflection points of the SC transition in the M region; squares/triangles show the onsets/offsets of the transition in the CDW region. Filled and open symbols correspond to sample #1 and #2, respectively. Dashed lines are guides for the eye.

References

[1] M. V. Kartsovnik, D. Andres, W. Biberacher, P. Christ, T. Togonidze, E. Steep, E. Balthes, H. Müller, and N. D. Kushch Synth. Met. **120**, 687 (2001).
[2] D. Andres, M. Kartsovnik, W. Biberacher, H. Weiss, E. Balthes, H. Müller, and N. Kushch, Phys. Rev. B **64**, 161104(R)(2001).
[3] H. Ito, M. V. Kartsovnik, H. Ishimoto, K. Kono, H. Mori, N. D. Kushch,G. Saito, T. Ishiguro, and S. Tanaka, Synth. Met. **70**, 899 (1995).
[4] M. Fisher, Phys. Rev. Lett. **65**, 923 (1990).
[5] T. Ishiguro, K. Yamaji, and G. Saito, *Organic Superconductors*, Springer-Verlag, Berlin, Heidelberg 1998.
[6] A. M. Gabovich, A. I. Voitenko, and M. Ausloos, Phys. Rep. **367**, 583 (2002).

Slow Oscillations of Interlayer Magnetoresistance in Quasi-two-dimensional Metals [1]

M. Kartsovnik and W. Biberacher [2]

The high-field magnetoresistance (MR) of a number of layered organic metals characterized by a weakly warped cylindrical Fermi surface (FS) exhibits prominent slow oscillations superposed on the fundamental Shubnikov-de Haas (SdH) oscillations. Since the behavior of these slow oscillations strongly resembles that of the SdH effect, they have been supposed to originate from additional very small pockets of the (FS). However, band structure calculations, which usually correctly reproduce the FS topology of organic metals [1], do not explain such small groups of carriers.

We have performed detailed studies of the oscillating interlayer MR of the organic metal β-(BEDT-TTF)$_2$IBr$_2$ at various orientations of the applied magnetic field. Our results provide an unequivocal evidence that the slow oscillations do not reveal any new carriers but are ultimately caused by a weak warping of the single cylindrical FS in this Q2D metal. We propose a theoretical explanation of the phenomenon, which appears to be in good agreement with the experiment.

The experiment was performed on a high-quality $[R(290\mathrm{K})/R(2\mathrm{K}) \geq 3000]$ single crystal with the dimensions $0.6 \times 0.3 \times 0.12\mathrm{mm}^3$. The sample was mounted in a measuring cell of a ^{3}He-cryostat allowing for the measurement of the resistance at different orientations of the magnetic field produced by a 14 T superconducting magnet. The field orientation was defined by the angle θ between the field direction and the normal to the highly conducting *ab*-plane of the sample.

Fig. 1 shows an example of the oscillating MR as a function of magnetic field B at temperatures $T = 0.56$ and 1.4 K. The fundamental SdH oscillations clearly observed at the lower temperature are periodic in a $1/B$ scale and have the frequency $F = 3930$ T. This is fully consistent with previous observations [2]. These oscillations reveal a slightly warped cylindrical FS with the cross-section occupying $\approx 55\%$ of the Brillouin zone area. The amplitude of these oscillations is modulated by the factor $\cos(2\pi F_{\mathrm{beat}}/B - \gamma)$, where $F_{\mathrm{beat}} = \frac{1}{2}(c\hbar/2\pi e)(A_{\mathrm{max}} - A_{\mathrm{min}})$ is determined by the difference between the maximum and minimum cross-sections, A_{max} and A_{min}, of the warped FS cylinder, and γ is a phase offset [3].

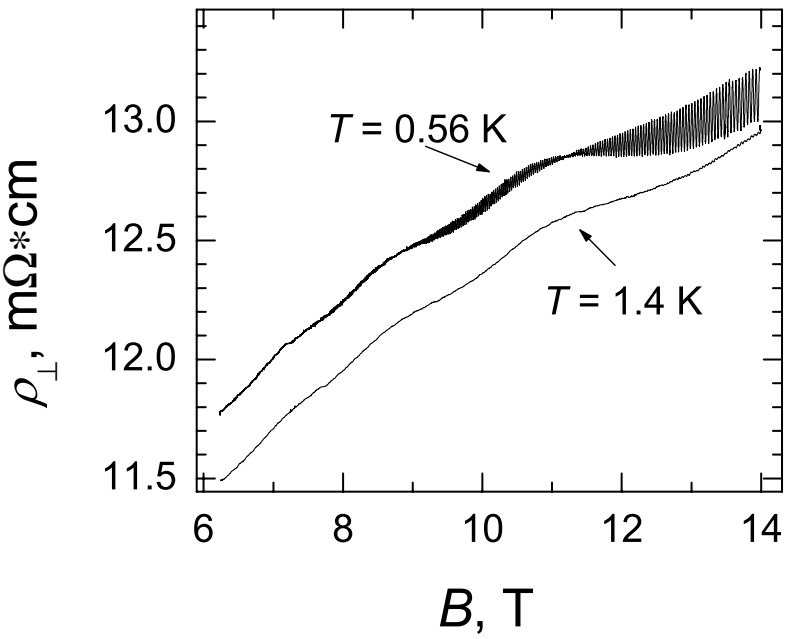

Figure 1: Interlayer resistivity of β-(BEDT-TTF)$_2$IBr$_2$ versus magnetic field.

[1] This work is supported by the EU ICN, contract No.: HPRI-CT-1999-40013.

[2] In collaboration with P. Grigoriev, L.D. Landau Institute for Theoretical Physics, Chernogolovka, Russia, and GHMFL, MPI&CNRS, Grenoble, France

Besides the rapid SdH oscillations, the MR exhibits oscillations with a ~ 100 times lower frequency. The most prominent feature of these oscillations illuminating their nature is the dependence of their frequency on the field orientation. Fig. 2a shows the frequencies of the rapid and slow oscillations as functions of angle θ. While $F(\theta)$ obeys the $1/\cos\theta$-law typical of a cylindrical FS, the non-monotonic behavior of the lower frequency $F_{\rm slow}(\theta)$ can hardly be explained by some peculiar form of a FS pocket. On the other hand, it obviously correlates with the angular dependence of the MR background shown in Fig. 2b: $F_{\rm slow}$ rapidly decreases at approaching the angles corresponding to the peaks of the background MR. The latter occur at $\theta \approx +33^\circ$ and -20° and manifest the so-called angle-dependent MR oscillations (AMRO) [2] originating from the quasi-two-dimensional character of the electronic system. At the same angles the beats of the fundamental SdH oscillations vanish, their frequency $F_{\rm beat}$ going to zero. One can therefore suggest that $F_{\rm slow}(\theta)$ is directly related to $F_{\rm beat}(\theta)$. Indeed, detailed field sweeps made at different θ's show that the maxima of the slowly oscillating component of MR are located near the beat nodes (see e.g. Fig. 1), i.e. $F_{\rm slow}(\theta) = 2F_{\rm beat}(\theta)$.

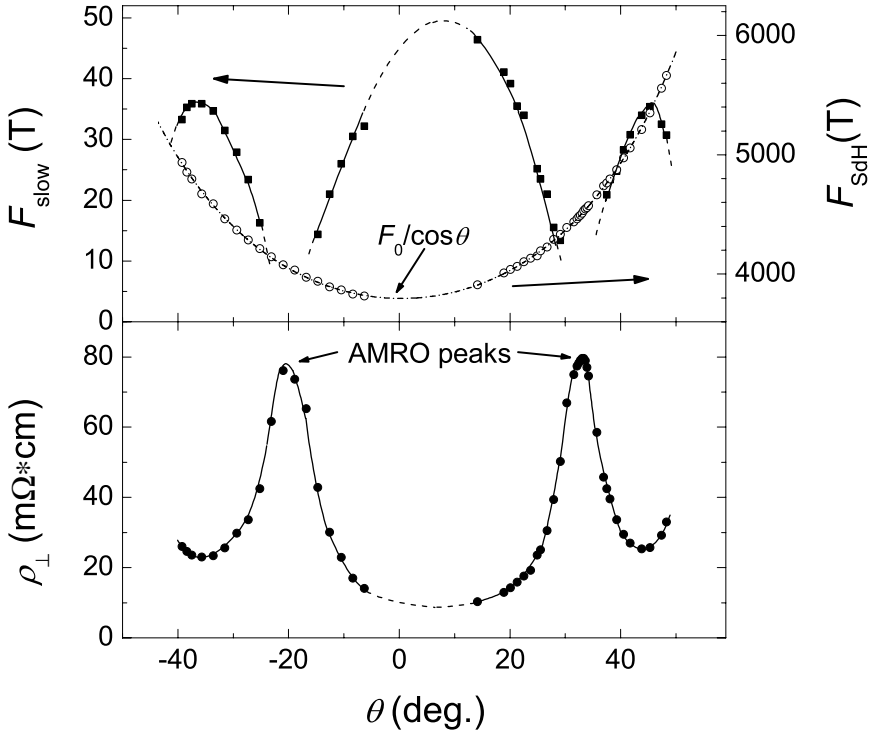

Figure 2: (a) - frequency of the slow oscillations (solid squares, left scale) and fundamental SdH oscillations (open circles, right scale) oscillations as a function of angle θ; (b) - angular dependence of the background resistivity.

To understand this result, one should take into account that in general the interlayer MR contains several factors oscillating in magnetic field. The amplitudes of the oscillations are modulated, due to the warping of the cylinder, with the frequency $F_{\rm beat} = (2t_\perp/\varepsilon_F)F \ll F$ (here, $t_\perp$ is the interlayer transfer integral and ε_F is the Fermi energy). The product of two oscillating quantities with modulated amplitudes $\tilde{\alpha}$ and $\tilde{\beta}$ yields a slowly oscillating term, e.g. $(1+\tilde{\alpha}\cos x)(1+\tilde{\beta}\cos x) = 1 + (\tilde{\alpha} + \tilde{\beta}\cos x + (\tilde{\alpha}\tilde{\beta}/2)\cos 2x + \tilde{\alpha}\tilde{\beta}/2$. Here, the last term is responsible for slow oscillations with the frequency $2F_{\rm beat}$.

In particular, when the cyclotron energy $\hbar\omega_c = \hbar eB/mc$ (where ω_c is the cyclotron frequency and m is the effective cyclotron mass) is comparable to $t_\perp$, both the relaxation time τ and interlayer velocity v_z give significant contributions to the SdH effect and the oscillating part of the interlayer conductivity $\tilde{\sigma}_{zz}$ can be expressed as [4]:

$$\sigma_{zz} \propto 2\cos\left(\frac{2\pi\mu}{\hbar\omega_c}\right)\cos\left(\frac{4\pi t_\perp}{\hbar\omega_c} - \frac{\pi}{4} + \phi\right) R_D R_T + \sqrt{\frac{\hbar\omega_c}{2\pi^2 t_\perp}}\cos\left(2\frac{4\pi t_\perp}{\hbar\omega_c} - \frac{\pi}{2} + \phi\right) R_D^{*2}. \qquad (1)$$

Here, μ is the chemical potential and $\phi = \arctan(\hbar\omega_c/2\pi t_\perp)$. The first term on the right-hand side of Eq.(1) describes the fundamental SdH oscillations with the amplitude damped by the scattering and

temperature damping factors [5], R_D and R_T, respectively, and modulated with the frequency $F_{\text{beat}} = 2t_\perp m/e\hbar$. It is the second term in Eq. (1) which describes the slow oscillations with $F_{\text{slow}} = 2F_{\text{beat}}$. Local minima of the slowly oscillating conductivity (hence maxima in magnetoresistance) should occurs at the same fields as the beat nodes, if one neglects the phase offset ϕ. The latter phase offset causes a small but finite difference between the positions of the beats and the slow oscillations. Thus, the data shown in Fig.1 are in very good agreement with the predictions of Eq.(1).

It is important to note that the term responsible for the slow oscillations does not depend on the chemical potential μ. Therefore, it is not sensitive to the temperature smearing of the Fermi distribution and macroscopic inhomogeneities of the sample. This is why the slow oscillations, despite being determined by the cyclotron motion on the same orbits as the fundamental SdH oscillations, survive up to much higher temperature. From the field and temperature dependencies of the slow oscillations one can extract a valuable information on electron scattering processes [4].

Finally, we would like to note that the above consideration suggests that the slow oscillations are a general feature of clean quasi-two-dimensional metals. They are expected to develop when the cyclotron energy becomes comparable with the interlayer transfer energy.

References

[1] T. Ishiguro, K. Yamaji and G. Saito, *Organic Superconductors*, 2nd Edition, Springer-Verlag, Berlin, 1998.
[2] M.V. Kartsovnik, V.N. Laukhin, J. Phys. I France 6 (1996) 1753
[3] P.D. Grigoriev, M.V. Kartsovnik, W. Biberacher, N.D. Kushch and P. Wyder, Phys. Rev. B **65**, 060403(R) (2002).
[4] M.V. Kartsovnik, P.D. Grigoriev, W. Biberacher, N.D. Kushch and P. Wyder, Phys. Rev. Lett. **89**, 126802 (2002).
[5] D. Shoenberg, *Magnetic oscillations in metals*, Cambridge University Press, Cambridge, 1984.

Evidence of Charge Ordering in $La_{2-x}Sr_xCuO_4$

F. Venturini, Q.-M. Zhang, R. Hackl [1]

Copper-oxide systems are characterized by several competing instabilities such as long-range antiferromagnetism, charge and spin ordering, and superconductivity. In this panoply, one of the more vexing questions is the origin of superconductivity and, in particular, the high transition temperatures T_c. It has been argued [1] that the ordering of the originally two-dimensional charge distribution in the planes into one-dimensional structures or "stripes" (Fig. 1) could be a precursor of superconductivity. The observation of stripes, however, and their properties and relationship to other instabilities in the cuprates is a matter of ongoing discussion. While the existence seems to be proved at least for some of the compounds the electrodynamics is still an open issue. Some clues could be found in systems with static stripes, i.e. whenever the putative charge instability couples strongly to the lattice. However, in most of the compounds, in particular at doping levels in the metallic state the stripes are usually fluctuating and do not lead to anisotropies in the conductivity, for instance. Consequently, one has to look for indirect rather than for direct indications.

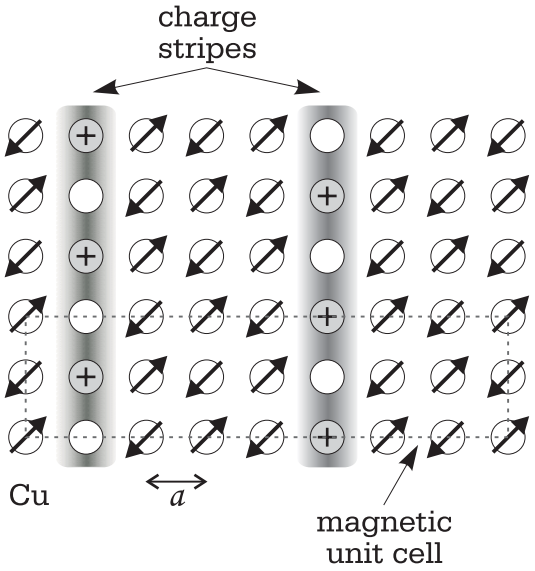

Figure 1: Sketch of charge ordering in the CuO_2 plane.

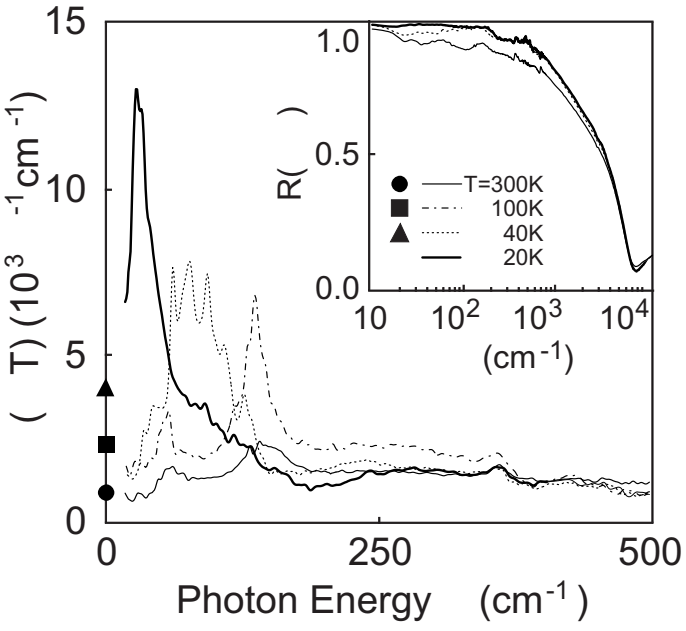

Figure 2: Far infrared spectra of $La_{1.90}Sr_{0.10}CuO_4$.

One way to look at stripes is the scenario of density waves. The subject is well studied both theoretically and experimentally [2]. Among other things an enhanced conductivity is found below the transition for energies smaller than the gap. This is indeed found in the infrared spectra of underdoped $La_{2-x}Sr_xCuO_4$ with $x = 0.10$ (Fig. 2) [3]. The spectra at high temperatures show a conductivity $\sigma(\omega, T)$ which is typical for cuprates at this doping level: $\sigma(\omega, T)$ decreases very slowly with ω.

Upon lowering T a new structure starts to develop in the energy range between 0 and 200 cm^{-1}. It gains intensity very rapidly and softens. At 20 K just below T_c the conductivity

[1] In collaboration with P. Calvani, S. Lupi, A. Lucarelli, M. Ortolani, A. Nucara, Università di Roma "La Sapienza", P. Giura, ESRF, and N. Kikugawa and Toshizo Fujita University of Hiroshima.

This work is supported by the DFG, the DAAD, and the Alexander von Humboldt Foundation.

is as high as 13,000 $\Omega^{-1}\mathrm{cm}^{-1}$. Below the peak $\sigma(\omega,T)$ extrapolates to the dc value indicating the stability of the analysis. At all temperatures even at $T = 300$ K the dc conductivity measured by conventional transport is smaller than the conductivity in the low-energy peak. Since this non-monotonicity of the conductivity is observed for all underdoped metallic samples [4] it can be considered robust.

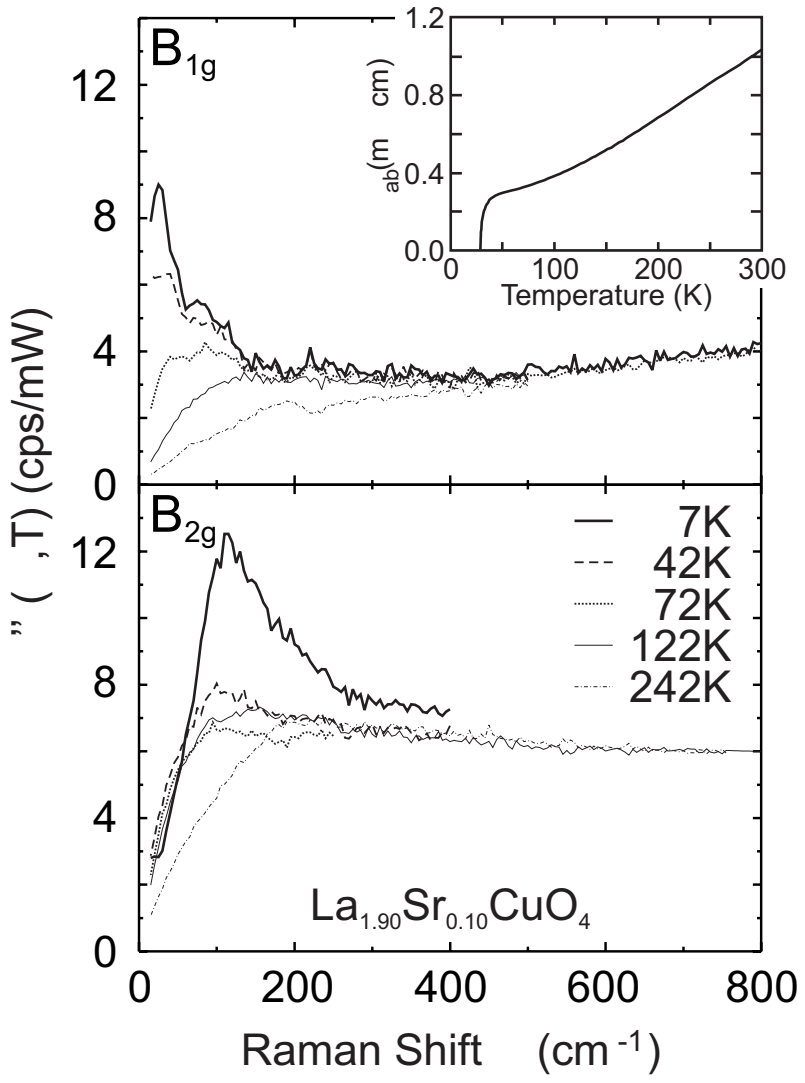

Figure 3: Raman spectra of $La_{1.90}Sr_{0.10}CuO_4$.

In the Raman spectra (Fig. 3) there are corresponding structures being, however, observed in B_{1g} symmetry only. While the response in B_{2g} symmetry is similar as in other high-T_c compounds a completely unexpected evolution with temperature is found in B_{1g} symmetry. At high temperature the B_{1g} spectra are much flatter at $\omega \to 0$ than the B_{2g} spectra indicating a larger B_{1g} relaxation rate. As expected for metallic behavior the B_{2g} spectra become more steep upon cooling. However, in contrast to other underdoped cuprates where the B_{1g} spectra flatten on cooling as a consequence of a metal-insulator transition [5] a pile up of spectral weight towards low energies is observed here. The corresponding relaxation rate not only decreases but even crosses the B_{2g} rate at approximately 100 K where the slopes in the two symmetries are approximately equal. Hence, the "Raman conductivity" $\chi''(\omega,T)/\omega \propto \sigma(\omega,T)$ in B_{1g} symmetry or, equivalently, along the copper-oxygen bonds is substantially higher than the conventional conductivity indicating 1D conduction channels at low temperature.

The onset temperature for the observed phenomenon is at approximately 250 K for $x = 0.19$ and increases by a factor of 2 with decreasing x as can be seen in the compilation of the presently existing infrared data (Fig. 4). In the figure the maximum conductivity of the peak at finite energy is plotted as a function of temperature for various samples at doping levels $0.03 \leq x \leq 0.26$. At $x = 0.26$ no transition is found, and the data can be interpreted in terms of a single component Drude-type of response. At $x = 0.19$ the transition is below room temperature. At lower doping the crossover can only be found by extrapolation.

References

[1] V. Emery and S. Kivelson, Nature **374**, 434 (1995).

[2] G. Grüner, *Density Waves in Solids*, Frontiers in Physics **89**, Addison-Wessely (1995).

[3] F. Venturini *et al.*, Phys. Rev. B **66**, 060502(R) (2002).

[4] A. Lucarelli *et al.*, Phys. Rev. Lett. accepted for publication (2002).

[5] F. Venturini *et al.*, Phys. Rev. Lett. **89**, 107003 (2002).

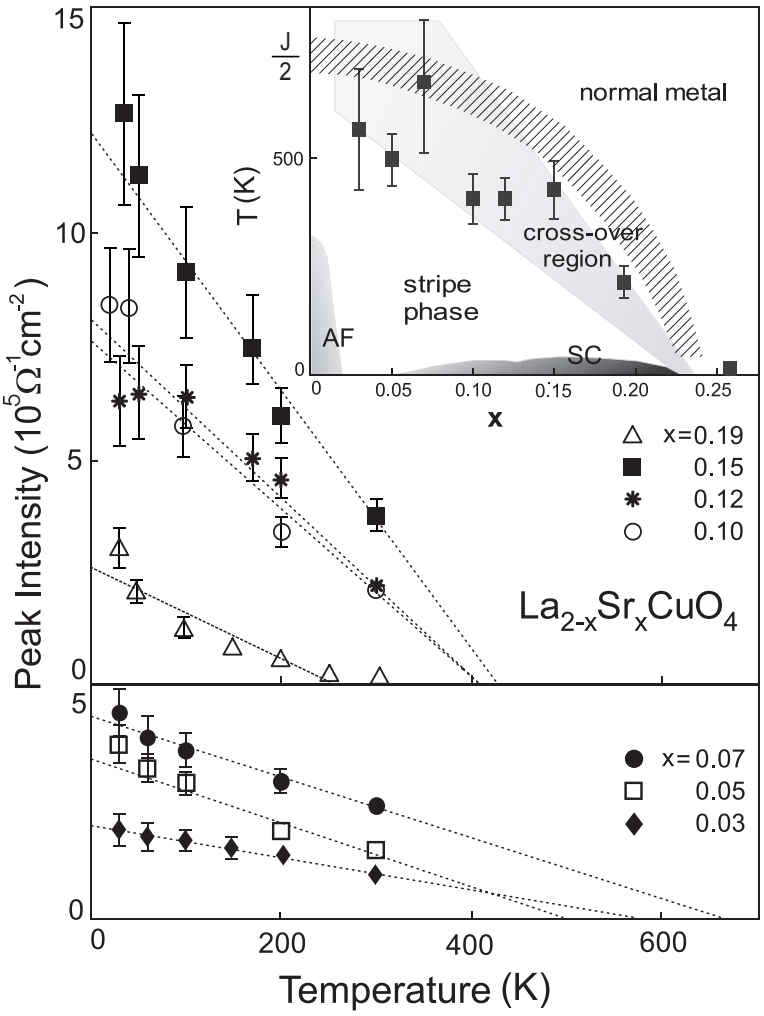

Figure 4: Onset temperature for stripe formation [4].

Study of the Raman Response at High Energy Transfers

F. Venturini, Q.-M. Zhang, R. Hackl [1]

Many scenarios aiming to explain the properties of the copper-oxygen compounds consider unconventional electron dynamics such anyons obeying neither Bose nor Fermi statistics, flux phases with spontaneous circulating currents, coupling to chiral spin waves (Fig. 1) or pairing driven by a reduction of the kinetic rather than the potential energy. [1] There is no simple experimentum crucis which would allow to either pinpoint one or to exclude another possibility. However, in most of the cases unconventional dynamics leave their fingerprints. For instance, anyons and circulating currents would violate time-reversal symmetry. Kinetic energy pairing would lead to a violation of the conductivity sum rules in an energy range of at least a few eV [2, 3, 4] and chiral excitations produce light-scattering spectra of A_{2g} symmetry which are forbidden for the usual carrier response [5]. These are some motives why we started studying the Raman response at high energy transfers and performing a complete symmetry analysis.

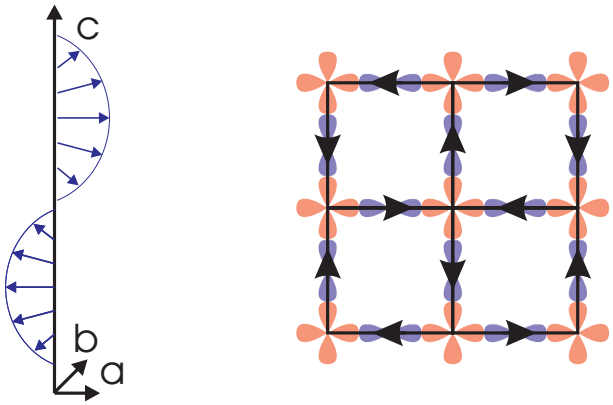

Figure 1: Chiral spin wave (left) and sponaneous circulating currents in the CuO_2 plane (right).

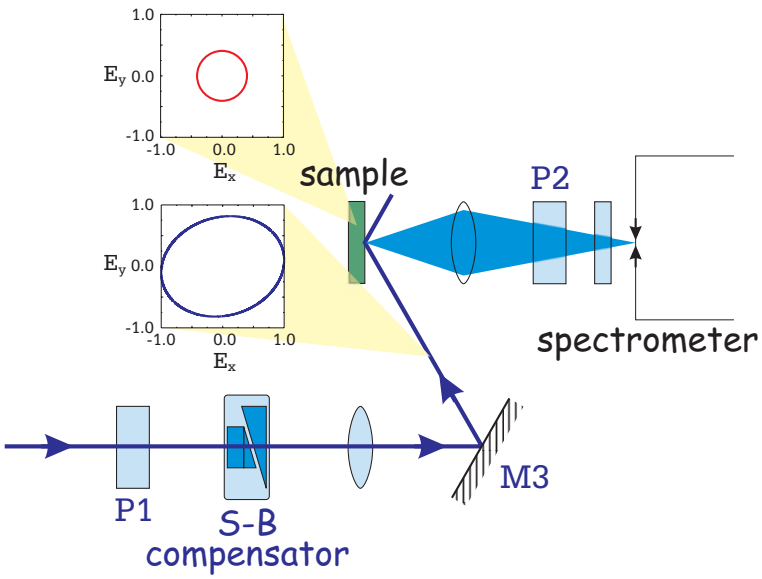

Figure 2: Sketch of the experimental setup. For circularly polarized light inside the sample (red) the incoming laser light must be polarized elliptically (blue).

Experimentally this is more demanding than looking at small energy transfers. First, the spectrometer has to be calibrated since the sensitivity varies by more than an order of magnitude in the range of interest. Second, the polarization states of the incoming and outgoing photons must be determined precisely. This includes the preparation of both linear and circular polarizations of the exciting light *inside* the sample. Since the light hits the sample at a large angle of incidence in order to prevent directly reflected laser light to penetrate optical elements or to enter the spectrometer, the polarization state outside the sample is different from the desired one inside (Fig. 2). In principle it is possible to determine the A_{2g} response by measuring

[1] In collaboration with H. Berger, EPF Lausanne, B. Revaz, University of Geneva, Y. Ando, CRIEPI, Tokyo, and N. Kikugawa and Toshizo Fujita University of Hiroshima.

This work is supported by the DFG and the Alexander von Humboldt Foundation.

3 spectra but it is good customs to get a complete set of 6 polarization combinations (Fig. 3) which allow a consistency check of the obtained spectra. This is a necessary but, unfortunately, not sufficient condition for the subtraction procedure to return a correct result. However, for the time being subtleties, though important ones, will not be considered. If the spectra are satisfactorily consistent[2] the A_{2g} response, for instance, can be calculated as

$$A_{2g} = \frac{1}{3}[rr + xy + x'y' - \frac{1}{2}(xx + x'x' + rl)]$$

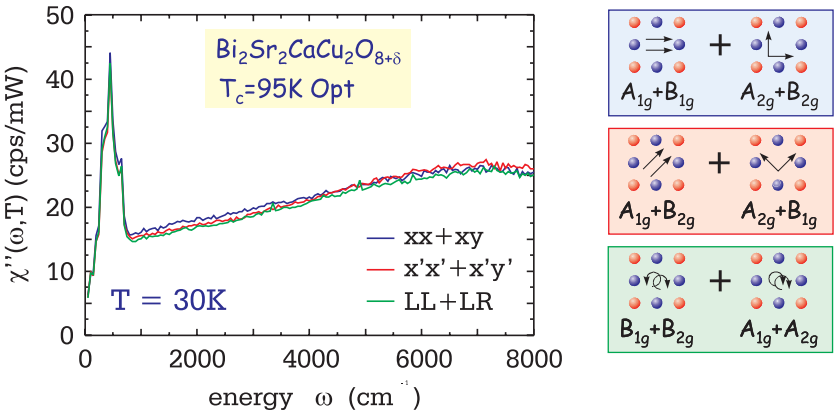

Figure 3: Check of consistency of the Raman spectra of $Bi_2Sr_2CaCu_2O_{8+\delta}$. Each curve corresponds to the sum of two polarization combinations as shown on the right-hand side.

with the symbols x, y and x', y' denoting polarizations parallel and diagonal to Cu-O bonds, respectively. r and l stand for right and left circularly polarized light (see Fig. 3). The other symmetries can be obtained by similar sums.

The results for AF $Bi_2Sr_2CaCu_2O_{8+\delta}$ (Bi-2212) are shown in Fig. 4. The most prominent feature is the two-magnon peak at approximately 3000 cm^{-1} in B_{1g} symmetry. It originates from the simultaneous flip of two nearest-neighbor AF ordered spins. In this energy range substantial intensity is found also in A_{1g} symmetry while the A_{2g} and B_{2g} spectra are comparably weak. Below 1500 cm^{-1} the A_{2g} response cannot be distinguished from zero. As expected there are no phonon lines in A_{2g} which in turn are strong in A_{1g} and B_{1g} symmetry below 1500 cm^{-1}. If there are indeed chiral excitations they couple very weakly to the light.

The question is whether there is an A_{2g} component also superconducting samples and an indication of an interaction between A_{2g} excitations and the paired electrons. This was investigated in an optimally doped single crystal of Bi-2212 with a T_c of 95 K (Fig. 5). The magnon is still present in B_{1g} symmetry but is shifted down to approximately 1600 cm^{-1} indicating the persistence of magnetic correlations at this doping level. A small increase of the peak frequency and the evolution of a dip between the pair-breaking feature at approximately 500 cm^{-1} and the magnon is found at the transition to the superconducting state.

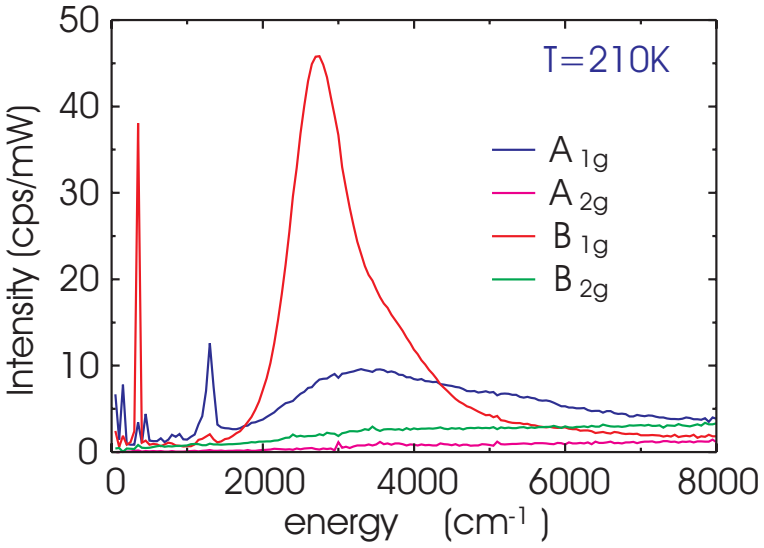

Figure 4: Raman spectra of antiferromagnetic (AF) Bi-2212 for the energy range $0-1$ eV.

[2] We are aware that there is room for individual taste.

In the three other symmetries no magnon features are found any more. The A_{2g} continuum is still very weak if not zero below 500 cm^{-1} but has comparable intensity at high energy transfers. Below T_c a small modification of the A_{2g} spectrum is observed. At the moment, however, it must doubted that the tiny A_{2g} peak at 30 K is statistically significant given the typical inconsistencies between the polarization combinations of approximately 1 count/s (see Fig. 3).

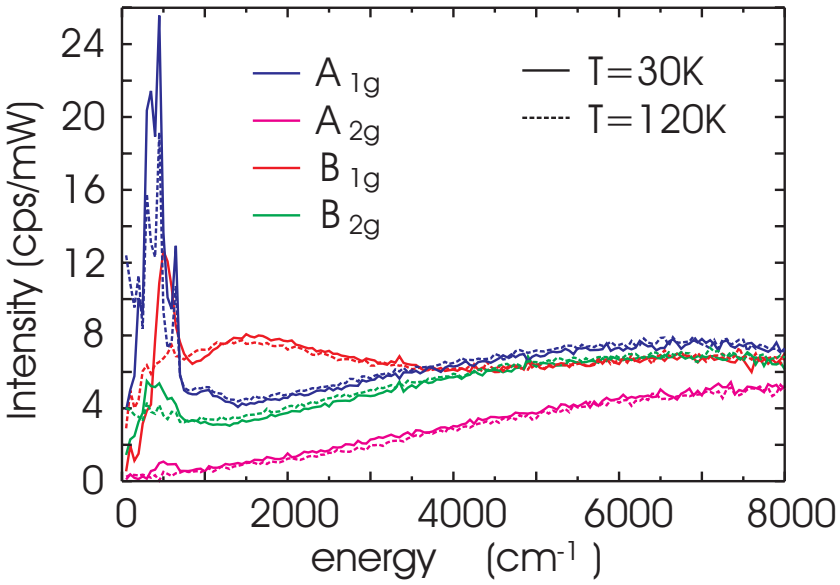

Figure 5: Spectra of Bi-2212 above and below $T_c = 95$ K.

References

[1] E.W. Carlson, V.J. Emery, S.A. Kivelson, and D. Orgad, cond-mat/0206217 (2002) and refences therein.
[2] M. Rübhausen, A. Gozar, M. V. Klein, P. Guptasarma, and D. G. Hinks, Phys. Rev. B **63**, 224514 (2001).
[3] A.F. Santander-Syro, R.P.S.M. Lobo, N. Bontemps, Z. Konstantinovic, Z.Z. Li, H. Raffy, cond-mat/0111539 (2001).
[4] H.J. A. Molegraaf, C. Presura, D. van der Marel, P. H. Kes, and M. Li, Science **295** 2239-2241 (2002).
[5] P.E. Sulewski, P.A. Fleury, K.B. Lyons, and S.-W. Cheong, Phys. Rev. Lett. **67** 3864 (1991).

Coexistence of Pseudogap and Superconductivity in Electron Doped High-Temperature-Superconductors

B. Welter, Y. Krockenberger, L. Alff, R. Gross [1]

The origin of the pseudogap phenomenon and its relation to superconductivity remains one of the most interesting unsolved questions concerning high-temperature superconductors. There are mainly two scenarios explaining the relation between the pseudogap and superconductivity. In the first scenario, the pseudogap and superconductivity are assumed to result from independent physical mechanisms associated with different order parameters. The second scenario is based on the supposition that the pseudogap is a precursor to superconductivity.

The relatively low critical fields of electron doped high-temperature superconductors give us the possibility to study the normal state at low temperatures. Tunneling studies on $Pr_{2-x}Ce_xCuO_4$ (PCCO) in this regime reveal a pronounced gaplike structure at energies comparable to the superconducting gap [1], [2]. Precedent measurements in fields up to 20 T have proven that this pseudogap is a true normal-state phenomenon and not due to some remnant superconductivity [3]. As to the doping dependence, our measurements have shown that the modulation and size of the pseudogap decrease with increasing doping [3]. Starting from these results we have continued our investigations by studying the influence of temperature on the pseudogap in more detail.

Fig. 1 shows tunneling spectra of underdoped $Pr_{2-x}Ce_xCuO_4$, taken in a field of 14 T applied perpendicular to the ab-planes for various temperatures from 4 K to 21 K. At 4 K a distinct gap is found which is filled with increasing temperature, finally disappearing at a temperature T^* of about 19 K. Similar measurements from another group on PCCO-Pb-junctions have shown that this behavior cannot be explained by thermal smearing [2]. Fig. 2 summarizes our results on three differently doped $Pr_{2-x}Ce_xCuO_4$ thin film grain boundary junctions [4]. T^* is displayed as a function of electron doping and compared to the critical temperature T_c. There are two important observations to be emphasized. First, in contrast to hole doped systems, $T^* \leq T_c$. Second, T^* decreases with increasing doping, consistent with our previous measurements. Now the question arises whether this pseudogap regime for $T^* \leq T_c$ exists only when superconductivity is quenched by a magnetic field or whether pseudogap and superconductivity coexist at low temperatures and zero field as suggested in Fig 2.

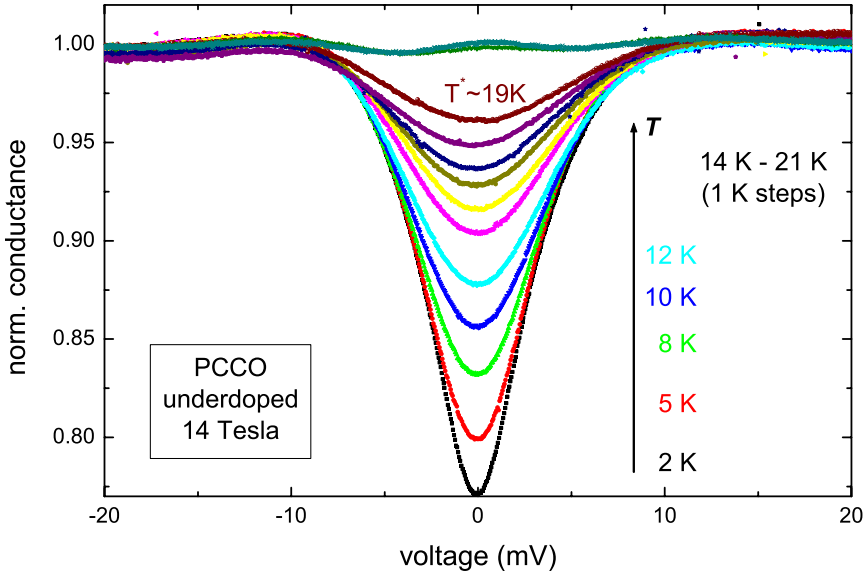

Figure 1: Differential conductance spectra of an underdoped $Pr_{2-x}Ce_xCuO_4$ grain boundary junction for temperatures ranging from 2 K to 21 K in a field of 14 T.

[1] In collaboration with D. Manske, Freie Universität Berlin, and M. Naito, NTT Basic Research Laboratories, Japan.

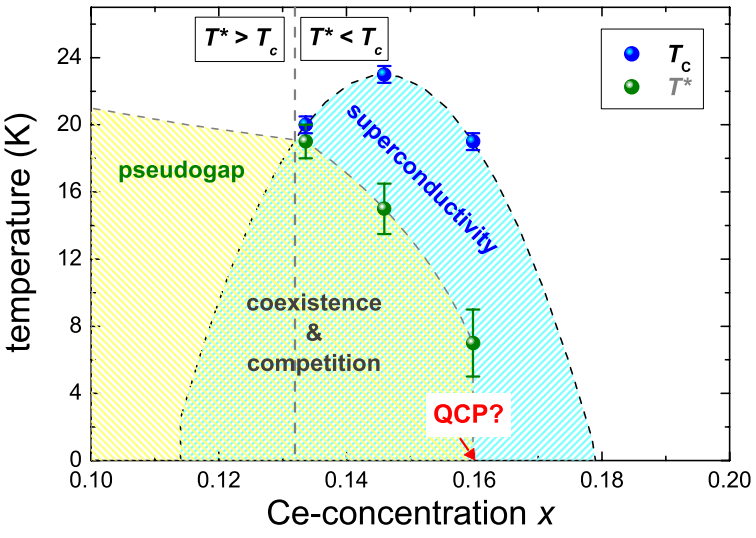

Figure 2: T^* and T_c of $Pr_{2-x}Ce_xCuO_4$ as a function of doping

One important argument in favor of the second assumption is the distribution of spectral weight in the $G(V)$-curves [5]. The conservation of states rule implies that the integrated (normalized) conductance has to be the same in the superconducting and in the normal phase. Fig. 3 shows the result of two normalization methods applied to the same tunneling spectrum, taken at 2 K and 0 T on the underdoped $Pr_{2-x}Ce_xCuO_4$-sample. In curve (i), background conductance effects were removed by normalizing the measured conductance curve by a function of the form $f(V) = a + b \cdot \ln(\cosh(c \cdot V))$, which was fitted to the high energy range of the spectrum. Looking at this normalized spectrum at 2 K and 0 T, it is immediately clear that the area A is larger than the sum of the areas B_1 and B_2.

This means that there is a considerable loss of states near E_F. However, the conservation of states is recovered, if the tunneling curve at 2 K and 0 T is normalized by the spectrum taken at the same temperature but in a field of 15 T which suppresses superconductivity. This strongly suggests a coexistence of the superconducting gap with the pseudogap below T_c, thus ruling out the possibility of preformed pairs as origin of the pseudogap. Very similar results were found in underdoped $Bi_2Sr_2CaCu_2O_y$ [6], indicating a possible common origin of the pseudogap in electron and hole-doped cuprates.

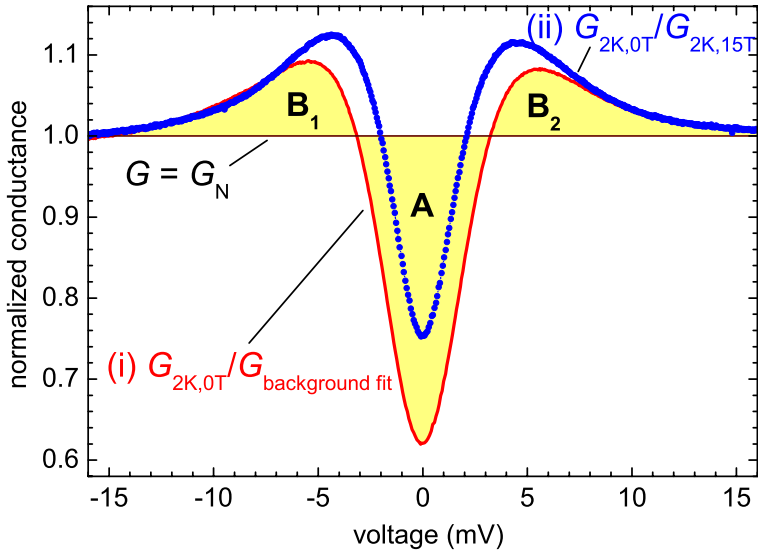

Figure 3: Tunneling spectra of $Pr_{2-x}Ce_xCuO_4$ at 2K and 0T, normalized by a background fit (i) and by the spectrum taken at 2K and 15T(ii).

References

[1] S. Kleefisch, B. Welter, A. Marx, L. Alff, R. Gross and M. Naito, Phys. Rev. B, **63**, 100507(R) (2001)
[2] A. Biswas, P. Fournier, V. N. Smolyaninova, R. C. Budhani, J.S. Higgins and R. L. Greene, Phys. Rev. B, **64**, 104519 (2001)
[3] B. Welter, Y. Krockenberger, M. Schonecke, A. Marx, L. Alff and R. Gross, Annual Report WMI 2001
[4] L. Alff, Y. Krockenberger, B. Welter, R.Gross, D. Manske and M. Naito, submitted to Nature (2002)
[5] B. Welter, Y. Krockenberger, L. Alff, M.Naito and R. Gross, to be published by Physica C (2002)
[6] A. K. Gupta, K.-W. Ng, cond-mat/0202450 (2992)

Analytic two–fluid description of superconductivity and fermionic superfluidity

Dietrich Einzel

Abstract. This work considers the problem of finding simple analytical forms for the temperature dependent thermodynamic and reactive response functions within the weak coupling theory of clean conventional and unconventional superconductors and Fermi superfluids. These are of central importance for a microscopic two–fluid description of superconductivity and superfluidity. In particular we derive very accurate analytic expressions for the entropy, specific heat, spin susceptibility and current of the normal component, formed by the thermal excitations (Bogoliubov quasiparticles), as well as for the superfluid density and hence the magnetic penetration depth, describing the response of the condensate. The results apply to both conventional and unconventional superconductors as well as to (triplet–) paired neutral systems like the A– and B– phases of superfluid ^{3}He or the core of neutron stars.

Equilibrium properties of superconductors and Fermi superfluids. We consider charged and neutral pair–correlated Fermi systems in which the fermionic states are characterized by a momentum $\mathbf{p}=\hbar\mathbf{k}$, an infinite (parabolic) band dispersion $\varepsilon_{\mathbf{p}}=E_{\rm F}+\xi_{\mathbf{p}}$, with $E_{\rm F}$ the Fermi energy, a group velocity $\mathbf{v}_{\mathbf{p}}=\nabla_{\mathbf{p}}\varepsilon_{\mathbf{p}}/\hbar$ and a density of states at the Fermi energy $N_{\rm F}$. The order parameter $\Delta_{\mathbf{p}}$ is assumed to be of the general form:

$$\Delta_{\mathbf{p}\sigma\sigma'}=\Delta_0(T)\ f_{\mathbf{p}}\left[\delta_{s,0}\ i\tau^2_{\sigma\sigma'}+\delta_{s,1}\ \hat{\mathbf{d}}\cdot\left\{\vec{\tau}i\tau^2\right\}_{\sigma\sigma'}\right] \tag{1}$$

Here s denotes the total spin of the Cooper pair and distinguishes singlet ($s=0$) from triplet ($s=1$) pairing. $\Delta_0(T)$ is the temperature dependent gap maximum, $f_{\mathbf{p}}$ describes the (possibility of a) node structure of the gap, to be specified below, and $\tau^i, i=1,2,3$ are the Pauli spin matrices. The momentum–dependent energy gap characterizes the spectrum $E_{\mathbf{p}}$ of thermal excitations, the so–called Bogoliubov quasiparticles $E_{\mathbf{p}}=[\xi^2_{\mathbf{p}}+|\Delta_{\mathbf{p}}|^2]^{1/2}$. The statistical physics of the gas of thermal excitations can be formulated in terms of the Fermi momentum distribution, taken at the quasiparticle energy $E_{\mathbf{p}}$, $\nu_{\mathbf{p}}=\nu(E_{\mathbf{p}})=\left[\exp\left(E_{\mathbf{p}}/k_{\rm B}T\right)+1\right]^{-1}$ and its energy derivative $\varphi_{\mathbf{p}}=-\partial\nu(E_{\mathbf{p}})/\partial E_{\mathbf{p}}$.

Thermodynamic and response functions of the quasiparticle system can be defined by introducing a vertex $a_{\mathbf{p}}\equiv a(\hat{\mathbf{p}},\xi_{\mathbf{p}},E_{\mathbf{p}})$, with normal state limit $a^{\rm N}_{\mathbf{p}}=a(\hat{\mathbf{p}},\xi_{\mathbf{p}})$. This allows for the distinction of different physical quantities like (i) the *entropy* $\sigma_{\rm B}(T)$ ($a^2_{\mathbf{p}}=\xi^2_{\mathbf{p}}/T$), (ii) the *heat capacity* $C^{\rm B}(T)$ ($a^2_{\mathbf{p}}=E^2_{\mathbf{p}}-(T/2)\partial\Delta^2_{\mathbf{p}}/\partial T$) (iii) the *current response* $K^{\rm B}_{\mu\mu}(T)=n^{\rm B}_{\mu\mu}/m$ ($a^2_{\mathbf{p}}=v^2_{\mathbf{p}\mu}$) and (iv) the *spin susceptibility* $\chi^{\rm B}(T)$ ($a^2_{\mathbf{p}}=(\gamma\hbar/2)^2$) by defining generalized Bogoliubov quasiparticle response functions $\mathrm{R}_a(T)$ through:

$$\mathrm{R}_a(T) \;=\; \frac{1}{V}\sum_{\mathbf{p}\sigma}\varphi_{\mathbf{p}}a^2(\hat{\mathbf{p}},\xi_{\mathbf{p}},E_{\mathbf{p}})=N_{\rm F}\left\langle\int_{-\mu}^{\infty}d\xi_{\mathbf{p}}\varphi_{\mathbf{p}}a^2(\hat{\mathbf{p}},\xi_{\mathbf{p}},E_{\mathbf{p}})\right\rangle_{\rm FS} \tag{2}$$

with normal state limit $\mathrm{R}^{\rm N}_a(T)=\lim_{\Delta_{\mathbf{p}}\to 0}\mathrm{R}_a(T)$. Here $n^{\rm B}_{\mu\mu}$ denotes as usual the components of the normal fluid density tensor. For a given vertex $a_{\mathbf{p}}$ one may construct generalized quasiparticle Yosida functions as the ratios:

$$Y_a(T)\equiv\mathrm{R}_a(T)/\mathrm{R}^{\rm N}_a(T) \tag{3}$$

An accurate interpolation procedure. The general idea is to use the exact asymptotic results available in the low temperature limit and near the transition temperature and connect them in oder to have approximate analytical forms for intermediate temperatures. The behavior in the low temperature limit has been discussed in ref. [3] and can be summarized as:

$$\lim_{T\to 0}Y_a(T) \;\equiv\; Y_{a00}(T)=\begin{cases}a^2_0(T)Y_{00}(T) & ;\ \text{isotropic gaps}\\ C_a\{f_{\mathbf{p}}\}\left(\frac{k_{\rm B}T}{\Delta_0}\right)^{\mu_a\{f_{\mathbf{p}}\}} & ;\ \text{nodal gaps}\end{cases} \tag{4}$$

The function $Y_{00} = (2\pi\Delta/k_{\rm B}T)^{1/2}\exp(-\Delta/k_{\rm B}T)$ describes the activated behavior of the low T quasiparticle response in the case of isotropic gaps and $c_0^2(T) = 1, 1, (3/\pi^2)(\Delta/k_{\rm B}T)$ and $(3/\pi^2)(\Delta/k_{\rm B}T)^2$ in the cases of the spin susceptibility, normal fluid density, entropy and heat capacity, respectively. For systems with nodal quasiparticles, the quantities C_a and μ_a, which depend on both the vertex $a_{\mathbf{p}}$ and the gap symmetry $f_{\mathbf{p}}$ under consideration, have been discussed in ref. [3]. Near $T_{\rm c}$, the generalized Yosida functions read to leading order in $x = 1 - T/T_{\rm c}$:

$$Y_a(T) = Y_a(T_{\rm c}^-)\,(1 - s_a x) \tag{5}$$

Here s_a denotes the temperature slope of the response functions just below the transition temperature. Explicit results for s_a for various pairing symmetries have been discussed in refs. [1] and [2] and cannot be presented here for lack of space. In order to connect the asymptotic results in the two limits of $T \to 0$ and $T \to T_{\rm c}$, we propose the following interpolation procedure for the generalized Yosida function: $Y_a^{\rm int}(T) = Y_{a0}(T)\left[1 + c_a\,(T/T_{\rm c})^{\kappa_a}\right]$; $Y_{a0}(T) = Y_{a00}(T)\left[1 + \beta_a(k_{\rm B}T/\Delta_0(0))\right]$. The coefficient β_a has to be introduced for each vertex $a_{\mathbf{p}}$ such that the deviation of $Y_a^{\rm int}(T)$ from $Y_a(T)$ can be reduced further at intermediate temperatures. Fixing the coefficient c_a by the condition $Y_a^{\rm int}(T_{\rm c}) \equiv Y_a(T_{\rm c}^-)$, leads to the following analytic expression, which is exact for both $T \to 0$ and T just below $T_{\rm c}$ (slope included):

$$Y_a^{\rm int}(T) \;=\; Y_{a0}(T)\left[1 - \left(\frac{T}{T_{\rm c}}\right)^{\kappa_a}\right] + Y_a(T_{\rm c}^-)\frac{Y_{a0}(T)}{Y_{a0}(T_{\rm c})}\left(\frac{T}{T_{\rm c}}\right)^{\kappa_a} \tag{6}$$

The exponent κ_a is determined by requiring, that the slope of $Y_a^{\rm int}(T)$ is fixed by the exact result $s_a\;\; T_{\rm c}\lim_{T\to T_{\rm c}^-}(dY_a(T)/dT) = Y_a(T_{\rm c}^-)s_a$. The result for the exponent κ_a reads: $\kappa_a = (s_a - T_{\rm c}Y'_{a0}(T_{\rm c})/Y_{a0}(T_{\rm c}))(1 - Y_{a0}(T_{\rm c})/Y_a(T_{\rm c}^-))$. Generally speaking, the interpolation procedure developed above, can be applied to *any* pair–correlated Fermi system without and with gap nodes, the latter specified by the function $f_{\mathbf{p}}$. The interpolation procedure has been applied to conventional superconductors or the B–phase of superfluid ^{3}He, where $f_{\mathbf{p}} = 1$ (s or p–wave, (pseudo–) isotropic), superconducting quasi–2–d hole–doped cuprates, where $f_{\mathbf{p}} = \cos 2\phi$ (d–wave, B_{1g}), and the heavy Fermion superconductor $\mathrm{UPt_3}$ where either of the pairing states $f_{\mathbf{p}} = \sqrt{2}\cos\theta\sin\theta$ (d–wave, E_{1g}) or $f_{\mathbf{p}} = (3\sqrt{3}/2)\cos\theta\sin^2\theta$ (f–wave, E_{2u}) have been discussed in the literature. The deviations between the interpolated and the exact results are seen to be mostly negligible, in many cases within the (sub–) percent regime for intermediate temperatures. For lack of space the reader is referred to refs. [1] and [2] for further details.

Summary and Conclusion. The temperature–dependent thermodynamic and reactive response functions $\mathrm{R}_a(T)$ manifest the *normal component* of a microscopic two–fluid description. The main result of this work is an analytic form for such a two fluid description of superconductivity and fermionic superfluidity.

References

[1] D. Einzel, accepted for publication in the J. Low Temp. Phys., March 2003
[2] D. Einzel, accepted for publication in the J. Low Temp. Phys. 2003
[3] D. Einzel, J. Low Temp. Phys. **126**, 867 (2002)

Quantum criticality in $YbRh_2(Si_{1-x}Ge_x)_2$

J.Custers[1], *P. Gegenwart*[1], *H. Wilhelm*[1], *O. Tovarelli*[1],*C. Geibel*[1], *N. Oeschler*[1], *F. Steglich*[1], *K. Ishida*[2], *Y. Kitaoka*[2], *K. Neumaier*

[1]Max-Planck-Institute für Chemie fester Stoffe, Dresden, Germany
[2]Department of Physical Science, Osaka University, Japan

Heavy-fermion (HF) metals are ideally suited for studies of quantum criticality, which has become of increasing interest especially after the discovery of high temperature superconductivity in the cuprates. HF metals contain a dense lattice of certain lanthanide ($4f$) or actinide ($5f$) ions which are, at sufficiently low temperatures ($T \ll T_K$, the Kondo temperature) strongly coupled to the surrounding Fermi sea of delocalized (s, p, d) conduction electrons. In this way the local magnetic $4f/5f$ moments, that exist well above T_K, are eventually screened by conduction electrons, yielding the formation of unusual electronic quasiparticles, the heavy fermions. These are "composite fremions" consisting of a dominating local f ("spin") part, which is complemented by an itinerant conduction electron ("charge") component.

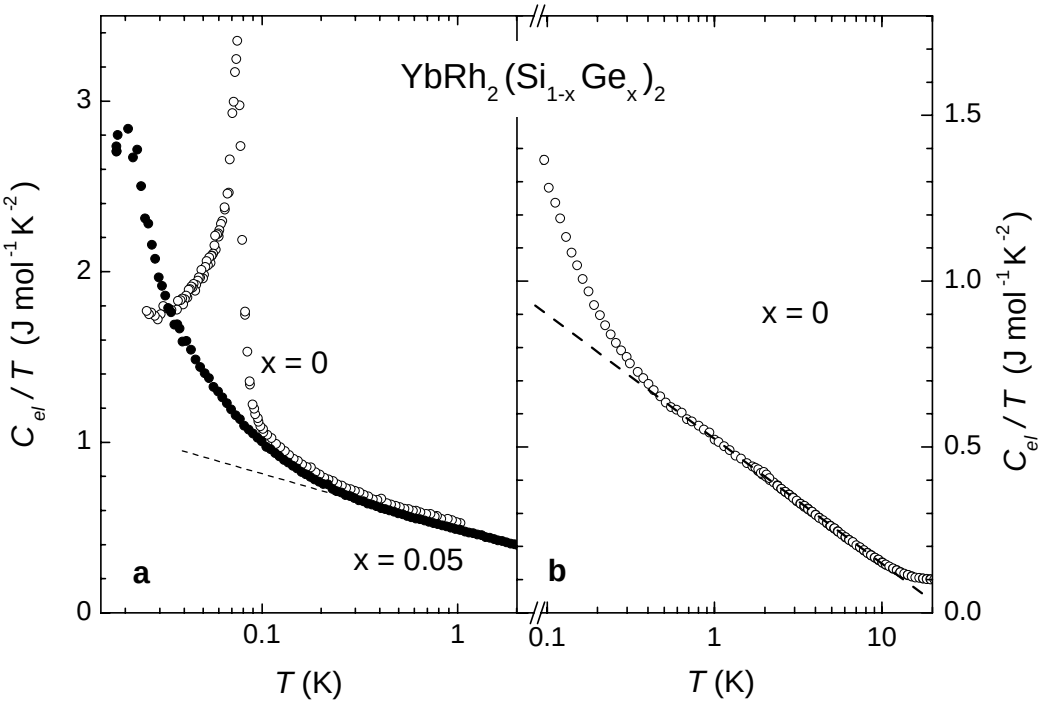

Figure 1: Zero-field electronic specific heat divided by temperature for $YbRh_2(Si_{1-x}Ge_x)_2$.

HF metals are sometimes in close vicinity to an antiferromagnetic (AF) instability. In this case a modest pressure or chemical doping is sufficient to bring the metal to its quantum critical point (QCP), at which $T_N \to 0$ in a continuous way. In the vicinity of the QCP, pronounced deviations from the behavior of a heavy Landau Fermi Liquid (LFL) in physical properties are observed. These so-called non-Fermi-Liquid (NFL) phenomena are related to the actions of strong low-lying AF spin fluctuations (associated with the QCP) that mediate the coupling between the quasiparticles. Two different theoretical scenarios have been proposed to describe this AF QCP: a spin density wave (SDW) and a localized moment (LM) scenario. In the SDW scenario, magnetic properties are associated with the spin polarization of the Fermi surface, and NFL behavior results from the scattering of quasiparticles off quantum critical spin

fluctuations in the magnetization. Three dimensional (3D) spin fluctuations only couple to quasiparticles along hot lines around the Fermi surface separated by the wavevector Q of the AF order. Only in case of strong magnetic frustration, the 3D system of the AF spin fluctuations ("spin fluid") may be decoupled into 2D spin fluids. With this assumption, all electrons on the Fermi surface are strongly scattered by the critical magnetic mode. In the LM scenario heavy electrons are a composite bound state, formed between the local magnetic moments and the high energy conduction electrons via the "Kondo effect". The break up of these composite fermions at the QCP is responsible for the NFL behavior. To get direct information on the question how the heavy electron decays into the quantum critical state, one has to tune the system away from quantum criticality at sufficiently low temperatures to observe how the LFL state is influenced by the strong quantum fluctuations near the QCP [1, 2, 3].

The tetragonal compound $YbRh_2(Si_{1-x}Ge_x)_2$ provides the possibility to carry out such a study. The undoped ($x = 0$) compound lies close to a QCP [1, 2, 3], with a tiny antiferromagnetic ordering temperature $T_N = 70\,\mathrm{mK}$ that can be suppressed to zero by a small magnetic field of $B \perp c = 0.06\,\mathrm{T}$ (see Fig.1). Applying external pressure increases T_N. The extrapolation of $T_N(p) \to 0$ yields $p_c = -0.3(1)\,\mathrm{GPa}$, reflecting that a small expansion of the unit cell volume would tune $T_N \to 0$. This can be achieved by the substitution of Si by the isoelectronic, but larger, Ge.

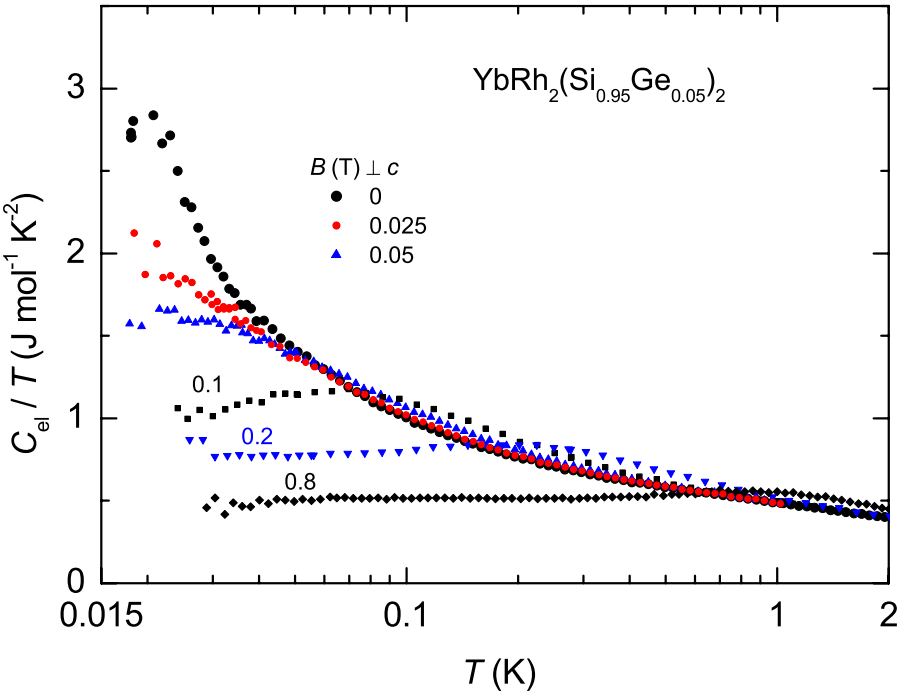

Figure 2: Electronic specific heat divided by temperature for $B = 0$ and $0 \leqq B \leqq 0.8T$.

For the $x = 0.05$ sample we observe a tiny AFM phase transition anomaly in the electronic specific heat coefficient $C_{el}(T)/T$ at T_N as low as 20 mK. Above $T > 0.3\,\mathrm{K}$, the zero field properties of $YbRh_2(Si_{0.95}Ge_{0.05})_2$ are essentially identical to those of the stoichiometric compound. In both cases $C_{el}(T)/T$ exhibits a logarithmic divergence $\propto -\log T$ between 0.3 and 10 K. In the low-T paramagnetic regime ($T_N < T \leq 0.3\,\mathrm{K}$), $C_{el}(T)/T$ shows a pronounced upturn. The volume thermal expansion coefficient divided by temperature, $\beta(T)/T$, develops, upon cooling, a similar pronounced upturn from the high temperature $\log T$ dependence. Since thermal expansion is insensitive against both hyperfine and impurity effects, the low-T upturn in $\beta(T)/T$ gives evidence for an intrinsically electronic, rather than a nuclear or extrinsic origin of the upturn in $C_{el}(T)/T$ vs T curves.

In the measurements of the field dependence of the electronic specific heat in $YbRh_2(Si_{0.95}Ge_{0.05})_2$ the magnetic field was applied perpendicular to the crystallographic c-axis, i.e., within the easy magnetic plane (see Fig.2). At high fields above 0.1 T, $C_{el}(T)/T$ is almost temperature independent, as expected in a LFL. A weak maximum is observed in $C_{el}(T)/T$ at a characteristic temperature $T_0(B)$ which grows linearly with increasing field. This indicates that entropy is transferred from the low tem-

perature upturn to higher temperatures by applying a magnetic field. At lower fields, the temperature region over which $C_{el}(T,B)/T = \gamma(B)$ does not depend on T shrinks towards zero. These results indicate the formation of a field-induced heavy LFL state at a characteristic scale $T \leq T_0(B)$. As the field is lowered, $\gamma(B)$ (LFL contribution to the specific heat) diverges, suggesting an ever increasing component of the zero-field upturn in the specific heat, if the samples were located exactly at the QCP (see Fig.3). It is this observation that confirms that the upturn in the specific heat observed in zero field is fundamentally electronic in character, and should therefore be associated with the intrinsic specific heat at the quantum critical point.

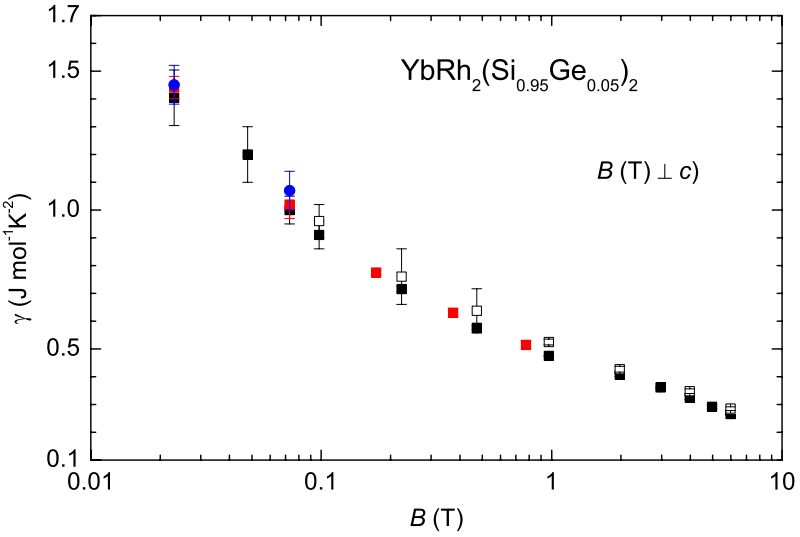

Figure 3: Electronic specific heat coefficient γ plotted versus the magnetic field $B \perp c$.

References

[1] P. Gegenwart, J. Custers, C. Geibel, K. Neumaier, T. Tayama, O. Trovarelli, F. Steglich,
Magnetic-field induced quantum critical point in $YbRh_2Si_2$.
Phys. Rev. Lett. **89**, 056402 (2002).

[2] F. Steglich, N. K. Sato, N. Aso, P. Gegenwart, J. Custers, K. Neumaier, H. Wilhelm, C. Geibel, O. Trovarelli,
Recent trends in heavy-fermion physics.
Physica C, accepted for publication (2002).

[3] J. Custers, P. Gegenwart, Neumaier, H. Wilhelm, N. Oeschler, K. Ishida, Y. Kitaoka, C. Geibel, F. Steglich,
Quantum criticality in $YbRh_2Si_2$.
J. Phys. Condens. Matter, submitted for publication (2002).

Pulsed NMR in the Nuclear Spin Ordered Phases of Solid ^{3}He in a Silver Sinter

Carmen Millan-Chacartegui, Erwin A. Schuberth, Frank Deppe and Stephan Schöttl [1]

To obtain the exact spin structure of the nuclear magnetically ordered phases of solid ^{3}He, namely in the bcc lattice called U2D2 and the high field phase which both appear below about 1 mK, we started a project of neutron scattering from the solid at the Hahn-Meitner Institute, Berlin. This experiment faces three main difficulties: Firstly, to cool the solid to temperatures below 1 mK (or even much lower in the case of the hcp lattice), secondly to keep it there under neutron flux, and thirdly to grow a single crystal within the sintered material needed for this purpose. As a first step we have performed pulsed NMR measurements in the ordered phases of solid ^{3}He in a silver sinter of 700 Å particle size down to temperatures of 600 μ K at various molar volumes. The samples remained in the ordered state for as long as 110 h.

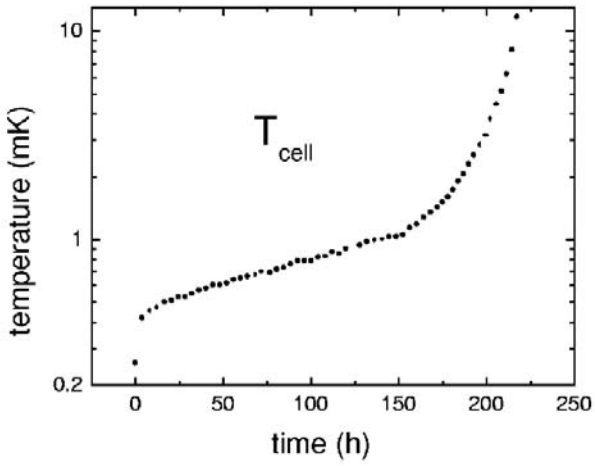

Figure 1: Temperature of the nuclear stage after demagnetization determined by pulsed NMR on ^{63}Cu. The faster warming after 150 h is due to external heating.

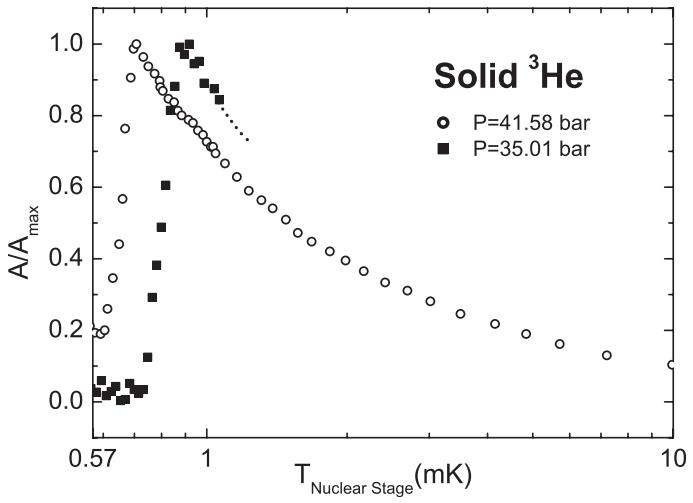

Figure 2: NMR intensity of solid ^{3}He vs the cell temperature at two different pressures.

In order to establish the spin structure of the nuclear magnetically ordered phases of solid ^{3}He by neutron scattering as we plan to do at HMI, Berlin, it is crucial that a single crystal can be formed in the sinter, which is required in order to cool ^{3}He and to keep the solid in the ordered state for sufficiently long time even under neutron irradiation. For checking these goals we designed a cell for pulsed NMR measurements on solid ^{3}He in a 700 Å sinter (the cell design is given in the diploma thesis of F. Deppe, TU Munich 2002). We started to look for the existence of a single crystal which would be indicated by the characteristic line splitting of the U2D2 phase. The cell temperature and its warmup behavior after demagnetization of our 0.9 mole $PrNi_5$ nuclear stage was monitored by pulsed NMR on a copper sample thermally connected to it.

[1] In collaboration with the Hahn-Meitner-Institute, Berlin

This work was supported by the EU, project No.: HPRN-CT-2000-00166.

The Fast Fourier Transform of the free induction decay of the solid ^{3}He signal was used to establish the magnetization of the solid in the paramagnetic phase, the frequency, and the full width at half maximum of the NMR line.

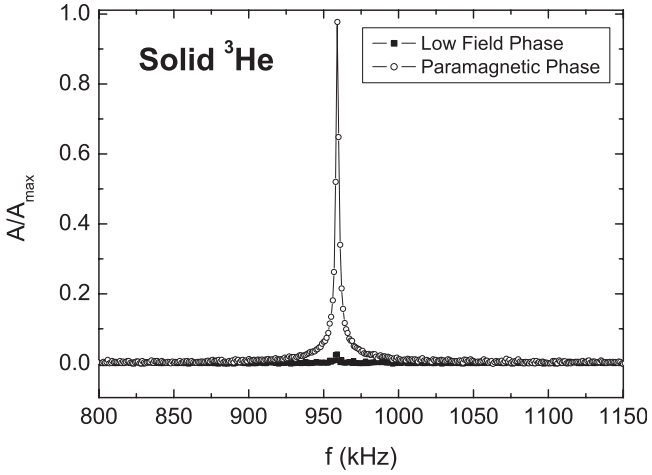

Figure 3: Pulsed NMR spectra of solid ^{3}He in a 700 Å silver sinter in the paramagnetic phase and in the LFP at $T = 600\mu$K, $p = 35.04$ bar. The tipping angle was $\approx 10^\circ$.

Fig. 1 shows the warm-up behavior of the cell after demagnetization. The faster warming after 150 h is due to additional external heating. In Fig. 2 the NMR signal intensities of a solid ^{3}He sample grown at 41.6 bar (i.e. 23.4 cc/mole) are plotted vs the temperature of the nuclear stage which is practically identical to that of the cell body. In the paramagnetic phase these intensities are proportional to the magnetization of the solid. We found neither a line splitting nor a line broadening in the ordered solid although we scanned the frequency range from 200 kHZ to 2 MHz. The tipping pulse used was around 8° to avoid the nonlinear spin dynamics observed previously by Matsushita et al. [1].

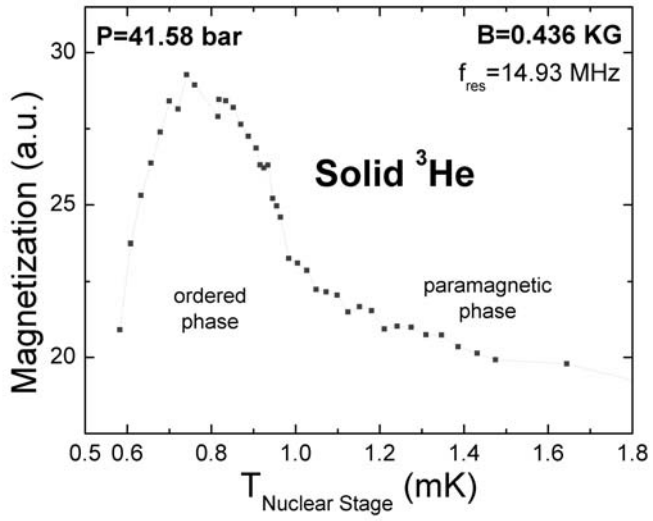

Figure 4: NMR intensity of solid ^{3}He in a 700Å Ag sinter.

In a subsequent run with a sample grown at 35.04 bar (and hence a with a molar volume of 24.14 cc, close to the melting curve) we found that the signal intensity decreased practically to zero. This is probably due to a more complete cooling of all the solid ^{3}He in the NMR coil because now T_N was 0.87 mK instead of 0.52 mK in the previous case. Again, a scan across the above frequency range with tipping angles of either 10° or 90° showed no line splitting and only a weak signal from the protons of the coil wire insulation. In Fig.3 we present an NMR spectrum from solid ^{3}He in a silver sinter in the low field ordered state with essentially zero intensity. We also cooled the 41.58 bar sample into the high field phase and measured NMR spectra and line intensities there. The result shows the expected enhancement for this weak ferromagnetic phase, see Fig. 4.

The large drop of the line intensity in the ordered state to zero is very peculiar. It can have several origins: either we still missed additional lines due to unfavorable tipping angles, or we had many crystallites and therefore low intensity in a wide frequency range, or we do not have the U2D2 phase in the sinter.

References

[1] T. Matsushita et al. JLTP **105**, 67 (1996)

Effect of Rare Earth Ion Substitution on the Magnetic and Transport Properties of $Pr_{0.7}RE_{0.04}Sr_{0.26}MnO_3$ (RE = Er, Tb and Ho) [1]

N. Rama[a,b] J.B. Philipp[c], Matthias Opel[c], A. Erb[c], V. Sankaranarayanan[a], M.S. Ramachandra Rao[a,b], and R. Gross[c]

[a] Materials Science Research Centre, Indian Institute of Technology Madras, Chennai-600 036, India
[b] Department of Physics, Indian Institute of Technology Madras, Chennai-36, India
[c] Walther-Meissner-Institute, Bavarian Academy of Sciences, D-85748, Garching, Germany

Within a bilateral German-Indian cooperation project, the effect of rare earth ion (RE = Er, Tb, Ho) substitution on the magnetic and electrical transport properties of $Pr_{0.74}Sr_{0.26}MnO_3$ (PSMO) has been studied. By the substitution of magnetic and non-magnetic ions with different ionic radii on the A-site of the perovskite type manganite PSMO both the effect of A-site disorder and the effect of the magnetic ions on the electric transport and magnetic properties can be studied. We found that even for a small substitution of Pr by Er, Tb, or Ho there that is a significant change in the nature of the transport and magnetic sample properties. This we attribute to the increase in the average A-site disorder. The sample substituted by magnetic Ho^{3+} ions is found to behave anomalously as compared to the samples substituted with non-magnetic rare earth ions. This anomalous behaviour is most likely caused by the magnetic coupling of the magnetic moments of the Ho and Mn ions.

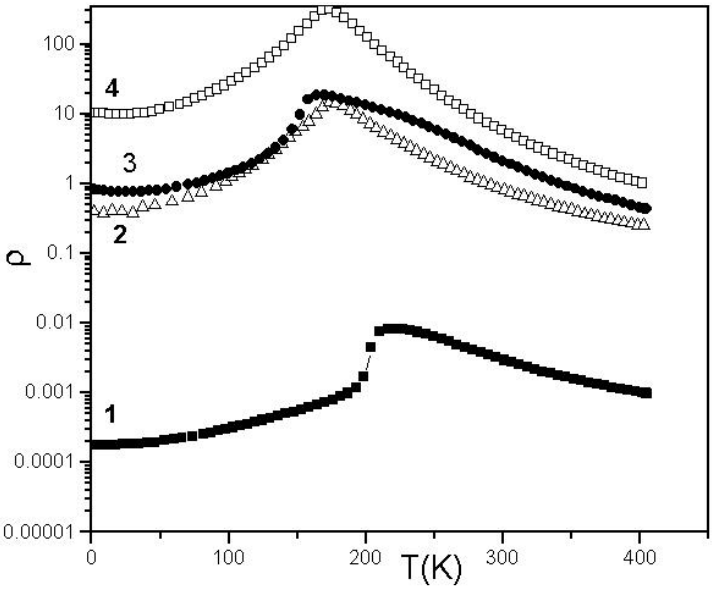

Figure 1: Resistivity versus temperature for the pure and RE substituted PSMO. Curves 1,2,3 and 4 represent the resistivity data of pure PSMO (0.26), Tb^{3+} substituted PSMO (0.26), Ho^{3+} substituted PSMO (0.26) and Er^{3+} substituted PSMO (0.26), respectively.

For our study polycrystalline samples of the composition $Pr_{0.7}RE_{0.04}Sr_{0.26}MnO_3$ (RE = Er, Ho, Tb) have been prepared by the conventional solid-state method. Stoichiometric amounts of preheated Pr_6O_{11}, Er_2O_3, Ho_2O_3, Tb_4O_7, $SrCO_3$ and MnO_2 were weighed and mixed thoroughly in an agate mortar and fired in an alumina crucible at 950°C for 24 h. The calcined powders were reground and heated again at 1250°C for another 24 h. The resultant powder was then pressed into pellets of 8 mm diameter and sintered in air at 1350°C for 24 h and finally furnace cooled. In our study we concentrated on the effect of the substitution of Er^{3+}, Ho^{3+} and Tb^{3+} ions at the Pr-site on the transport and magnetic properties of $Pr_{0.7}RE_{0.04}Sr_{0.26}MnO_3$ (PSMO (0.26)). Since within the framework of the double exchange model the Mn^{4+} concentration is one of the factors that determines the Curie temperature T_C, we have doped the system such that they have the same Mn^{4+} concentration.

The temperature dependence of electrical resistivity ρ of the four samples is shown in Fig. 1. The metal to insulator (MI) transition, a characteristic feature of the doped manganites, at a temperature T_P roughly

[1] This work was done within a German-Indian science and technology cooperation project funded by the BMBF (project IND 01/009).

corresponding to the maximum in the $\rho(T)$ curves is clearly seen for all samples. Furthermore, it is evident that all RE substituted samples show much higher resistivity over the entire temperature range of our measurements (400 K to 2 K) as compared to pure PSMO (0.26). We found, that the resistivity value at the maximum in the resistivity versus temperature curve is largest for the Er^{3+} substituted PSMO (0.26) and lowest for the Tb^{3+} substituted PSMO (0.26) sample. This is in accordance with A-site disorder that can be estimated using the expression $\langle\sigma^2\rangle = \sum_i y_i r_i^2 - (\sum_i y_i r_i)^2$ [1]. That is the resistivity increases with increasing A-site disorder.

The sharp drop in the resistivity versus temperature curve that is observed for the pure PSMO (0.26) sample just below the metal to insulator (MI) transition at the temperature $T_P \simeq 220$ K, is absent in the substituted samples. This suggests that the MI transition in the substituted samples is much more gradual than in the pure sample. This gradual transition may arise due to the onset of a percolative transport behaviour [2]. At temperatures above T_P, the temperature dependence of the resistivity can be well described within the adiabatic polaron hopping model giving $\rho(T) = \rho_0(T)\, T\, \exp(-E_A/k_B T)$ [3] (see Fig. 2). The values of activation energy obtained for the various substituted compounds by fitting the experimental data by the polaron hopping expression is found to increase with increasing A-site disorder.

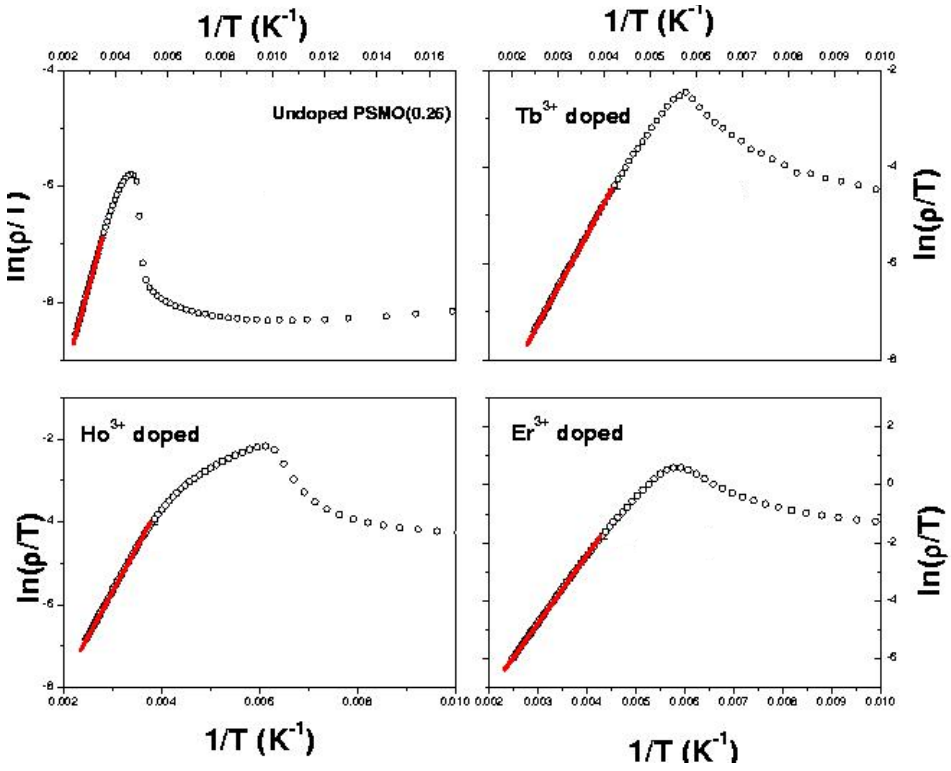

Figure 2: $\ln(\rho/T)$ plotted versus $1/T$ for the pure PSMO (0.26) sample as well as for the Tb^{3+} substituted PSMO (0.26), the Ho^{3+} substituted PSMO (0.26), and the Er^{3+} substituted PSMO (0.26) compound. Also shown are the fits of the high temperature data to the adiabatic polaron model. For the fits, a temperature interval extending from 294 K, 250 K, 274 K, and 248 K to 400K, respectively, was used. The symbols represent the data points and the solid line the fit according to the adiabatic polaron hopping model.

Fig. 3 shows the magnetization versus temperature curves for the investigated samples. It is seen that the magnetization data have minima around 60 K, which is attributed to the Pr^{3+} sublattice ordering [4]. Pr ordering is seen in the Ho^{3+} substituted sample even though it has a $\langle\sigma^2\rangle$ value comparable to that of the Er^{3+} substituted PSMO (0.26) sample, where it is not seen clearly. Among the rare earth ion substituted PSMO (0.26) samples, the Ho^{3+} substituted PSMO (0.26) behaves differently from the others. This anomalous behaviour of the Ho^{3+} sample is related to the magnetic moment of the Ho^{3+} ions. Recently, it has been reported that the moments of the Ho^{3+} ions couple to those of the Mn ions in $La_{0.7}Ca_{0.3}MnO_3$ [5]. However, it has also been proven by neutron diffraction that the Pr sublattice orders

ferromagnetically most likely due to a coupling between the Pr moments and the Mn moments [4]. This effect is clearly seen in Pr systems doped with calcium (PCMO), where the saturation moment at high fields and low temperature is at least 10% higher than the value measured for the corresponding La compounds such as LCMO or LSMO.

When the PSMO system is substituted with other rare earth ions the coupling among the Pr and Mn ions may be weakened due to the decrease in the number of Pr ions. This phenomenon in combination with A-site disorder makes the system more resistive. However, in the Ho^{3+} substituted PSMO (0.26) sample this effect could be slightly offset by the possible coupling between Mn and Ho ions. This is reflected by the fact that the Ho^{3+} and Tb^{3+} substituted PSMO (0.26) compounds have nearly the same resistivity even though the Ho^{3+} sample should have had higher resistivity according to its larger disorder. A similar effect has been found by us for the Ho^{3+} substituted LCMO sample in comparison to the Y^{3+} sample even though both have the same $\langle\sigma^2\rangle$ value [5].

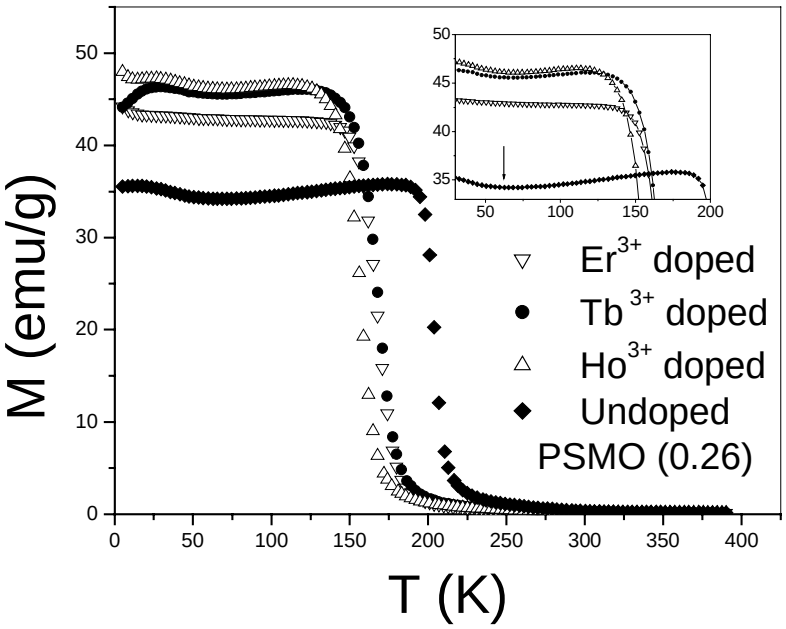

Figure 3: Temperature dependence of the magnetization. The arrow indicates the onset of Pr ordering.

In summary, our study shows that the substitution of even a small amount (0.04%) of the Pr ions in PSMO (0.26) by other RE ions results in a significant change in the electrical transport and magnetic properties. We also found that the Ho^{3+} substituted sample behaves anomalously compared to the Er^{3+} and Tb^{3+} substituted samples. This anomalous behaviour of the Ho^{3+} doped sample most likely arises from a coupling between the magnetic moments of the Ho^{3+} and Mn ions.

References

[1] L. M. Rodriguez -Martinez et al., Phys Rev. B **54**, R15622 (1996); see also L. M. Rodriguez-Martinez et al., Phys Rev. B **58** 2426 (1998)
[2] E. Dagotto et al., Phys. Rep. **344**, pp. 1-153 (2001).
[3] Holstein, Ann. Phys. **8**, 343 (1959).
[4] J. G. Park et al., Phys Rev. B **60**, 14804 (1999).
[5] V. Ravindranath, et al., Phys. Rev. B **63**, 184434 (2001).

Low-frequency $1/f$ Noise in Doped Manganite Grain Boundary Junctions

J. B. Philipp, L. Alff, A. Marx, and R. Gross [1]

The doped manganites have attracted large interest in recent years because of the complex interplay of charge, spin, orbital and structural degrees of freedom and their potential use in magnetoelectronic devices. By growing epitaxial thin films on bicrystal substrates artificial grain boundaries (GB) can be introduced into manganite thin films. Recently, in such artificial manganite GB junctions a large two-level tunneling magnetoresistance (TMR) with TMR values up to 300% at 4.2K has been demonstrated [2]. The charge transport mechanism across the structurally distorted GB region is still discussed controversially. In order to get more insight into the nature of charge transport across the GB, we have performed a systematic analysis of the low frequency $1/f$-noise in single GB junctions formed in epitaxial $La_{2/3}Ca_{1/3}MnO_3$ films deposited on $SrTiO_3$ bicrystal substrates. The $La_{2/3}Ca_{1/3}MnO_3$ films typically had a Curie temperature $T_C = 210\,\mathrm{K}$. After film deposition the films were annealed *ex situ* at 950°C in pure oxygen atmosphere. Then, microbrigdes straddling the grain boundary are patterned into the films using optical lithography and Ar-ion beam etching.

The noise properties of the GBJ's were measured by biasing the junctions at a constant current I and measuring the low-frequency voltage fluctuations. The measurements were performed as a function of temperature (4.2–300 K) and applied magnetic field (up to 12 T) applied within the film plane parallel to the GB barrier. The measured voltage noise is quantified by the frequency independent normalized voltage noise power $P_{\mathrm{octave}} = \int_{f_1}^{2f_2} S_V/V^2 df$, where S_V is the spectral density of the voltage fluctuations and $f_2 = 2f_1$.

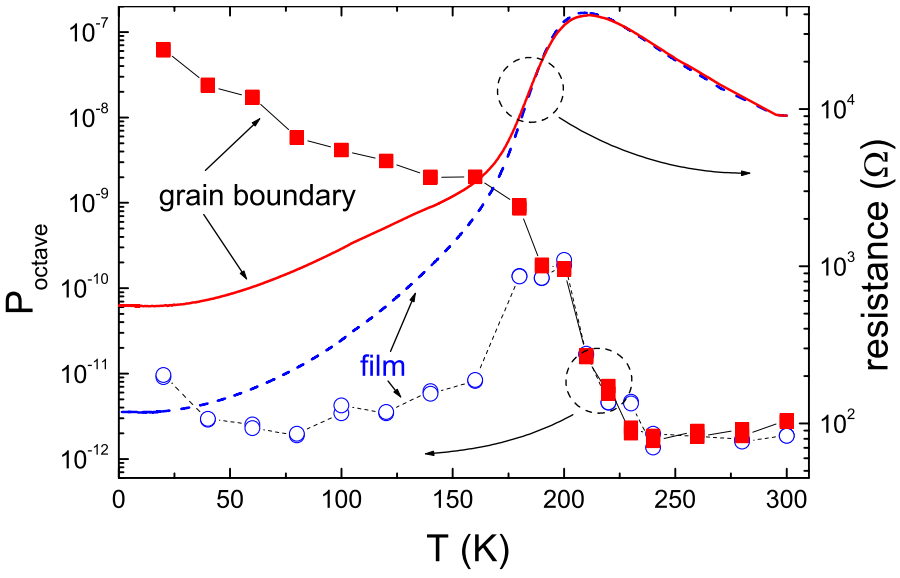

Figure 1: Temperature dependence of the normalized noise power P_{octave} with (full symbols, solid line) and without GB (open symbols, dashed line). For comparison the temperature dependence of the resistance is also shown.

Fig. 1 shows the temperature dependence of P_{octave} for two $La_{2/3}Ca_{1/3}MnO_3$ microbridges of the same geometry. However, only one microbridge contains a GB. The $1/f$ noise for the microbridge with the GBJ is rapidly increasing with decreasing T for $T < 220\,\mathrm{K}$. In contrast, the noise of the microbridge without GBJ is almost temperature independent except for a noise peak close to the Curie temperature $T_C \simeq 220\,\mathrm{K}$. We recently showed that this noise peak can be suppressed by a small applied magnetic field and is related most likely to magnetic fluctuations at the paramagnetic to ferromagnetic transition in the doped manganites [3]. The key result of Fig. 1 is the fact that below T_C the $1/f$ noise power of the microbridge with GBJ can be attributed to the GBJ alone.

[1] This work is supported by the Deutsche Forschungsgemeinschaft.

Fig. 2 shows the dependence of normalized octave noise power P_{octave} on a magnetic field applied within the film plane parallel to the GB for different values of the bias current I_b. Fig. 2 shows two experimental facts. First, the noise power decreases with increasing bias current for all applied fields for $I_b \gtrsim 10\,\mu$A. Second, the noise power decreases with increasing magnetic field for bias current values below about $200\,\mu$A. Whereas for $I_b \lesssim 100\,\mu$A the noise decreases by more than one order of magnitude by increasing the magnetic field to 12 T, for $I_b \gtrsim 200\,\mu$A the noise is only weakly dependent on the applied magnetic field.

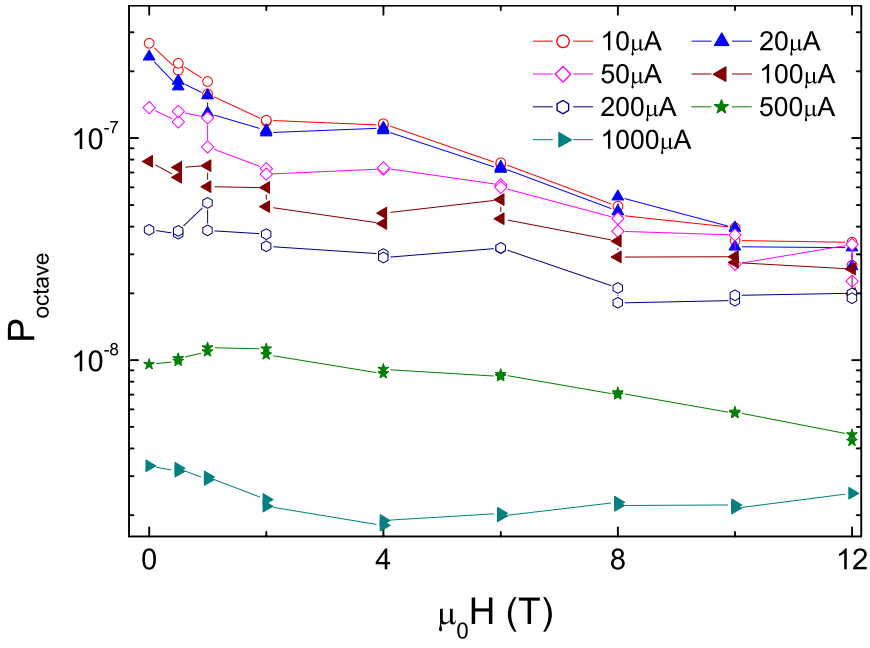

Figure 2: Magnetic field dependence of the normalized noise power for a $La_{2/3}Ca_{1/3}MnO_3$ GBJ in the octave from 100 to 200 Hz at $T = 40$ K for different values of the bias current I_b.

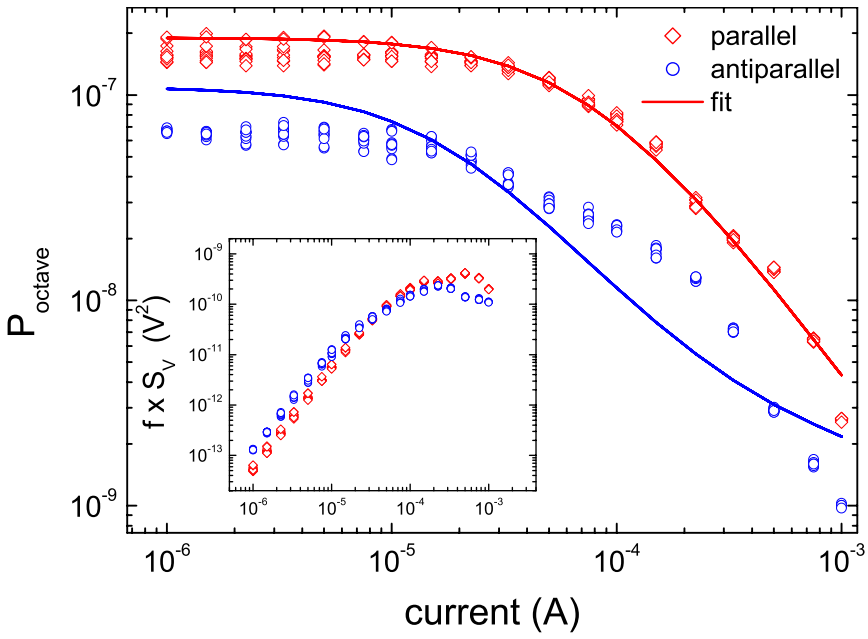

Figure 3: Normalized noise power P_{octave} vs bias current I_b for parallel (full symbols) and antiparallel magnetization direction in the GBJ electrodes (open symbols) at $T = 40$ K. The solid lines are fits to the data within a small signal analysis [2]. The inset shows the noise power $f \times S_V$ vs the bias current I_b.

Fig. 3 shows the dependence of the normalized noise power P_{octave} on the bias current I_b for both the parallel and antiparallel magnetization direction in the GBJ electrodes at $T = 40$ K. Both for the parallel and antiparallel magnetization orientations there is only a very weak bias current dependence of the normalized noise power for small bias currents followed by a rapid decrease of P_{octave} at large bias current values. As illustrated in the inset of Fig. 3, the quantity $f \times S_V(I_b)$ shows a nonlinear dependence on the bias current.

Both the dc electrical transport and the low-frequency noise properties can be consistently understood in

a junction model assuming a strongly distorted region at the GB containing a large number of localized states or traps with fluctuating magnetic moments. The localized defect states are capable of trapping and releasing charge carriers. This charge carrier trapping and release processes lead to local variations of the barrier height and, thus, to fluctuations of the tunneling conductance. Furthermore, the magnetic field dependence of the noise suggests that the charge traps are associated with a magnetic moment $\mathbf{S}_L$ with a fluctuating orientation. The increase of P_{octave} with decreasing T is expected within our model due to the increase of the spin polarization in the junction electrodes with decreasing temperature [1]. Then, with increasing spin polarization the fluctuations of the orientation of the localized moments results in increasing fluctuations of the local barrier height.

Applying a magnetic field was found to continuously decrease the junction noise P_{octave} up to 12 T for bias currents $\leq 200\,\mu$A as shown in Fig. 2. Here, the applied magnetic field tends to align the localized magnetic moments of the charge traps in the barrier region and thus reduces the fluctuations of the local barrier height. However, in order to explain the magnetic field dependence of P_{octave} up to the largest applied field of 12 T the fluctuating magnetic moments associated with the localized states cannot be considered as free moments but rather as (weakly) interacting moments forming a spin

glass like state. The competition of ferromagnetic double exchange and antiferromagnetic superexchange between neighboring Mn ions in the manganites depends sensitively on doping, structural disorder, and bond angles. For bulk $La_{2/3}Ca_{1/3}MnO_3$ the ferromagnetic double exchange is dominating. However, for the structurally distorted GB region there is certainly a strongly suppressed double exchange. Therefore, at the grain boundary there may be regions with locally dominating ferromagnetic and antiferromagnetic exchange [4]. Because of the distorted nature of the GB it is plausible to assume that there is an arrangement of interacting magnetic moments strongly resembling a spin glass in the GB barrier.

References

[1] C. Höfener, J. B. Philipp, J. Klein, L. Alff, A. Marx, B. Büchener, and R. Gross, Europhys. Lett. **50**, 681 (2000).
[2] J. B. Philipp, C. Höfener, S. Thienhaus, J. Klein, L. Alff, and R. Gross, Phys. Rev. B **62**, 9248 (2000).
[3] P. Reutler, A. Bensaid, F. Herbstritt, C. Höfener, A. Marx, and R. Gross, Phys. Rev. B **62**, 11619 (2000).
[4] M. Ziese, C. Srinitiwarawong, and C. Shearwood, J. Phys.: Condens. Matter **10**, L569 (1998).

Metallic Nanometer Devices for Advanced Quantum Electronics [1]

J. Schuler, M. Tober, F. Deppe,[2] *C. Probst, K. Neumeier, A. Marx, R. Gross*

The steady reduction of lateral dimensions in the field of semiconductor technology entails the demand to take into account and to make use of quantum effects in future designs of electronic devices. It is obvious that quantum effects in nanostructures can provide access to interesting new physics and a rich field of very promising future applications based on conceptually new operating mechanisms of electronic devices. So far in electronic devices mostly quantum effects arising from the quantization of the electronic level structure have been exploited. However, in a new class of quantum devices the coherent superposition of quantum states is intended to be used. Such devices are required for quantum information processing (QIP).

The new approach of QIP is relies on basic principles of quantum mechanics. Instead of using the classical bits based on two well defined classical states ("0" and "1") for encoding information, in QIP so-called quantum bits (qubits) based on the superposition $a|0\rangle + b|1\rangle$ of two basis states $|0\rangle$ and $|1\rangle$ are used. Thus, the elementary unit in quantum information processing (QIP) is a two level quantum system called qubit. Computational operation are performed by the creation of coherent quantum superposition states and their manipulation by unitary transformations. Whereas qubits can be implemented by various physical systems, solid state based qubits are of particular interest, since they possibly meet the requirement of scalability and large-scale integration needed for useful quantum computers. Particularly interesting solid state systems are *superconducting* qubits, since here all electrons are condensed into a macroscopic quantum state which is separated by a gap from the large number of quasi-particle states. Due to this gap the entanglement of the quantum state with the quasiparticle states resulting in decoherence is reduced. Hence, the phase coherence time in superconducting qubits is expected to be sufficiently high.

Another very promising device based on the discrete nature of charge is the single electron transistor (SET). It consists of two tunnel junctions and a capacitively coupled gate electrode. As the region between the two tunnel junctions is only weakly connected to the rest of the electrical circuit, it is usually referred to as the *island* of the SET. The number of excess charge carriers on the island n (additional or missing electrons) always is an integer number. Electrical transport through the SET can only be established by electrons tunneling through both junctions separately [1]. By applying a voltage to the gate electrode the energy levels of the electronic states on the island can be changed, and thus the transport of electrons through the device can be drastically influenced. For sufficiently low voltages applied across the two junctions tunneling of electrons across the device can be blocked due to the charging energy of the electron(s) on the island and on the leads (*Coulomb Blockade*).

To observe single charge effects the involved energy scale has to be sufficiently large compared to rivaling effects such as thermal excitations. The underlying energy scale for single charging effects is the Coulomb energy E_C, which has to meet the requirement $E_C = \frac{e^2}{2C} \gg k_B T$, where e is the electron charge, C the total SET capacitance, k_B Boltzmann's constant, and T the temperature. For an Al/AlO_x/Al-tunnel junction with total capacitance of the range of 1 fF, the Coulomb energy corresponds to a temperature of 1 K. Therefore, it is necessary to investigate SET effects at temperatures in the mK regime. Apart from the standard SET there is a great variety of SET-like structures e.g. a SET with ferromagnetic components (island and/or leads) [3, 4], single electron pumps, charge qubits etc.

The study of single electron devices and solid state based qubits requires the development of the technological basis for the fabrication of the required nanostructures. Therefore, we have developed optimized nanofabrication processes allowing for the fabrication of metallic nanostructures, which consist

[1] In collaboration with H. Takayanagi, NTT Basic Research Laboratories, Atsugi, Japan.

[2] Present address: NTT Basic Research Laboratories, Atsugi, Japan.

of normal metals, superconductors, and ferromagnetic metals to realize SET-like structures as well as superconducting flux qubits [2]. In order to fabricate well-defined (Josephson) tunnel junctions we have developed an oxidation process which allows for a complete in-situ preparation of the junctions using a shadow evaporation process.

Sample Preparation

The preparation of SET-structures and flux qubits is usually done by employing electron beam lithography and a mix&match-process. In a first process step auxiliary structures (alignment marks, optional bond pads, and the leads) are patterned using a special photolithographic lift-off process, which was realized by utilizing the image-reversal properties of the Clariant AZ 5214E photo resist. This variant of the process leads to a smooth leveling off of the lead structures, which greatly improves the reproducibility of the process. On top of the developed resist layer an optional 5 to 10 nm thick Cr and a 20 - 40 nm Au layer are deposited by a sputter-process.

After this first lift-off step, the sample is spin-coated with a two layer resist system. The bottom layer consists of 690 nm-thick PMMA/MAA which is covered by a top layer of 70 nm-thick PMMA 950k. Afterwards, the SET/qubit structure is exposed using electron beam lithography and developed in a two-step process, where the profile of the two-layer resist can be adjusted. The profile of the resist system shows a considerable undercut of up to more than 400 μm on each side of the structure, so that the *shadow evaporation* technique can be applied in the next process step. Aluminum is used as the basic material for almost all SET/qubit structures, as it can be easily evaporated using our electron beam evaporation source and as it forms a homogeneous oxide barrier, that provides a tunnel barrier. The oxide thickness can easily be controlled by adjusting the O_2-pressure and the oxidation temperature of the atmosphere, to which the aluminum is exposed after deposition for a certain period of time. To keep the oxidation process well-controlled the SET/qubit structure itself has to be fabricated in an *in-situ* process. The shadow evaporation technique offers this possibility. Here, Al or other materials are evaporated using an electron beam evaporation source under different angles with respect to the sample surface. In between the individual evaporation steps the Al can be oxidized. After a subsequent lift-off step the sample can once again be patterned using photolithography if required (e.g. leads and bond pads). Figure shows a completed SET structure.

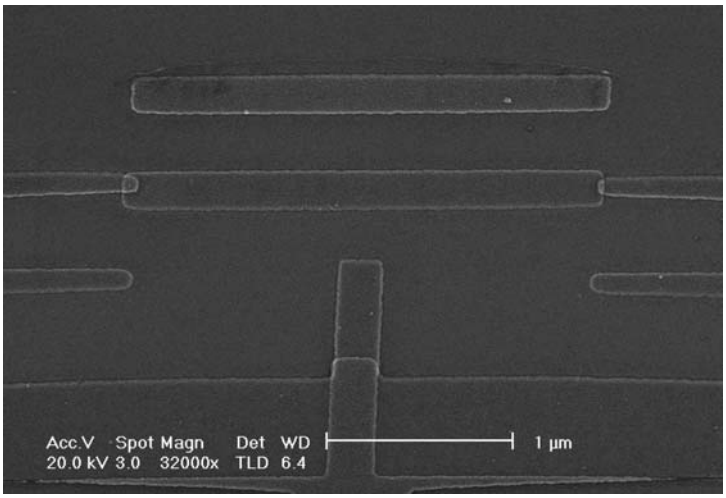

Figure 1: A scanning electron microscopy image of a SET structure. The leads are 100 nm wide, the island is 200 nm wide and 1.1 μm long. The gate electrode is separated by 300 nm from the island.

Experimental Setup

The dilution insert (see page 67) for the experiments on SET/qubit structures in the millikelvin range has been completed. To meet additional requirements for both noise measurements and experiments on highly sensitive SET/qubit structures the design of the insert has been modified. The preamplifier of the SQUID system, which has to be integrated into the insert required a partial redesign of the top of the dilution insert. Furthermore, a test insert has been constructed and realized which allows to investigate the optimal thermal coupling of the STAR Cryoelectronics SQUID to the lHe bath. The vacuum line of the dilution unit has been modified to accommodate a semi-rigid coaxial line which is required to

provide microwave signals to excite transitions between the qubit states. The thermal coupling of this high-frequency line at 4.2 K and the mechanical connection between 1 and 4 K as well as the coupling of the microwave radiation into the samples still need to be tested. For electrical transport measurements the unit is equipped 48 highly filtered lines which are thermally anchored at 4.2 K and 1 K. A tightly closed sample holder which is thermally weakly coupled to the mixing chamber and copper-in-powder based rf filters are presently implemented.

References

[1] T. Dittrich, P. Hänggi, G. Ingold, B. Kramer, G. Schön, and W. Zwerger, *Quantum Transport and Dissipation*,VCH-Verlag (1998), chapter 3, *Single Electron Tunneling*.
[2] T. P. Orlando, J. E. Mooij, L. Tian, C. H. van der Wal, L. S Levitov, S. Loyd, J. J. Mazo, Phys. Rev. B **60**, 15398 (1999).
[3] C. D. Chen, Watson Kuo, D. S. Chung, J. H. Shyu, and C. S. Wu, Phys. Rev. Lett. **88**, 047004 (2002).
[4] H. Imamura, Y. Utsumi, and H. Ebisawa, Phys. Rev. B **66**, 054503 (2002).

Orbital Order and Anisotropic Transport Properties in Doped Manganites Induced by Epitaxial Coherency Strain[1]

J. Klein, J. B. Philipp, D. Reisinger, M. Opel, A. Marx, A. Erb, and R. Gross

The physics of the hole doped perovskite manganites is determined by a complex interplay between structural, magnetic, electronic, and orbital degrees of freedom. It has been pointed out by Millis *et al.* that uniform compression, as realized by hydrostatic pressure, increases the electron hopping amplitude favoring a ferromagnetic metallic state [1, 2]. In contrast, biaxial strain, as realized in epitaxial thin films grown on substrates with significant lattice mismatch or in heterostructures required for magnetoelectronic devices, enhances the Jahn-Teller distortions favoring an insulating state due to the tendency of the electrons to become localized [2]. The investigation of the structural, electronic, and magnetic properties of biaxially strained manganite thin films and heterostructures is of great interest to gain more insight into the physics of these materials and their dependence on lattice distortions as well as to clarify the impact of strain in heterostructures used in magnetoelectronic devices such as magnetic tunnel junctions.

It has been found recently that thin films of the doped manganites may be structurally, magnetically, and electronically nonuniform at large compressive strain imposed by lattice mismatch to the substrate [3, 4]. This has been explained in terms of a nonuniform strain distribution due to island formation in the Stranski-Krastanov growth mode. However, also homogeneous, coherently strained thin films and superlattices of doped manganites display novel properties [5]- [13]. Recently, we have analyzed the magnetic and transport properties of high quality homogeneous $La_{2/3}Ca_{1/3}MnO_3$ (LCMO) films that have been grown coherently strained (tensile strain) on $SrTiO_3$ (STO) substrates in a layer-by-layer growth mode using UHV laser molecular beam epitaxy (L-MBE) [14, 15]. In contrast to previous studies, transport properties have been measured both parallel and perpendicular to the substrate [16, 17]. A key result of this study was that biaxial strain results in highly anisotropic transport properties of LCMO: Whereas insulating behavior and non-linear IVCs are observed perpendicular to the biaxially strained plane (parallel to the *c*-axis), the *ab*-plane transport was metallic below the Curie temperature T_C. We further have shown that this behavior is not due to interface effects between different layers [18, 19], but is an *intrinsic* property of the biaxially strained LCMO films. We suggested strain induced orbital ordering as the possible origin of the observed behavior in agreement with theoretical predictions [10, 20]. Here, we report on the anisotropic transport properties of coherently strained $La_{2/3}Ba_{1/3}MnO_3$ (LBMO) films grown on $NdGaO_3$ (NGO) substrates. Whereas for the LCMO films on STO substrates a tensile in-plane strain is established, a compressive in-plane coherency strain is realized for the LBMO films on NGO. Therefore, a different type of orbital ordering is expected for LBMO and LCMO films discussed in Ref. [16].

We have grown LBMO films both on (100) $SrTiO_3$ ($a \simeq 3.905$ Å) and (110) $NdGaO_3$ ($\frac{1}{2}\sqrt{a^2+b^2} \simeq 3.863$ Å) substrates using L-MBE [14, 15]. The lattice mismatch between the STO and NGO substrate and LBMO ($a_{\mathrm{bulk}} \simeq 3.91$ Å in pseudocubic notation) is 0.1% and 2.6%, respectively, resulting in almost strain-free films for the former and a large in-plane compressive strain for the latter. Hence, comparing the transport properties of the LBMO films grown on these substrates allows to clarify the role of the in-plane compressive coherency strain. The growth parameters were as follows: The films were deposited at a substrate temperature of 780°C and an oxygen pressure of 200 mTorr from stoichiometric targets using a KrF excimer laser. Layer-by-layer growth of the films was confirmed by a high pressure RHEED system showing clear growth oscillations [14, 15]. The interface and surface roughness of the films was studied by x-ray reflectometry and atomic force microscopy and found to be of the order of a single unit cell. X-ray analysis showed that the LBMO films grow coherently strained on NGO substrates up to a

[1]This work was supported in part by the Deutsche Forschungsgemeinschaft and the BMBF (project 13N8279).

thickness of about 60 nm. That is, the in-plane lattice parameter of the LBMO film is reduced, while the out-of-plane lattice constant is increased, leading to a tetragonal lattice distortion with $c/a \simeq 1.026$. The tetragonal distortion can be viewed as a Jahn-Teller like distortion, which results in an increased Jahn-Teller splitting of the Mn e_g levels and, in turn, in a tendency of the electrons to become localized. It also favors a C-type antiferromagnetic ordering [20]. For details of the sample fabrication, see [16, 17].

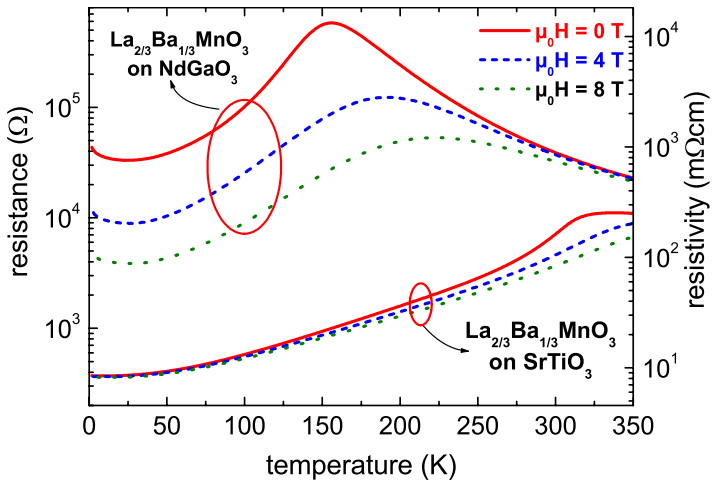

Figure 1: Resistance versus temperature curves measured along the *ab*-plane direction for two 68 nm thick LBMO films grown on a (100) $SrTiO_3$ (strain-free) and a (110) $NdGaO_3$ substrate (compressive in-plane strain) for 0, 4, and 8 T.

Fig. 1 shows the *ab*-plane resistance versus temperature, $R(T)$, curves of LBMO films on STO and NGO substrates. The curves have been obtained by standard four-probe measurements on several 10 μm wide and several 100 *mu*m long microbridges. The strain-free film on STO shows the usual behavior with peak temperature T_p in the $R(T)$ curve, which roughly gives the paramagnetic insulator to ferromagnetic metal transition, of about 320 K. Fig. 1 shows that the coherency strain shifts T_p down to 170 K. This strain induced shift of T_p has been discussed in detail recently [12]. In addition, a strongly increased resistivity and large magnetoresistance is observed at low T.

In Fig. 2 the $R(T)$ curves the *c*-axis direction are shown. These curves have been obtained by three-probe measurements on the mesa structures shown in the inset. The contact resistance between the LBMO layer and the in-situ deposited Au layer was checked carefully and found to be well below $10^2 \Omega\mu m^2$ over the entire temperature range. Whereas for the almost strain-free LBMO film on STO the *c*-axis transport is similar to the *ab*-plane data, i.e. the transport properties are about homogeneous, for the strained film on NGO a clear difference is obtained below $T_p \simeq 170$ K. Whereas the *ab*-plane transport shows a metallic behavior (R decreases with T), the *c*-axis resistance shows a strong increase with decreasing T and is by many orders of magnitude larger than the *c*-axis resistance of the strain-free film.

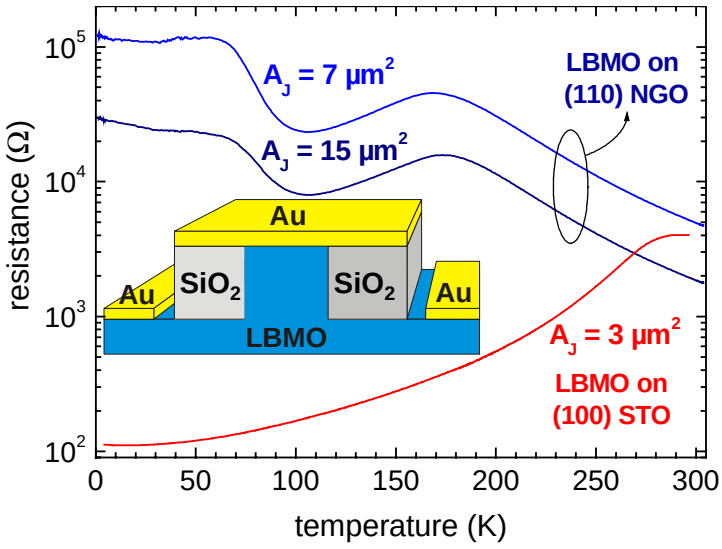

Figure 2: R vs. T curves measured along the *c*-axis direction using mesa structures with area A_J patterned into a LBMO film grown on a (100) STO (strain-free) and a (110) NGO substrate (compressive in-plane strain). The inset shows a cross-sectional view of the mesa structure.

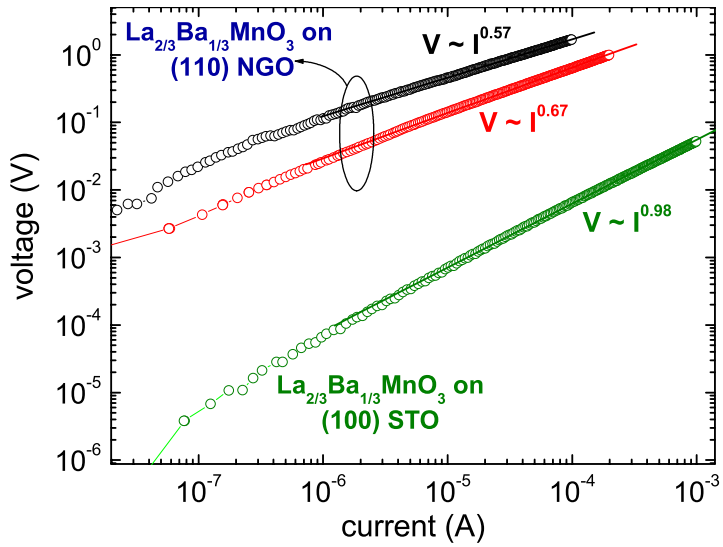

Figure 3: IVCs measured at 4.2 K along the *c*-axis direction of a LBMO film grown on a (100) STO (strain-free) and a (110) NGO substrate (compressive in-plane strain). The lines are linear fits to the data.

A clear different also is seen in the *c*-axis current-voltage characteristics (IVCs) plotted in Fig. 3. Whereas linear (ohmic) IVCs are measured for the strain-free film, strongly nonlinear IVCs with $V \propto I^{0.65\pm0.1}$ are obtained for the strained film. This is completely analogous to the strained LCMO films, for which $V \propto I^{0.25\pm0.05}$ has been observed [16, 17].

In Fig. 4 we have plotted the *c*-axis $R(T)$ curves for different bias current I_b and applied magnetic fields H. Whereas for linear IVCs the measured R is independent of I_b, a clear I_b dependence of R is expected for nonlinear IVCs. This is indeed observed. Fig. 4 clearly shows a deviation of the $R(T)$ curves obtained for different I_b below $T^\star \simeq 100$ K at $H = 0$. That is, the nonlinearity in the IVCs becomes pronounced below $T^\star$. This temperature is shifted to lower values by applying a magnetic field.

Discussing our experimental observations we note that in the case of inhomogeneously strained films (e.g. due to island growth), it is plausible to assume a phase separated state with ferromagnetically and antiferromagnetically ordered clusters [3, 4]. However, this not likely for the our LBMO films grown on NGO in a layer-by-layer growth mode resulting in coherently strained, homogeneous films. The same was found for coherently strained LCMO films grown on STO [16]. Furthermore, from our detailed transport experiments with current in- and out-of-plane, we have strong evidence against a phase separated state in the strained LBMO films. In the presence of nano-scale phase separation it is very difficult to explain how insulating behavior can be achieved in *c*-axis direction whereas transport along the *ab*-plane is still metallic.

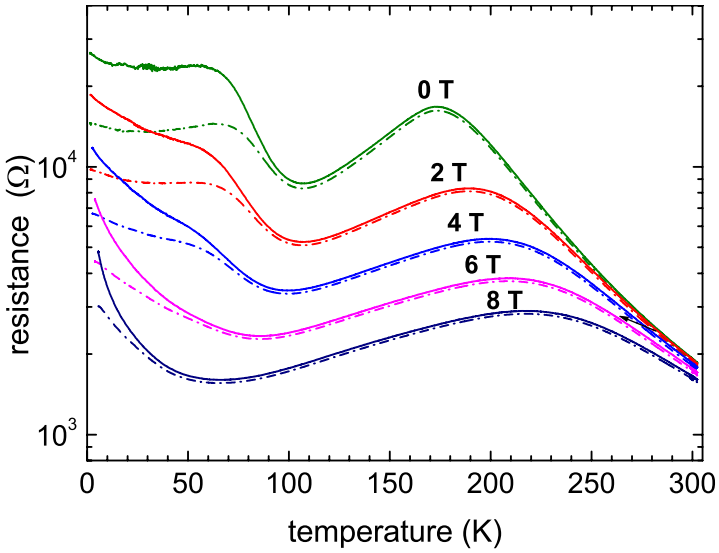

Figure 4: R vs. T curves measured along the *c*-axis direction for a strained LBMO film grown on a (110) NGO (compressive in-plane strain) for 0, 2, 4, 6, and 8 T. The solid lines are obtained for $I = 1\,\mu$A, the dotted for $I = 10\,\mu$A.

The most obvious explanation for the anisotropic transport in strained LBMO films is a biaxial coherency strain induced orbital ordering. It is expected that biaxial strain results in different spin structures, such as ferromagnetic (F), layer-type antiferromagnetic (A) and chain-type antiferromagnetic (C) states and, hence, different magnetotransport characteristics [10, 20]. For tensile in-plane strain ($c/a < 1$, as present for LCMO films on STO [16]), a transition from the conventional double exchange mediated, orbital dis-

ordered F state to the orbital ordered A state, which is composed mainly by $d_{x^2-y^2}$ states, is expected. In contrast, for compressive in-plane strain ($c/a > 1$, as present for our LBMO films on NGO), a transition from the orbital disordered F state to the orbital ordered C state, which is composed mainly by $d_{3z^2-r^2}$ states, is expected. Whereas in the F state the spins are aligned parallel in adjacent planes, in the C state the spins are aligned parallel along chains in *c*-axis direction with neighboring chains having opposite spin directions. That is, the gradual transition from the F to the C state is accompanied by a reduction of saturation magnetization in agreement with our experiments. We note, however, that for an ideal C state no metallic transport along the *ab*-plane is expected in contrast to our experimental findings. This is due to the almost full spin polarization of the charge carriers in the doped manganites, which prevents the charge carriers to hop along the *ab*-plane direction with alternating direction of the localized core spins in the ideal C state. The fact that we still observe metallic transport along the *ab*-plane at low T then suggests that we do not have an ideal C state but more likely a canted or disordered F state with C type antiferromagnetic correlations. This is confirmed by the observed magnetic field dependence of the *ab*-plane transport. First, a large magnetoresistance is observed at low temperatures (see Fig. 1). This can naturally be explained by the spin ordering effect of the applied magnetic increasing the spin alignment in the canted or disordered F state. Second, the nonlinearity of the *c*-axis IVCs is reduced by an applied field (see Fig. 1). This again can be explained by the fact that the field strengthens the orbital disordered, ferromagnetic metallic F state.

In summary, we have investigated the magnetotransport of coherently strained (compressive) LBMO films and compared to our recent results on strained (tensile) LCMO films [16]. The compressive strain in the LBMO films was found to induce anisotropic transport properties at low T with metallic and insulating behavior for the current along the *ab*-plane and *c*-axis direction. It has been shown that this behavior is not due to interface effects or phase separation. We suggest a strain induced orbital ordering as the possible origin of the observed behavior in agreement with theoretical predictions. However, the strain is not sufficient to induce a full orbital ordering, i.e. a transition from a orbital disordered, ferromagnetic F state to an ideal orbital ordered, antiferromagnetic C state. Our results suggest a transition from a orbital disordered, ferromagnetic F state to a canted or disordered F state with C type antiferromagnetic correlations.

References

[1] A. J. Millis *et al.*, Phys. Rev. Lett. **74**, 5144 (1995); see also Phys. Rev. Lett. **77**, 175 (1996).
[2] A. J. Millis *et al.*, J. Appl. Phys. **83**, 1588 (1998).
[3] A. Biswas *et al.*, Phys. Rev. B **61**, 9665 (2000).
[4] A. Biswas *et al.*, Phys. Rev. B **63**, 184424 (2001).
[5] H. L. Ju *et al.*, J. Appl. Phys. **83**, 7073 (1998).
[6] H. W. Zandbergen *et al.*, Phys. Rev. B **60**, 10259 (1999).
[7] J. Z. Sun *et al.*, Appl. Phys. Lett. **74**, 3017 (1999).
[8] M.G. Blamire *et al.*, J. Magn. Magn. Mat. **191**, 359 (1999).
[9] Moon-Ho Jo *et al.*, Appl. Phys. Lett. **75**, 3689 (1999).
[10] Y. Konishi *et al.*, J. Phys. Soc. Jpn. **68**, 3790 (1999).
[11] K. Dörr *et al.*, J. Phys.: Cond. Matter **12**, 7099 (2000).
[12] Yafeng Lu *et al.*, Phys. Rev **B 62**, 15806 (2000).
[13] A. Vigliante *et al.*, Europhys. Lett. **54**, 619 (2001).
[14] R. Gross *et al.*, in *Superconducting and Related Oxides: Physics and Nanoengineering IV*, D. Pavuna and I. Bosovic eds., SPIE Conf. Proc. **Vol. 4058** (2000), pp. 278–294.
[15] J. Klein *et al.*, J. Magn. Magn. Mat. **211**, 9 (2000); see also Supercond. Sci. Technol. **12**, 1023 (1999) and Phys. Stat. Sol. (a) **189**, No. 3, 617-620 (2002).
[16] J. Klein, J. B. Philipp, G. Carbone, A. Vigliante, L. Alff, and R. Gross, Phys. Rev. **B 66**, 052414 (2002).
[17] J. Klein, J. B. Philipp, D. Reisinger, M. Opel, A. Marx, A. Erb, L. Alff, and R. Gross, J. Appl. Phys., to appear (2003).
[18] J.-H. Park *et al.*, Phys. Rev. Lett. **81**, 1953 (1998).
[19] M. J. Calderón *et al.*, Phys. Rev. B **60**, 6698 (1999).
[20] Z. Fang *et al.*, Phys. Rev. Lett. **84**, 3169 (2000).

Manganite Based Magnetic Tunnel Junctions [1] [2]

Yafeng Lu,[3] *J. Klein, J. B. Philipp, F. Herbstritt, D. Reisinger, M. Opel, A. Marx, and R. Gross*

For computer industry there is great interest in the possibility of fabricating a non-volatile random access memory which retains its information even after removing power from the device – an ideal memory. The new concept of a *non-volatile* Magnetic Random Access Memory (MRAM) has been proposed and will possibly revolutionize semiconductor memory and logic circuits in the near future. The basic elements for MRAMs are micron-sized magnetic tunnel junctions (MTJs), which consist of two ferromagnetic (FM) electrodes sandwiching a thin insulating (I) barrier. Since the discovery of a large tunneling magnetoresistance (TMR) at room temperature in MTJ devices in the early 90's, [1, 2] this research field has become very active.

The TMR ratio is defined as TMR $= (R_{ap} - R_p)/R_p = \Delta R/R_p$, where R_{ap} and R_p are the resistance of the MTJ for the antiparallel and parallel magnetization orientation in the FM junction electrodes. In Jullière's model [3], the TMR ratio is related to the spin polarization P_1 and P_2 of the conduction electrons at the Fermi level in the junction electrode as TMR $= 2P_1P_2/(1 - P_1P_2)$, i.e. within this simple model large TMR ratios are expected for electrodes with large spin polarization.

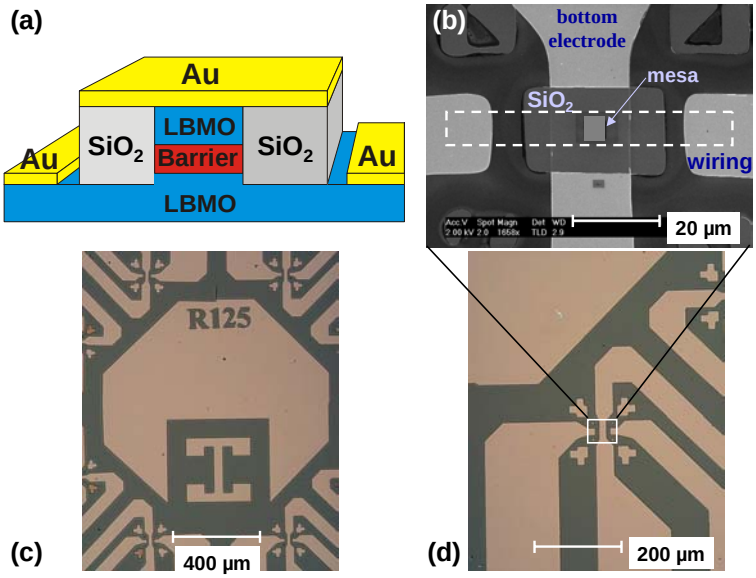

Figure 1: Cross-sectional view (a) of a manganite based MTJ and SEM micrograph (b) taken after the patterning of the mesa structure. The dashed white line indicates the wiring layer deposited in the final fabrication step to make contact to the top electrode in the mesa structure. (c) and (d) show optical micrographs of the sample layout. The micrographs have been taken after the patterning of the base electrode and contact pads.

Since the achievable magnitude of the TMR effect increases with increasing spin polarization, materials with full spin polarization are interesting candidates for MTJs. Therefore, the doped manganites, the double perovskite, CrO_2 or Fe_3O_4, which have been predicted to be so-called half-metals with a spin polarization close to 100%, have attracted much attention for MTJ devices. Since the discovery of the colossal magnetoresistance (CMR) in films of perovskite type rare earth manganese oxides, considerable effort has been devoted to the exploration of the applicability of the CMR materials in magnetoresistive devices operated in moderate magnetic fields of the order of a few hundred Gauss at room temperature. It turned out quite early that manganite based spin dependent tunneling devices (see Fig. 1) exploiting the high spin polarization of these materials are promising [4]- [12]. However, most experiments also showed that such devices have problems regarding the quality and microstructure of interfaces and barriers. These problems have to be solved to fabricate high quality MTJs with large TMR values in a reproducible way. In this context, the tunneling characteristics and magnetotransport properties have to be studied in more detail in order to clarify the nature of

[1] In collaboration with J. Simon, Th. Walter, W. Mader, University of Bonn.

[2] This work has been partly supported by the Deutsche Forschungsgemeinschaft and the BMBF (project 13N8279).

[3] Present address: Max-Planck-Institut für Mikrostrukturphysik, Halle.

charge transport in these junctions and, in turn, to find remedies for improving the performance of MTJs based on the doped manganites.

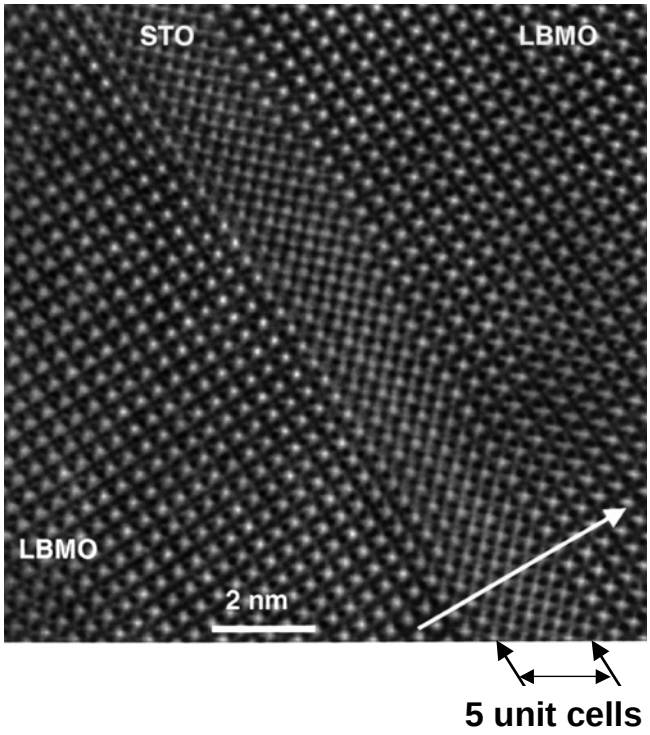

Figure 2: Cross-sectional High Resolution Transmission Electron Microscopy (HRTEM) image of a LBMO/STO/LBMO trilayer grown by L-MBE. The microstructure of the trilayer shows a perfectly epitaxial growth (J. Simon, University of Bonn).

We have studied the spin-dependent tunneling in $La_{2/3}Ba_{1/3}MnO_3$ (LBMO) based trilayer magnetic tunnel junctions employing $SrTiO_3$ (STO) and strained $La_{2/3}Ca_{1/3}MnO_3$ (LCMO) barrier layers. For the realization of manganite based MTJs we have grown heteroepitaxial LBMO/STO/LBMO and LBMO/LCMO/LBMO trilayer structures *in situ* on (001) STO substrates using UHV-Laser Molecular Beam Epitaxy (L-MBE) [13, 14]. Using RHEED and atomic force microscopy it could be shown that the manganite layers grow in a layer-by-layer growth mode on the STO substrate. The thickness of the base and top LBMO electrode typically was several 10 nm. The thickness of the STO barrier layer was varied between 1.6 nm and 10 nm. For the LBMO/LCMO/LBMO trilayer structures, the insulating, highly strained LCMO barrier layer was deposited under the same conditions as the LBMO electrodes (substrate temperature $T_S = 760^\circ$C and an oxygen pressure $p_{O_2} = 200$ mTorr) and had a thickness up to 30 nm. For the patterning of the junction structure optical lithography and Ar ion beam etching were employed. A cross-sectional view of the sample structure and optical as well as a scanning electron micrograph taken after the patterning of the mesa structure are shown in Fig. 1. In Fig. 2 a HR-TEM image of a LBMO/STO/LBMO trilayer structure is shown. It is evident that the trilayer structures can be grown in high quality. We note, however, that the HR-TEM images does not give valuable information on the magnetic disorder at the interfaces as well as on oxygen defects within the barrier layer.

For the MTJs with the STO barrier, the measured tunneling characteristics were found to deviate considerably from the ideal characteristics expected for elastic tunneling through an ideal barrier. The data indicate that inelastic multi-step tunneling as described by the Glazman-Matveev model [15] is present. The magnetic field dependence of the junction resistance was found to strongly depend on the barrier thickness and can show a complicated behavior due to both a complex magnetic state in the junction electrodes and magnetic interactions between the ferromagetic electrodes. For thin barriers ($t_b = 1.6$ nm) ferromagnetic pinhole coupling between the junction electrodes is observed. On increasing the barrier thickness ($t_b = 3$ nm), the two ferromagnetic layers are mostly decoupled. Then, a nearly flat high resistance plateau, where the magnetization direction is opposite in the junction electrodes, is obtained (see Fig. 3a) with a TMR $= 9.5\%$ at 150 K. For the junction with $t_b = 4.5$ nm (see Fig. 3b), two very sharp magnetoresistance peaks were found indicating that the switching fields of the two FM electrodes are close to each other. The TMR is 30% at 7 K at a bias current of 10 nA. However, the shape and the detailed values of the $R(H)$ loop were found to depend significantly on the magnetic history of the junction. The $R(H)$ curve of the junction with a 6 nm thick STO barrier layer (see Fig. 3c) shows multiple discrete resistance steps which most likely originate from a complex magnetic domain structure. A TMR ratio of

15% is obtained at 77 K. With further increasing the barrier thickness to $t_b = 10$ nm, the TMR strongly decreases. We note that a very large tunneling magnetoresistance up to $R_{ap} - R_p/R_p \simeq 1200\%$ was observed for some junctions which, however, was found to sensitively depend on the magnetic history [16].

The $R(H)$ curves in Fig. 3 also show a significant high field magnetoresistance. This most likely originates from a disordered interface layer (e.g. a canted LBMO phase). Assuming that a high field is required to align the interfacial magnetic moments parallel to the applied field, we can explain the significant variation of R also at high fields. Our data suggests that the decrease of the junction resistance at high fields is weaker for the junctions with large barrier thickness, although the interfacial layer should be about the same for junctions with different t_b. However, one has to take into account that the total junction resistance increases with increasing barrier thickness and, hence, the contribution of the interfacial layer becomes smaller with increasing barrier thickness.

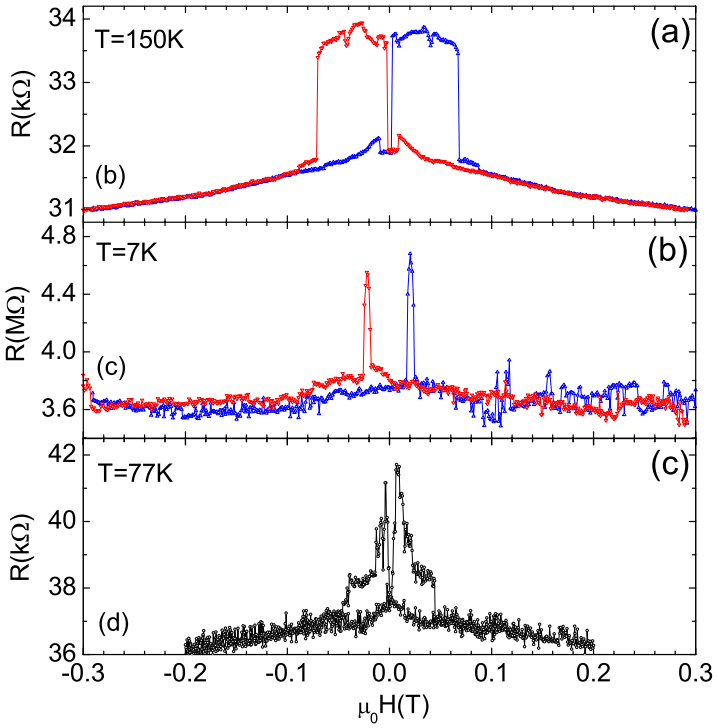

Figure 3: Resistance versus applied magnetic field curves of LBMO/STO/LBMO MTJs with different values of the nominal barrier thickness t_b and the junction area A_J: (a) $t_b = 3$ nm, $A_J = 10 \times 40\mu m^2$, $I_{bias} = 1\mu$ A; (b) $t_b = 4.5$ nm, $A_J = 8 \times 8\mu m^2$, $I_{bias} = 10$ nA; (c) $t_b = 6$ nm, $A_J = 10 \times 10\mu m^2$, $I_{bias} = 1\mu$A.

We also have fabricated MTJs with LBMO electrodes and a LCMO barrier. Since the lattice parameters of LCMO are significantly smaller than those of LMBO, the thin LCMO barrier layer is exposed to high tensile strain. It was shown recently, [17] that large biaxial strain results in orbital ordering and highly anisotropic transport properties of LCMO: Whereas insulating behavior and non-linear IVCs are observed perpendicular to the biaxially strained plane (parallel to the c axis), the in-plane transport is still metallic below the Curie temperature T_C, which however is reduced to values around 100 K due to the biaxial strain. It is evident that the strained insulating LCMO can be used as a tunneling barrier which can be easily grown on the LBMO base electrode

Fig. 4 shows the $R(H)$ curves of a LBMO/LCMO/LBMO junction with a 8 nm thick strained LCMO barrier at two different T. The measurement of the magnetization shows that the LCMO layer has a magnetic transition from a paramagnetic insulating to a magnetic state with strongly reduced magnetization and highly anisotropic transport properties around 100 K. [17] Therefore, at $T = 125$ K (Fig. 4a) we expect the LCMO layer to behave as a paramagnetic insulating tunneling barrier. At this T, the LBMO electrodes with $T_C \simeq 270$ K are ferromagnetic and we therefore expect $R(H)$ curves corresponding to those of a MTJs. This is indeed the case. The $R(H)$ curve in Fig. 4a clearly shows a sharp switching from a low to a high resistance state at around 7 mT when increasing the field starting a large negative magnetic fields. The same switching is observed at -7 mT when decreasing the field from large positive values. The measured TMR ratio of about 3% is quite small, however, this value is obtained for a large barrier thickness of 8 nm and is comparable to that obtained for STO barriers of the same thickness.

Usually, the TMR ratio is increasing with decreasing T. However, this is not the case here. Reducing T to values below the magnetic ordering temperature of the LCMO layer results in a strong magnetic coupling of the two junction electrodes. That is, the magnetization directions in both electrode are always parallel and no low field TMR effect can be observed. That is, by varying T the magnetic coupling between the junction electrodes can be switched on and off. At low T only the high field magnetoresistance is observed, that is caused by an orientation of the disordered, spin-glass like spin structure in the LCMO layer [17].

Our study of manganite based MTJs shows that the improvement and control of the interface layer between the manganite electrodes and the barrier layer is crucial to improve the magnetotransport properties of the junctions. We also showed that a strained insulating LCMO layer can be used as tunneling barrier. In this case the magnetic coupling between the junction electrodes could be switched on and off as a function of T due to a magnetic transition of the barrier layer.

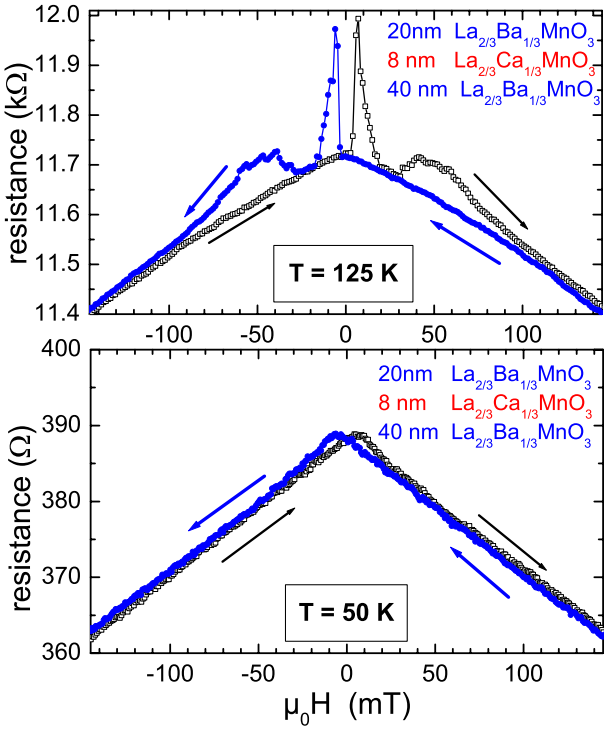

Figure 4: Resistance versus applied magnetic field curves for a LBMO/LCMO/LBMO junction above (125 K) and below (50 K) the magnetic ordering temperature of the strained LCMO barrier layer.

References

[1] J. S. Moodera, L. R. Kinder, T. M. Wong, R. Meservey, Phys. Rev. Lett. **74**, 3273 (1995).

[2] S. S. P. Parkin, K. P. Roche, M. G. Samant, P. M. Rice, R. B. Byers, R. E. Scheuerlein, E. J. O'Sullivan, S. L. Brown, J. Bucchigano, D. W. Abraham, Yu Lu, M. Rooks, P. L. Trouilloud, R. A. Wanner, and W. J. Gallagher, J. Appl. Phys. **85**, 5828 (1999).

[3] M. Jullière, Phys. Lett. **A 54**, 225 (1975).

[4] J. Z. Sun, W. J. Gallagher, P. R. Duncombe, L. Krusin-Elbaum, R. A. Altman, A. Gupta, Yu Lu, G. Q. Gong, and Gang Xiao, Appl. Phys. Lett. **69**, 3266 (1996).

[5] M. Viret, M. Drouet, J. Nassar, J. P. Contour, C. Fermon, and A. Fert, Europhys. Lett. **39**, 545 (1997).

[6] Moon-Ho Jo, N. D. Mathur, N. K. Todd, M. G. Blamire, Phys. Rev **B 61**, R14905 (2000).

[7] N. D. Mathur, G. Burnell, S. P. Isaac, T. J. Jackson, B.-S. Teo, J. L. MacManus-Driscoll, L. F. Cohen, J. E. Evetts, and M. G. Blamire, Nature **387**, 266 (1997)

[8] K. Steenbeck, T. Eick, K. Kirsch, K. O'Donnell, and E. Steinbeiß, Appl. Phys. Lett. **71**, 968 (1997).

[9] J. Klein, C. Höfener, S. Uhlenbruck, L. Alff, B. Büchner, and R. Gross, Europhys. Lett. **47**, 371 (1999); see also J. Magn. Magn. Mater. **211**, 150 (2000).

[10] R. Gross, L. Alff, B. Büchner, B. H. Freitag, C. Höfener, J. Klein, Yafeng Lu, W. Mader, J. B. Philipp, M. S. R. Rao, P. Reutler, S. Ritter, S. Thienhaus, S. Uhlenbruck, B. Wiedenhorst, J. Magn. Magn. Mater. **211**, 150 (2000).

[11] C. Höfener, J. B. Philipp, J. Klein, L. Alff, A. Marx, B. Büchner, and R. Gross, Europhys. Lett. **50**, 681 (2000).

[12] J. B. Philipp, C. Höfener, S. Thienhaus, J. Klein, L. Alff, and R. Gross, Phys. Rev. **B 62**, Rapid. Com., R 9248 (2000).

[13] R. Gross, J. Klein, B. Wiedenhorst, C. Höfener, U. Schoop, J. B. Philipp, M. Schonecke, F. Herbstritt, L. Alff, Yafeng Lu, A. Marx, S. Schymon, S. Thienhaus, W. Mader, SPIE Conf. Proc. **4058** (2000), pp. 278-294.

[14] J. Klein, C. Höfener, L. Alff, and R. Gross, Supercond. Sci. Technol. **12**, 1023 (1999), see also J. Magn. Magn. Mater. **211**, 9 (2000).

[15] L. I. Glazman and K. A. Matveev, Sov. Phys. JETP, **67**, 1276 (1988).

[16] Yafeng Lu, J. Klein, J. B. Philipp, F. Herbstritt, M. Opel, A. Marx, and R. Gross, J. Appl. Phys., submitted for publication (2002).

[17] J. Klein, J. B. Philipp, G. Carbone, A. Vigliante, L. Alff, and R. Gross, Phys. Rev. **B 66**, 052414 (2002).

Influence of Alkaline Earth Metals on A_2CrWO_6

J. B. Philipp, L. Alff, A. Erb, and R. Gross

Ordered double-perovskites $AA'BB'O_6$ are interesting materials for the spintronic devices because of their high spin polarization at the Fermi level [1], which according to band structure calculations is close to 100%, and their high Curie temperature T_C (e.g. $T_C = 635\,\mathrm{K}$ for Sr_2CrReO_6 [2]. In particular, due to these properties the double perovskite may be useful for spin injection into semiconductors at room temperature.

The polycrystalline samples were prepared from stoichiometric mixtures of $SrCO_3$, $BaCO_3$, $CaCO_3$, Cr_2O_3, La_2O_3 and WO_3 with purities in between 99.99% and 99.999%. The powders were thoroughly mixed, placed in Al_2O_3 crucibles and were repeatedly heated in a thermobalance under reducing atmosphere (H_2/Ar, 5/95%) with intermediate grinding. The final temperatures were increased from 1200°C for the first to up to 1550°C for the final firing. The use of the thermobalance allowed us to monitor the degree of reaction due to the accompanied weight loss of the samples. The samples were furthermore characterized by X-ray powder diffractometry to detect parasitic phases such as the insulating compound $SrWO_4$.

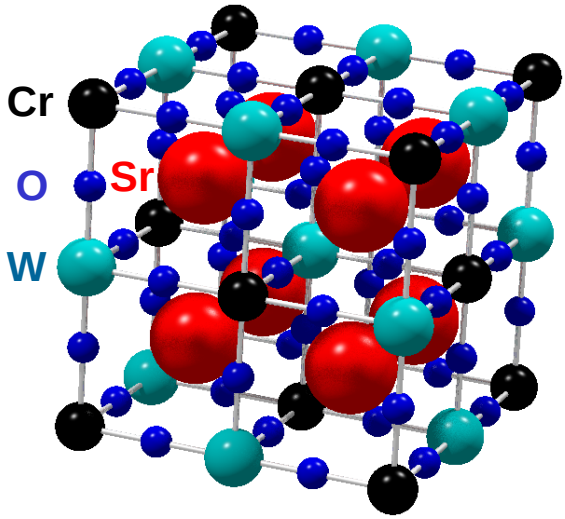

Figure 1: The crystal structure of Sr_2CrWO_6.

We first discuss the influence of the chemical pressure on A_2CrWO_6 due to different alkaline earth cations with different ionic radii [5] ($< r_{Ca} >= 1.34\,$Å, $< r_{CaSr} >= 1.39\,$Å, $< r_{Sr} >= 1.44\,$Å, $< r_{BaSr} >= 1.53\,$Å and $< r_{Ba} >= 1.61\,$Å all with coordination number 12). The tolerance factor t is a geometrical quantity, which characterizes the mismatch between the A and B cations in perovskite ABO_3 materials. It is given by

$$t = \frac{< r_A > + < r_X >}{\sqrt{2}(< r_B > + < r_X >)}.$$

For a perfect size match ($t = 1$), the B-O-B bond angle is 180°. For $t < 1$, rather than a simple contraction of bond distances, the octahedra tilt and rotate to reduce the excess space around the A site, resulting in an angle smaller than 180°. In Fig. 2d the tolerance factor calculated with bond valance parameters by the SPuDS program [6] is shown. The tolerance factor is varying form 0.94 (Ca_2) over 1.00 (Sr_2) to 1.06 (Ba_2). The crystal structure of the samples is determined by x-ray Rietfeld refinement. The Sr_2 compound is cubic (Fm-3m) with $a = 7.82$Å as expected for $t = 1$. The Cr-W disorder is about 23%. This value is larger than for the FeMo system. This is probably caused by the small difference in the ionic radii between Cr ($< r_{Cr^{3+}} >= 0.615\,$Å and W ($< r_{W^{5+}} >= 0.62\,$Å compared to Fe ($< r_{Fe^{3+}\,\mathrm{high\,spin}} >= 0.645\,$Å and Mo ($< r_{Mo^{5+}} >= 0.61\,$Å.

The SrCa samples are still cubic with $a = 7.73$Å, in contrast to the Ca_2 samples, where the tilt of the octahedra causes a distortion from the cubic system to the P21/n system with $a = 5.39$Å, $b = 5.45\,$Å, $c = 7.66\,$Å and $\beta = 90.1°$ which is predicted by the SPuDS program [6]. The Ba_2 sample has a hexagonal 6-layer structure (P62c) with $a = 5.70$Å and $c = 13.99\,$Å like $Ba_3Cr_2W_2O_9$ but with $Ba_3Cr_{1.5}W_{1.5}O_9$. It was not possible to prepare a phase pure SrBa sample, because there was always a phase separation in

a Ba-rich (P62c) and Ba-pure (Fm-3m) phase. These sturctual changes are different to the well studied system A_2FeMoO_6, where Ca_2 is monoclinic, Sr_2 is tetragonal and Ba_2 is cubic [3].

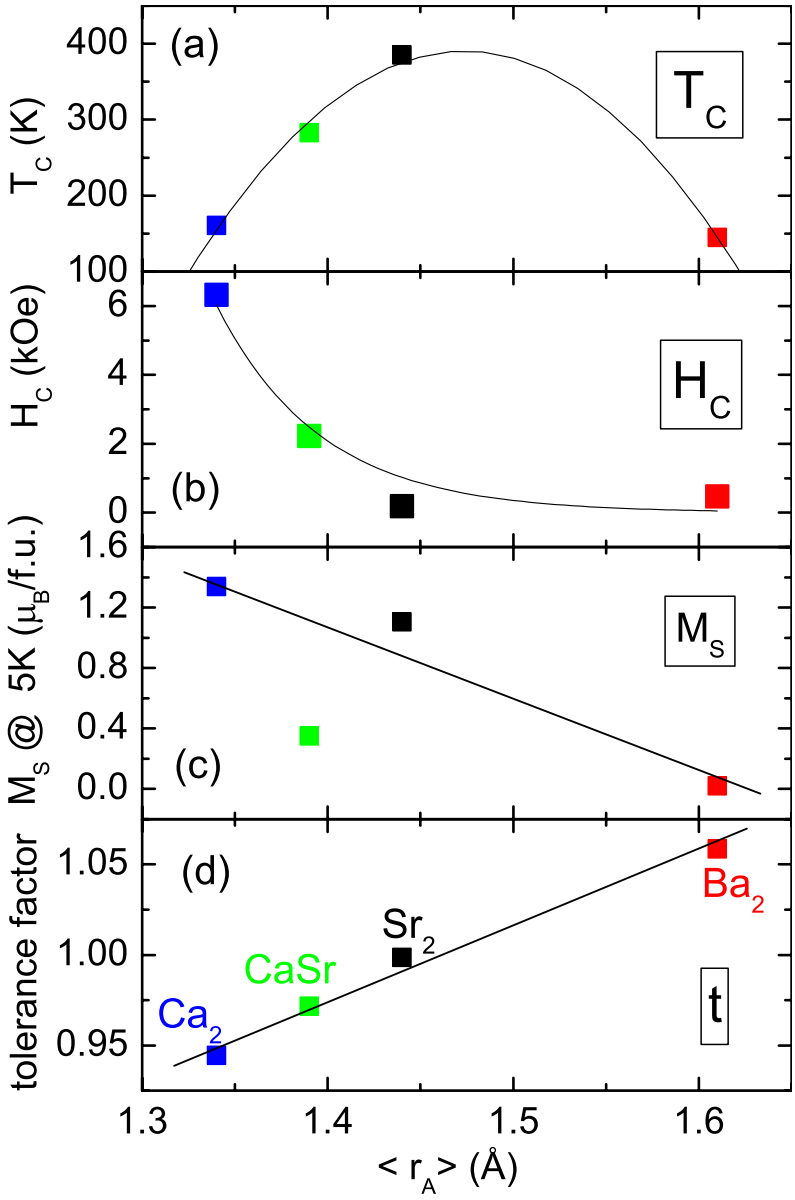

Figure 2: Curie temperature T_C (a), coercivity field H_C (b), saturation magnetization M_S at 5 K (c) and tolerance factor (d) for the series A_2CrWO_6 with A_2 =Ca_2, CaSr, Sr_2 and Ba_2 as a function of the ionic radii at the *A*-site.

The most remarkable effect of the chemical pressure is the change of the Curie temperature (see Fig. 2a). The Curie temperature has a maximum of ~ 400 K for the Sr_2CrWO_6 compound and decreases for the Ba_2CrWO_6 (140 K) and Ca_2CrWO_6 (165 K) compounds. An effect of the same order of magnitude is found in the system A_2CrReO_6 with Sr_2CrReO_6 (635 K) and Ca_2CrReO_6 (360 K) [2]. The effect in the systems A_2CrReO_6 and A_2CrWO_6 is much larger compared to the system A_2FeMoO_6, where the Curie temperature is varying between 310 K and 420 K [3]. In all the systems the maximum of the Curie temperature has been found for Sr containing compound.

Fig. 2b shows the decrease of the coercivity field with increasing ionic radius r. Also the saturation magnetization (at $T = 5$ K and $H = 7$ T) is decreasing with increasing ionic radius (see Fig. 2c). The reduced saturation magnetization for the CaSr sample is caused by a canted or antiferromagnetic spin order at low temperatures.

In Fig. 3 the normalized magnetization versus temperature is shown. The Ca_2 and Sr_2 samples have typical curves expected for ferromagnetic materials. For the Ba_2 sample the magnetization shows an upturn at very low temperatures, which so far is not understood. The CaSr sample shows a maximum in the magnetization versus temperature curve at 50 K, which indicates a antiferromagnetic or canted spin order.

The magnetic properties can now be explained taking into account two parameters. Firstly, the Cr-W bond length increases from Ca_2 over Sr_2 to Ba_2, which leads to a reduction of the magnetic interaction. Secondly, only for the Sr_2 the bond angles are equal to 180°, which leads to the strongest interaction in the double exchange or superexchange and results in the highest Curie temperature. We note that in doped manganites ($A^{3+}_{0.7}A'^{2+}_{0.3}MnO_3$) the Curie temperature shows a maximum for $t = 0.93$ and a drastic reduction of the Curie temperature is observed for smaller t [4].

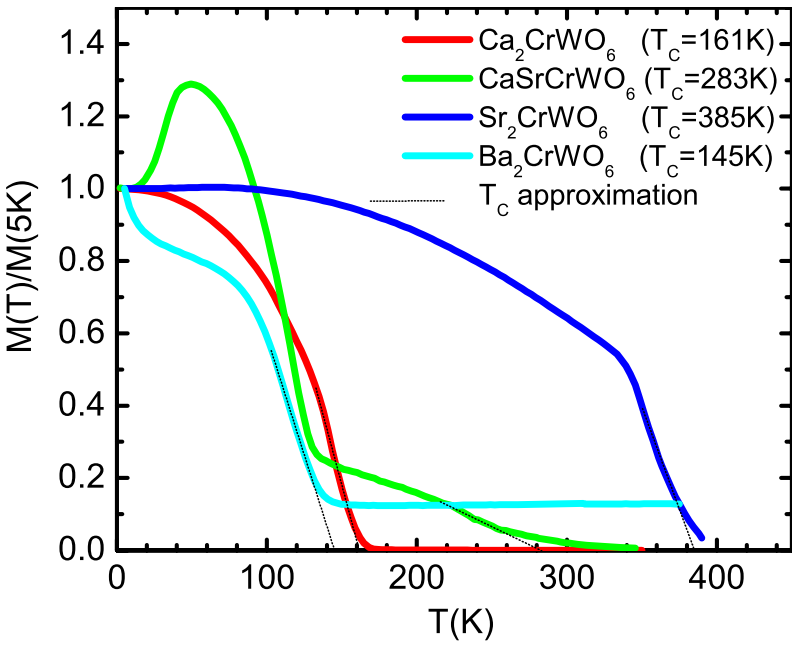

Figure 3: Normalized magnetization versus temperature for the series A_2CrWO_6 with A_2 =Ca_2, CaSr, Sr_2 and Ba_2). The applied field is $H = 100$ Oe and the samples are field cooled.

References

[1] K.-I. Kobayashi, T. Kimura, H. Sawada, K. Terakura, and Y. Tokura, Nature **395**, 677 (1998).

[2] H. Kato, T. Okuda, Y. Okimoto, Y. Tomioka, Y. Takenoya, A. Ohkubo, M. Kawasaki, and Y. Tokura, Appl. Phys. Lett. **81**, 328 (2002).

[3] C. Ritter, M. R. Ibarra, L. Morellon, J. Blasco, J. Garcia, and J. M. De Teresa, J. Phys.: Condens. Matter 12, 8295 (2000).

[4] H. Y. Hwang, S-W. Cheong, P. G. Radaelli, M. Marezio, and B. Batlogg, Phys. Rev. Lett. **75**, 914917 (1995).

[5] R. D. Shannon, Acta Crystallogr. Sec. A, 751 (1976).

[6] M. W. Lufaso and P. M. Woodward, Acta Cryst. B **57**, 725 (2001)

Epitaxial Growth of Magnetic Oxides Using Laser Molecular Beam Epitaxy [1]

D. Reisinger, P. Majewski, J. B. Philipp, M. Schonecke, B. Blass, K. Nielsen, M. Opel, A. Erb, L. Alff, R. Gross

Magnetoelectronics or spintronics is a new field of solid state physics. Whereas usual electronic devices are based on the transport and control of electronic charge, in spintronic devices both the charge and spin degrees of freedom of charge carriers are exploited to obtain new device functionality. Since most of todays electronic devices are based on semiconducting materials, there is a strong research effort to introduce the spin degree of freedom into semiconductors. At present there are two major strategies to achieve this goal. On the one hand, semiconductors can be made ferromagnetic by doping with magnetic impurities. On the other hand, spin polarized charge carriers can be injected into semiconductors. The latter strategy requires the combination magnetic materials having a high spin polarization at the Fermi level and high Curie temperature T_C with semiconductors to allow for effective spin injection into semiconductors at room temperature. Interesting materials are so-called semi-metals such as the doped manganites, the double perovskites, magnetite, CrO_2 or the Heusler compounds, which have (or are predicted to have) a full spin polarization at the Fermi level.

An important step towards a semiconductor base spin electronics is the epitaxial growth of materials with high spin polarization acting as spin injectors on semiconductors. Along this line, we are studying the growth of magnetic oxides on silicon. There are several magnetic oxides that are promising for spin injection due to their high spin polarization. First, there are the doped perovskite type manganites. For these materials a spin polarization of more the 96% has been experimentally demonstrated at 4.2 K. However, the maximum Curie temperature of this class of materials is less than 380 K (for $La_{2/3}Sr_{1/3}MnO_3$) what is not sufficient for room temperature applications. A further interesting class of materials are the double perovskites (see page 45), which have Curie temperatures up to 550 K. However, these materials have to be grown at substrate temperatures of the order of 700 K what is not compatible with standard silicon technology. Classical materials having high T_C values and high spin polarization are CrO_2 ($T_C \simeq 400$ K) and Fe_3O_4 (magnetite, $T_C \simeq 800$ K). In our work we have successfully grown magnetite on silicon. One of the major steps forward within the last year was the epitaxial growth of magnetite on silicon using a TiN/MgO bilayer buffer. In a new project, we also investigate the epitaxial growth of oxide based diluted magnetic semiconductors by doping Mn into the wide gap semiconductor ZnO. At present, there is still a considerable controversy about the question, whether or not Mn doped ZnO is a ferromagnet with high T_C and high spin polarization. We are planning clarifying experiments regarding this contrversy. We also note that oxide based semiconductors may be a good choice for the combination with magnetic oxides, since in this case complicated buffer layer systems may be not necessary.

Epitaxial growth of magnetite on Si(001)

An important step for the epitaxial thin film growth on Si is the removal of the amorphous silicon oxide layer prior to deposition. In our Laser Molecular Beam Epitaxy (L-MBE) system (see p. 57) this step can be done by a new high temperature laser heating setup [1], where the Si substrate is heated directly from the backside by an infrared laser. The substrate surface is monitored during the whole temperature variation by RHEED. The corresponding RHEED patterns are shown in Fig. . At low temperatures (Fig. a, $T_s = 600^\circ$), a large background RHEED signal is obtained due to diffusive scattering from the amorphous silicon oxide surface layer. Increasing the temperature, the signal from the (2×1) surface reconstruction becomes visible within a lightly streaky RHEED pattern at about $T_s = 900^\circ$ (Fig. b). The surface reconstruction takes place only

[1] This work is supported by the DFG and the BMBF

after oxygen and other impurities such as SiC have desorbed from the surface, i. e. if a sufficiently good vacuum is available. It is interesting to note, that at $T_s > 1100^\circ$C the (2×1) surface reconstruction disappears. A possible explanation is that the dimer bonds of the (2×1) surface displacement structure are dissolved at that temperature. Note that also the diffuse background signal has disappeared, demonstrating that the amorphous silicon oxide surface layer has completely been removed. After cooling, a stable and clean (2×1) surface is obtained with strong diffraction spots on the Laue circle of the 0^{th} order, faint streaks, and Kikuchi lines. The process described above thus yields clean Si(001) (2×1) surfaces without any chemical surface treatment.

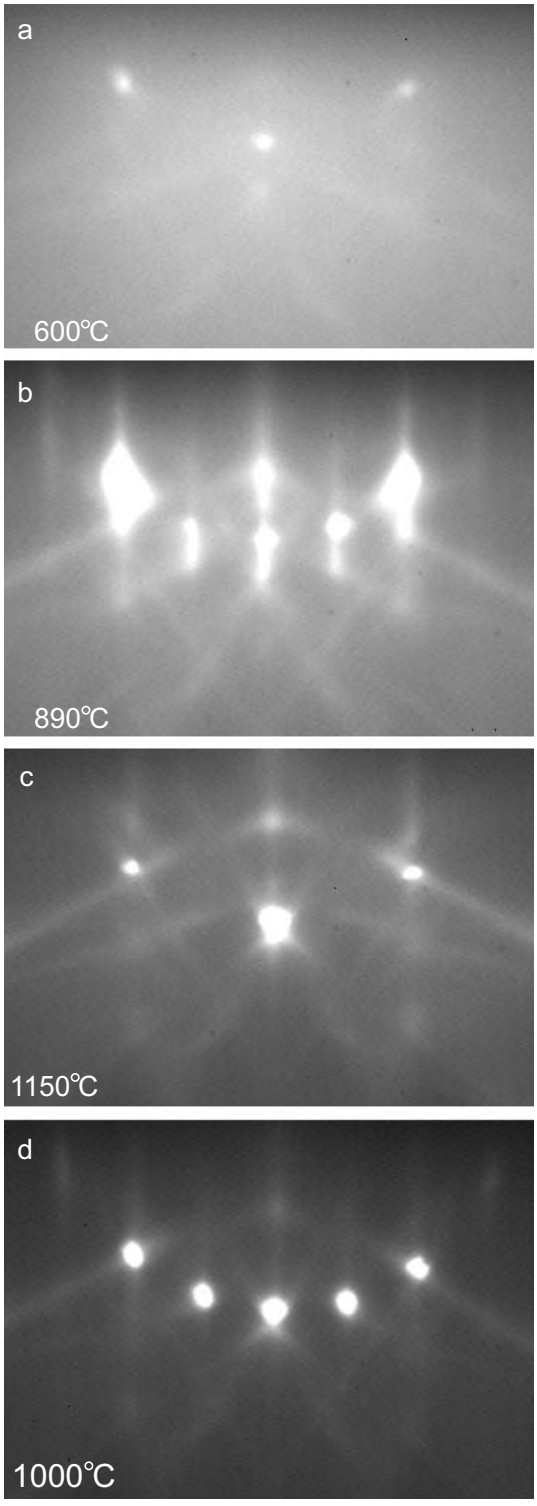

Figure 1: RHEED-pattern of the Si(001) surface at different temperatures.

After having obtained a clean Si surface we have grown TiN buffer layers by pulsed laser deposition. As a function of temperature we have found two different growth modes of TiN(001) on the clean Si(001) surface. For $T_s \geq 650^\circ$C a three-dimensional Volmer-Weber (island) growth mode is obtained. This is confirmed by optical microscopy showing islands which are oriented along the [110] direction of the Si(001) substrate. The size of the quadratic islands is about $3 \times 3\,\mu\text{m}^2$. It is not obvious why in this temperature range TiN grows with this preferential direction, since the lattice mismatch is considerable. We believe, that this is due to the 45° rotation of the dimer rows in the 2×1-reconstruction. The transition into the island growth mode itself is kinetic energy driven. For lower temperatures, a two-dimensional growth mode is obtained resulting in smooth films. It is most likely that the growth is in the so-called 5-on-4-cube-on-cube bulk superstructure with a lattice mismatch of about -2.4% [2, 3]. In this superstructure 5 TiN unit cells overlap 4 Si(100) unit cells. Subsequent to the TiN layer, a thin MgO intermediate layer ($T_s = 330^\circ$C, pure Ar atmosphere) and the magnetite layer (also $T_s = 330^\circ$C, pure Ar atmosphere) are grown by L-MBE without breaking vacuum (for details see [4, 5]).

The thickness of a completed heterostructure and the interface roughness can be determined from low angle x-ray reflectometry measurements by fitting the experimental data using a simulation software based on dynamical scattering. Fig. 2 shows a reflectometry measurement of a completed multilayer system consisting of a magnetite/MgO/TiN trilayer on Si(001). Note that the agreement between the simulation and the measurement is astonishingly good for the complicated heterostructure. From the refinement the layer thickness is obtained. In the example of Fig. 2 the values are 43 nm for magnetite, 3.9 nm for MgO, and 12 nm for TiN. The roughness of the surface

and interfaces between the different layers and the substrate, which causes a decrease of the oscillation amplitude with increasing angle, also can be estimated by fitting the experimental data. The determined roughness values are in the range between 0.3 nm and 0.7 nm. This is fully consistent with the roughness values measured by Atomic Force Microscopy (AFM).

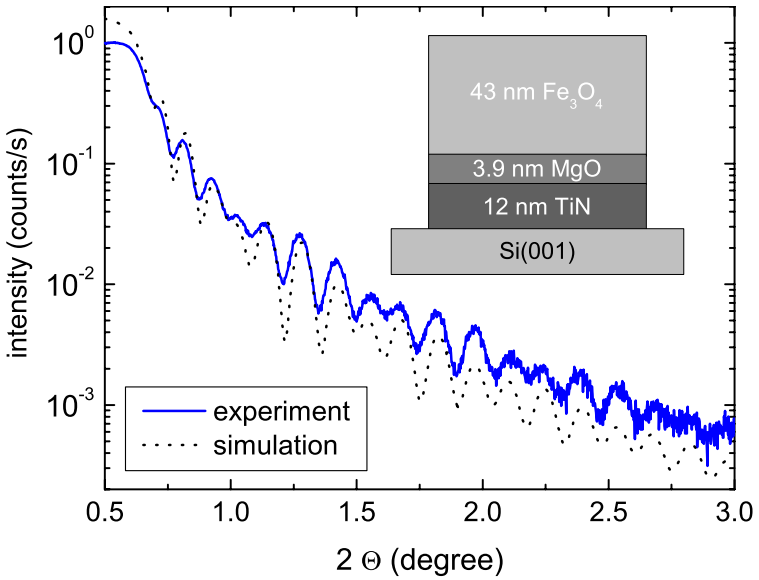

Figure 2: X-ray reflectometry measurement of a completed TiN/MgO/Fe_3O_4 heterostructure on Si(001) together with the result of the numerical simulation.

Our study shows that it is possible to grow magnetite epitaxial thin films on Si(001) substrates by L-MBE using a double buffer layer system of TiN and MgO. For the cleaning of the Si substrate we have used an *in situ* laser heating process which allows for a maximum substrate temperature of 1150°C. The substrate treatment and the whole growth process can be monitored directly be RHEED allowing the determination of the surface structure at each process step. By x-ray diffraction and AFM, the high epitaxial quality and small interface roughness of the multilayer structure has been confirmed. Magnetite thin films on Si substrates have the potential to become useful in spintronics for spin injection. The compatibility of the presented multilayer structure with the insulating material MgO may provide a way to fabricate a suitable tunneling barrier to overcome the resistivity mismatch between the ferromagnetic material (Fe_3O_4 in our case) and the semiconductor and thereby to achieve an effective spin injection. For further information see [4, 5].

Epitaxial growth of manganese doped ZnO

In a new project, we plan to grow manganese doped ZnO on ZnO substrates (homo-epitaxial growth). The key question of this study is whether or not a diluted magnetic semiconductor can be obtained by doping ZnO with magnetic impurities. A first step in our study is the measurement of the magnetic properties of the Mn doped ZnO films as a function of the Mn concentration. The key question is whether Mn favors to form clusters in ZnO or whether indeed a charge carrier mediated magnetism between Mn^{2+} ions is obtained. In order to get information on clustering of Mn, we are planning to do a detailed transmission electron microscopy analysis in cooperation with the University of Bonn (Prof. W. Mader).

References

[1] Z. Yu, J. Ramdani, J. A. Curless, C. D. Overgaard, J. M. Finder, R. Droopad, K. W. Eisenbeiser, J. A. Hallmark, W. J. Ooms, and V. S. Kaushik, J. Vac. Sci. Technol. B **18**, 2139 (2000).
[2] R. Chowdury, X. Chen, J. Narayan, Appl. Phys. Lett. **64**, 1236 (1994).
[3] P. R. Willmott, R. Timm, J. R. Huber, Appl. Surf. Sci. **127-129**, 105 (1998).
[4] D. Reisinger, B. Blass, J. Klein, J. B. Philipp, M. Schonecke, A. Erb, L. Alff, and R. Gross, Appl. Phys. A, submitted for publication (2002), cond-mat/0208495.
[5] D. Reisinger, M. Schonecke, T. Brenninger, M. Opel, A. Erb, L. Alff, and R. Gross, J. Appl. Phys., submitted for publication (2002)

A "Dry" millikelvin Cooler — Dilution Refrigerator with Pulse-Tube Precooling

K. Uhlig

Within the year 2002 the preliminary setup of our ^{3}He/^{4}He dilution refrigerator with pulse-tube precooling (PTR-DR) which we had made for testing the components of the refrigerator, was replaced by a state of the art cryostat construction which had been planned like this all along. Fig. 1 shows a schematic view of the lab with the refrigerator: The compressor, the rotary pumps and the roots pump are located in the basement just below the lab, and only the cryostat, the required electronics and the gas handling system are placed in the lab. The cryostat is suspended from a metal frame which is bolted to the ceiling of the lab. In this way the refrigerator is freely accessible from all sides when an experiment is mounted to the mixing chamber (for further information on dry mK systems, see [1, 2, 3]

The cryostat has been operated several times after these changes were made. The maximum achievable throughput of ^{3}He was 300 μmol/s (as compared to 60 μmol/s before). This upper limit is set by the pumping speed of the roots pump. The ^{3}He throughput (and in turn the cooling power of the refrigerator) could be increased by about a factor of two by either using a bigger roots pump or even better a turbo pump. There is a separate flange in the main pumping line of the fridge where a turbo pump can be installed.

In Fig. 2 we give a few technical details of the PTR-DR. The first graph (upper left) shows the temperature of the second stage of the pulse-tube refrigerator T_{pt2} as a function of the heat applied to the still, which is correlated with the ^{3}He throughput (Fig. 2, lower right). Depending on the ^{3}He throughput, T_{pt2} ranges between 3 K and 4 K. In upper right part of Fig. 2 we show the still temperature, which ranges between 600 mK and 800 mK. At these temperatures a good distillation rate of the ^{3}He can be expected. In our case it is between 90% and 94% in the temperature range indicated above. In the lower left part of Fig. 2 the inlet pressure of the ^{3}He, when it enters the cryostat, is plotted. It is of the order of 1 bar. This pressure can be maintained by the rotary pumps, a separate compressor is not required.

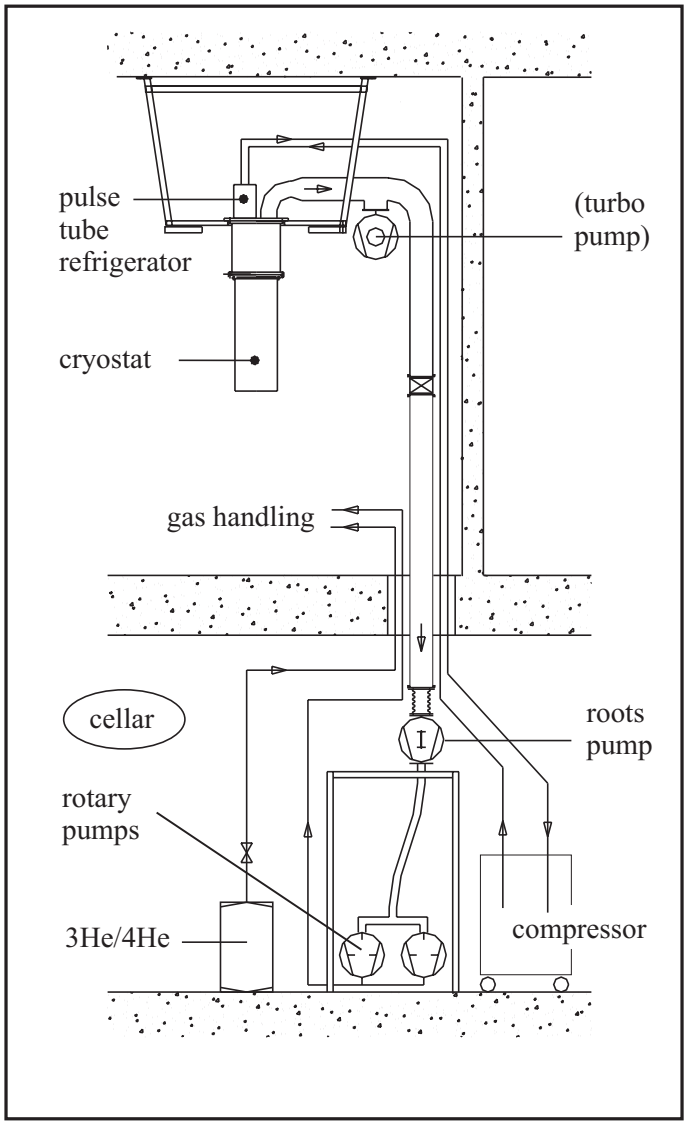

Figure 1: Schematic view of the laboratory for the dry mK cooler with the main components.

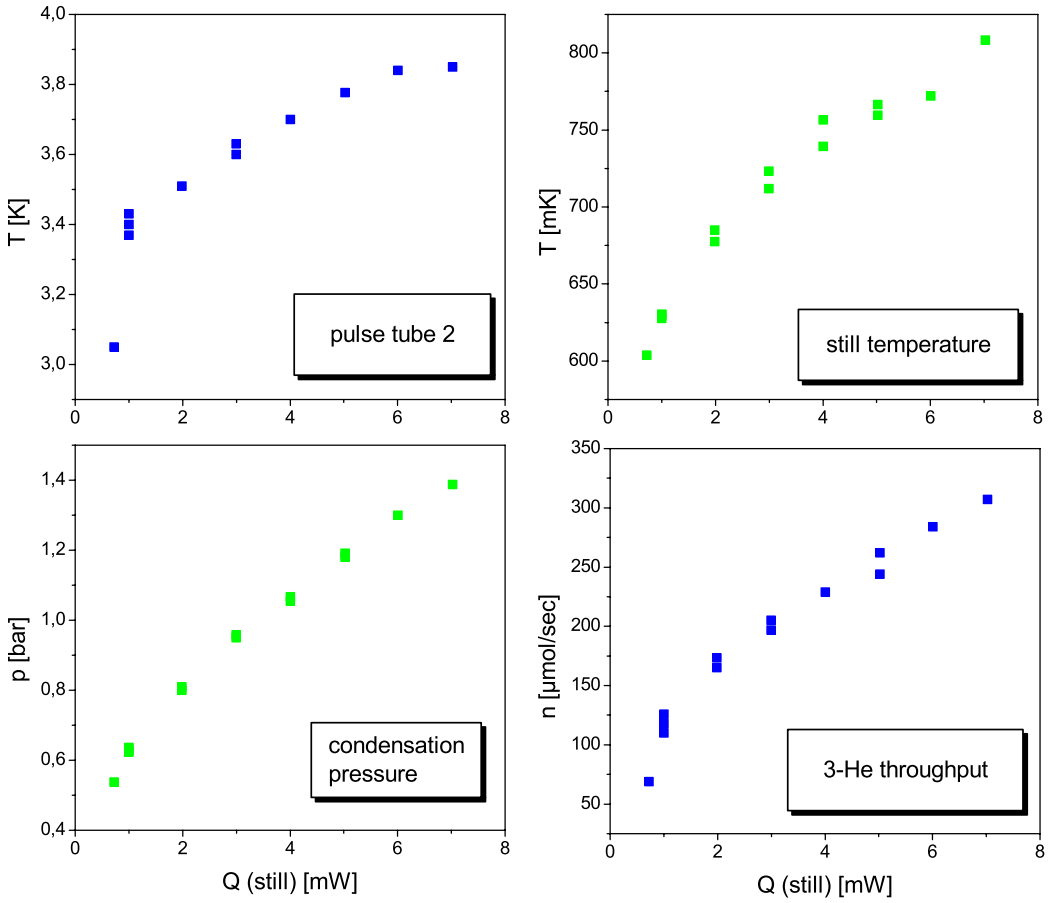

Figure 2: Temperature of the second stage of the pulse-tube refrigerator (upper left), temperature of the still (upper right), the inlet pressure of ^{3}He on entering the cryostat (lower left) and the ^{3}He throughput (lower right) plotted as a function of heat load applied to the still.

In the tests described here, the temperature of the mixing chamber varied between 9 mK and 13 mK, depending on the ^{3}He throughput. These achievable temperatures were solely determined by the performance of the heat exchangers of the dilution refrigerator and not by an external heat leak. In other words, lower temperatures are possible by inserting more heat exchangers.

Finally, we should mention that a PTR-DR similar to ours is intended for a cryostat, which is built to cool a novel superconducting bolometer at the James-Clerk-Maxwell Telescope on Hawaii. We have agreed with the coordinators of the project, the UK Astronomy Technology Centre in Edinburgh, on the support concerning the construction of the cryostat. So far, the Joule-Thomson heat exchanger and a pre-cooling circuit for the cryostat have been designed.

References

[1] *^{3}He/^{4}He dilution refrigerator with pulse-tube refrigerator precooling.*
Cryogenics **42**, 73-77 (2002).

[2] *Thermal shunt for quick cool-down of two-stage closed-cycle refrigerator.*
K. Uhlig,
Cryogenics **42**, 67-69 (2002).

[3] *^{3}He/^{4}He dilution refrigerator precooled by Gifford-McMahon cooler II. Measurements of the vibrational heat leak.*
K. Uhlig,
Cryogenics, accepted for publication (2002).

Differences in the Redox Behavior and the Metal Distribution of the Vermiculites from Santa Olalla and Ojen (Andalusia, Spain)

A. Lerf [1]

The 2-dimensionally constrained space in the interlayer galleries of the layered clay minerals forms a very peculiar reaction medium dominated by the bonding relationships between the negatively charged surfaces of the host lattice and the metal ions and the hydration water in the interlayer space. Up to now only the acid-base properties within this reaction milieu has been investigated thoroughly and used for catalysis. How the reaction conditions in the interlayer space are influenced by redox-active structural iron ions (within the octahedral sheets of the host layers) is nearly not studied. To elucidate this influence we have started a few years ago an investigation of the redox properties for some andalusian vermiculites containing a remarkable amount of structural iron. The success of oxidation and reduction reactions is proved via the determination of the Fe^{2+}/Fe^{3+}-ratios by means of Mössbauer spectroscopy.

The most recent results show a significant difference of the Fe^{2+}/Fe^{3+}-ratio for the vermiculites from Santa Olalla and Ojen. The highest ratio has been observed for samples intercalated with hydrazine: the highest value of the Fe^{2+}/Fe^{3+}-ratio for Santa Olalla amounts to 0.25, whereas it is 0.4 for the Ojen vermiculite. Even in these samples the extent of reduction can be increased considerably by thermal treatment. However, the highest degree of reduction has been achieved with the decomposition of the NH_4-vermiculite at 700 ^{o}C. The quadrupole splitting of part of the Fe^{2+} ions is unusually low for clay minerals. A possible explanation could be the creation of oxygen vacancies in the first coordination sphere of the iron ions due to water loss during heating. This result is quite exciting because the clay must act as catalyst for ammonia decomposition.

Apart from the differences in the redox behaviour both vermiculites show remarkable variations of the IR spectra in the range 3700 - 3650 cm^{-1} (stretching-vibrations of the structural OH-groups). These differences in the IR-spectra can be interpreted with differences in the metal ion distribution in the octahedral layer of the clay minerals, which is closely related with the chemical composition [1, 2, 3]. Under the assumption of a statistical distribution of the metal ions on the available octahedral sites it is possible to calculate the frequency of definite metal combination on three neighbouring sites forming the immediate surrounding of the structural OH-groups. Three different species are taken into consideration: Mg^{2+}, Fe^{2+} and R^{3+}, which stays for Fe^{3+} and Al^{3+}. With a contribution of more than 1 % the following combinations occur: in case of the Santa Olalla vermiculite $3Mg^{2+}$, $2MgFe^{2+}$, $2MgR^{3+}$, $Mg^{2+}2R^{3+}$ and $Mg^{2+}Fe^{2+}R^{3+}$; in case of Ojen there are the additional combinations $Mg^{2+}2Fe^{2+}$ and $Fe^{2+}2R^{3+}$ beside those observed for the Santa Olalla mineral. However, the amounts of these configurations in both minerals are significantly different. Each of the metal combinations is characterised by a definite vibration frequency, which seem to be nearly identical for the different 2:1 clay minerals. Though we can apply the assignment of Wilkins and Vedder [1, 2, 3] and compare the calculated distributions of the various combinations with the intensities of the IR absorption bands, which are in excellent agreement. Thus we can conclude that the distribution of the metal atoms in the vermiculites under study is nearly random and we have a homogeneous charge distribution on the clay layers, which is important for the intercalation chemistry.

The question arises how this result fits with our Mössbauer data, which show only minor differences in isomer shift and quadrupole splitting, the parameters sensitive on the metal ion distribution. However, the comparison of both sets of data is not straightforward. First, one has to be aware that those metal combinations without iron do not contribute to the Mössbauer spectra. Thus the contribution of the

[1] In collaboration with F.E. Wagner, Physics-Department of the TUM, J. Poyato, L. Perez-Maqueda and J.L. Perez-Rodriguez, Instituto de Ciencia de Materiales de Sevilla, Consejo Superior de Investigaciones Cientificas y Universidad de Sevilla; the project is supported by DAAD/Aciones Integradas

remaining combinations has to be readjusted to 100 %. Second, the extent to which the metal distribution will influence the quadrupole splitting is not really known. We consider this influence as small because the metals are next nearest neighbours and not located in the immediate coordination sphere, which is occupied by oxygen atoms only. Since the quadrupole splitting of the Fe^{2+} sites is twice as high as that of the Fe^{3+} we should have a higher chance to resolve different Fe sites in case of the Fe^{2+} ions. This is really the situation observed: whereas there is always one rather broad Fe^{3+} signal we observe two different Fe^{2+} sites. We assign the observed Fe^{3+} site to $2MgFe^{3+}$ and the Fe^{2+} site with the higher quadrupole splitting (which is the higher symmetric site) with $2MgFe^{2+}$ according to the most prominent metal atom combinations obtained from the above-mentioned calculation and the IR-spectra. The second Fe^{2+} signal is ascribed to other less symmetric combinations like $Fe^{2+}MgR^{3+}$. The ratio of both Fe^{2+} sites is in fair agreement with that calculated. The admixture of less prominent sites may lead only to a more or less continuous shift in the size of the quadrupole splitting depending on the differences in quadrupole splitting and their weight of contribution with respect to the prominent site.

Further work will stress the following points:

1. the application of these ideas to the explanation of the observed shifts in quadrupole splitting due to redox reactions,
2. the development of a thorough understanding of the mechanism of redox reactions in these trioctahedral clay minerals,
3. the use of intercalated species with reversible electron transfer (mainly dye molecule cations) as electron shuttles from external current sources to the structural Fe ions, that is, we would like to get information about the redox potentials of our clays,
4. the preparation of electron transfer chains for photocatalytic reactions via the cointercalation of various electron transfer mediators.

References

[1] W. Vedder, *Amer. Miner.* 49, 736 (1964).
[2] R.W.T. Wilkins, *Miner. Mag.* 36, 325 (1967).
[3] W. Vedder and R.W.T. Wilkins, *Amer. Miner.* 54, 482 (1969).

Quasielastic Neutron Scattering on Different Hydration States of Graphite Oxide

A. Lerf [1]

We have investigated graphite oxide (GO) at the neutron time-of-flight spectrometer V3/NEAT of Hahn-Meitner-Institut Berlin (HMI). The powder samples were prepared with three different degrees of hydration. In terms of mass of water added to mass of GO (2 g, 1 g and 0.25 g, respectively) these were 10%, 50% and 80%. Each degree of hydration was prepared once with ordinary water and once with deuterated water in order to separate the contribution of the GO from that of the hydration water. Spectra of the six samples were recorded at room temperature with two different energy resolutions of 66 μeV and 100 μeV, and measurement times of 8 to 15 hours, taking advantage of the full available beam time. A preliminary data correction for detector efficiency and sample geometry as well as conversion to S(q,w) could be done on site. The position of the structural Bragg peak depends on hydration and is consistent with x-ray Debye-Scherrer patterns, also taken at HMI. The latter finding proves that the samples can be related to the above-mentioned well-defined hydration degerees and that the hydration level of the corresponding H_2O and D_2O samples was comparable. Quasielastic scattering was found over the whole angle range with clear peaks centered around zero energy transfer. The quasielastic contribution to the spectra clearly increases with hydration degree. Therefore, the spectra promise to be an excellent base for developing models of the water motion. The available time was reduced by 12 hours due to reactor shutdown. We used this time for the preparation of samples of an extra hydration level. Having measured these, there was no more time for measurements at different temperatures.

[1] In collaboration with S. Schöttl, National Physical Laboratory, Teddington TW11 0LW UK; J. Pieper, Hahn-Meitner-Institut, Berlin. This work is supported by BENSC

Experimental Facilities and Infrastructure

Within the last two years, several new experimental facilities and various components of the technical infrastructure have been installed at the Walther-Meissner-Institute. On the following pages a brief overview is given on the main equipment and techniques that are available at the Walther-Meissner-Institute at present.

UHV-Laser-MBE

The Walther-Meissner-Institute operates a UHV-Laser-Molecular Beam Epitaxy (L-MBE) system for the growth of complex oxide heterostructures. The system has been designed to meet the special requirements of oxide epitaxy. The UHV cluster tool consists of the following main components:

- central transfer chamber.
- load-lock chamber with heater system for substrate annealing.
- laser deposition chamber with in-situ reflection high energy electron diffraction (RHEED) system and atomic oxygen source. The RHEED system has been modified to allow for the operation at high oxygen partial pressure up to 0.5 mbar.
- surface characterization chamber with UHV scanning force microscope (Omicron).
- metallization chamber with a four heart electron gun system and a liquid nitrogen cooled sample stage. The sample holder can be tilt for shadow evaporation.
- KrF excimer laser.

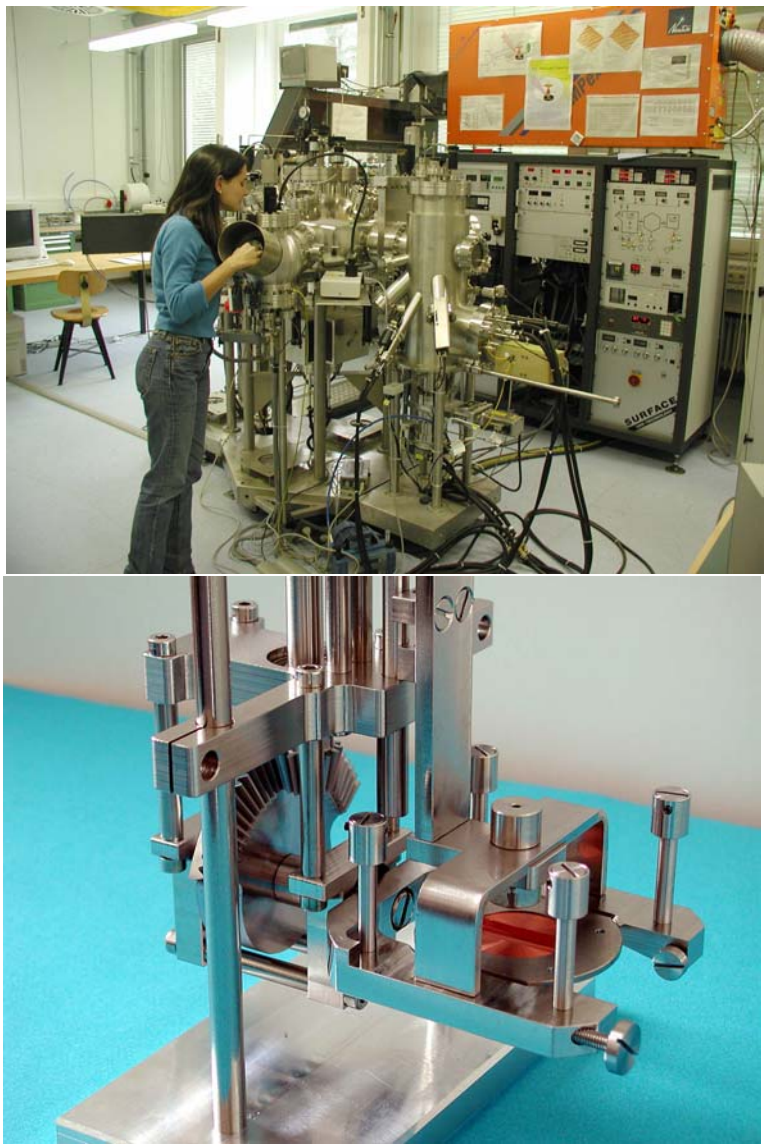

Figure 1: Top: UHV-Laser-Molecular Beam Epitaxy System. Bottom: Sample holder for metallization chamber allowing for evaporation under different angles.

The system is used for the growth of complex oxide heterostructures consisting of superconducting, magnetic and dielectric materials such as the high-temperature superconductors, the doped manganites, the double perovskites, magnetite etc..

During 2002, the laser molecular beam epitaxy system (laser-MBE) which was installed at the Walther-Meissner-Institut during 2001 has been extended and modified. In particular, the substrate heating system and the temperature control unit was changed from a resistive radiation heater to a new infrared laser heating system (see Fig. 3, left) including a pyrometer for determining the sample temperature. In addition, a source for atomic oxygen has been added. The main advantage of the new heating system is that only the substrate is heated while the surrounding parts are hardly affected (fig. 3, right). In this way one can achieve an essentially better vacuum at temperatures well above 1000°C. The achievable substrate temperature is limited by the melting point and the size of the substrate material (approx. 1410°C for a 5×5 mm^2 silicon substrate). The laser heating system has already been successfully used for removing the amorphous silicon oxide layer form the surface of silicon substrates at 1150°C. This is required for the epitaxial growth of oxide thin films on this substrate.

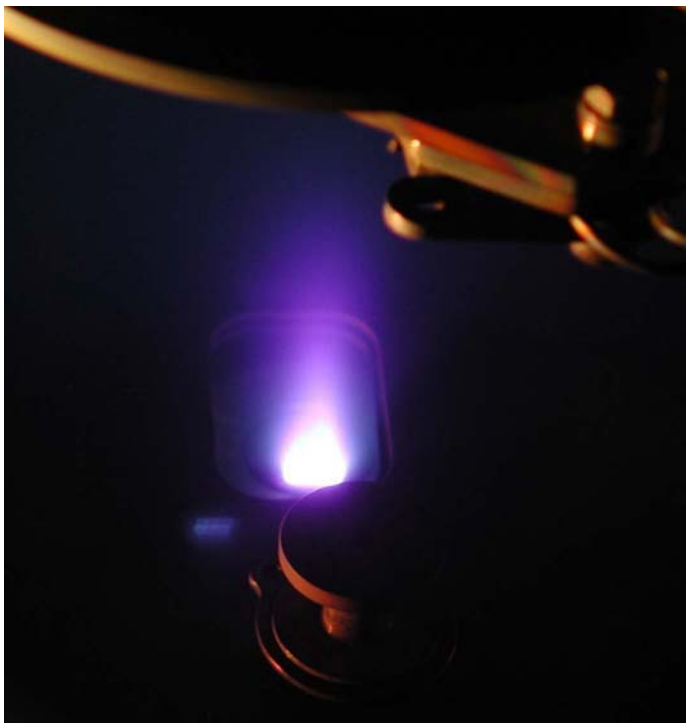

Figure 2: Pulsed Laser Deposition (PLD): When the pulse of the UV laser (KrF excimer laser, 248 nm) hits the target, the target material is ablated and the so-called laser "plume" containing highly excited atoms and molecules is formed.

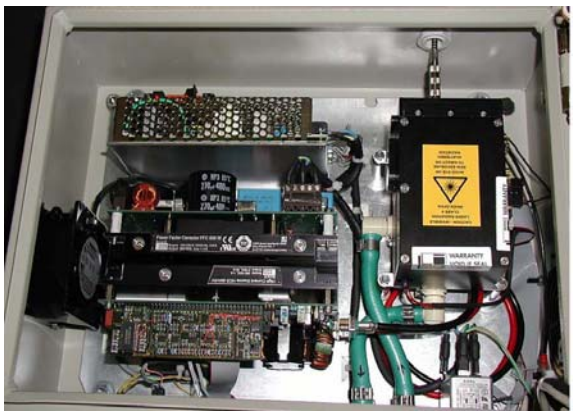

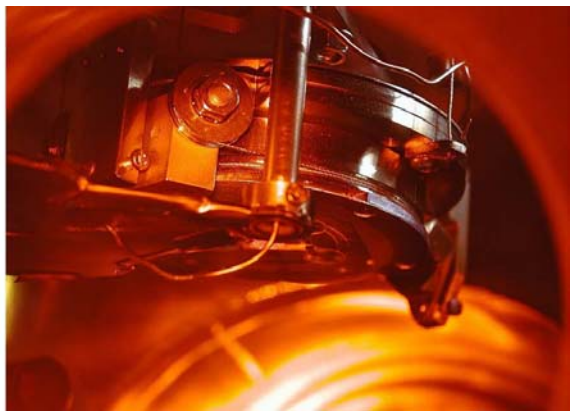

Figure 3: Components of the laser heating system: The substrate is heated using an IR diode laser head that is located in a separate box far away from the deposition chamber (left). The laser light is brought to the substrate (right) via an optical fiber.

Single Crystal Growth and Synthesis of Bulk Materials

Transition metal oxides are of great interest due to their various interesting physical properties (e.g. high temperature superconductivity, colossal magnetoresistance, ferroelectricity, nonlinear optical properties etc.) and their high potential for applications. In the last 2 years a new laboratory for the synthesis of bulk materials and single crystals has been built up at the WMI. With the installation of a four-mirror image furnace in the year 2002 the laboratory is now fully operational. With this furnace crystals of various high temperature superconducting materials or other transition metal oxides can be grown as single crystals using the traveling solvent floating zone technique. The furnace consists basically of 4 elliptical mirrors with a common focus on the sample rod and with halogen lamps in their other focus. By irradiation of the focused light the sample rod is locally heated and eventually molten. The molten zone can be moved up and down along the entire sample rod under simultaneous rotation. By repeated melting and crystallization of the sample seed selection takes place and the formerly polycrystalline rod is transformed into a single crystal. Single crystal growth can be performed with this furnace at maximum temperatures up to 2200°C in the pressure range from 10^{-5}mbar up to 10 bar and in oxydizing, reducing as well as inert atmosphere.

Figure 4: The four-mirror image furnace installed at the crystal laboratory of the WMI. Crystals can be grown by the floating zone and traveling solvent floating zone technique at temperatures up to 2200°C and pressures up to 10 bar.

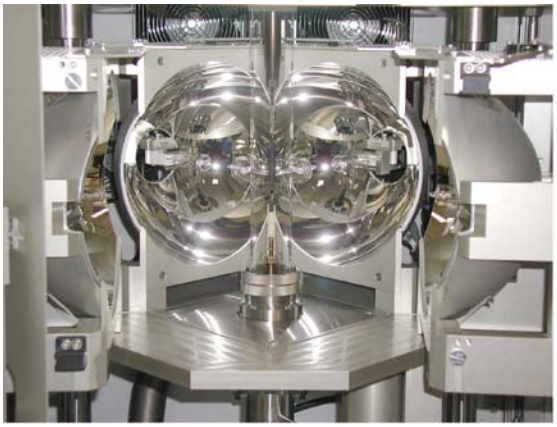

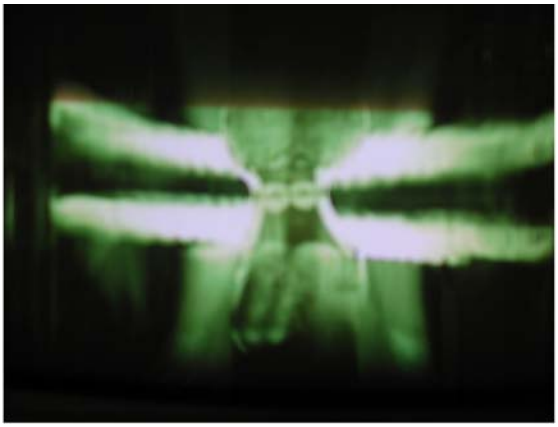

Figure 5: Left: Central part of the image furnace with the four elliptical mirrors. In the center one can see the quartz tube with the poly-crystalline rod. Right: View on the molten zone of TiO_2 (melting point: 1800°C) obtained by a CCD camera.

The X-ray diffraction systems

For x-ray analysis the Walther-Meissner-Institute operates two X-ray diffractometers (Bruker D8 Advance and D8 Discover). The two-circle system is used for powder diffraction. In this system the samples can be heated in oxygen atmosphere up to 1600°C. It is equipped with a Göbel mirror and an area detector to save measuring time. The second system is a high resolution four-circle diffractometer that can be used for reciprocal space mappings. It is equipped with a Göbel mirror and an asymmetric two-fold monochromator and allows for the texture analysis of thin film superlattices and single crystalline materials. In both systems measurements can be carried out fully computer controlled.

Figure 6: The two-circle X-ray diffractometer Bruker D8 Advance.

Beyond these two Bruker x-ray systems a Laue camera for single crystal analysis and a Debye-Scherrer camera are available.

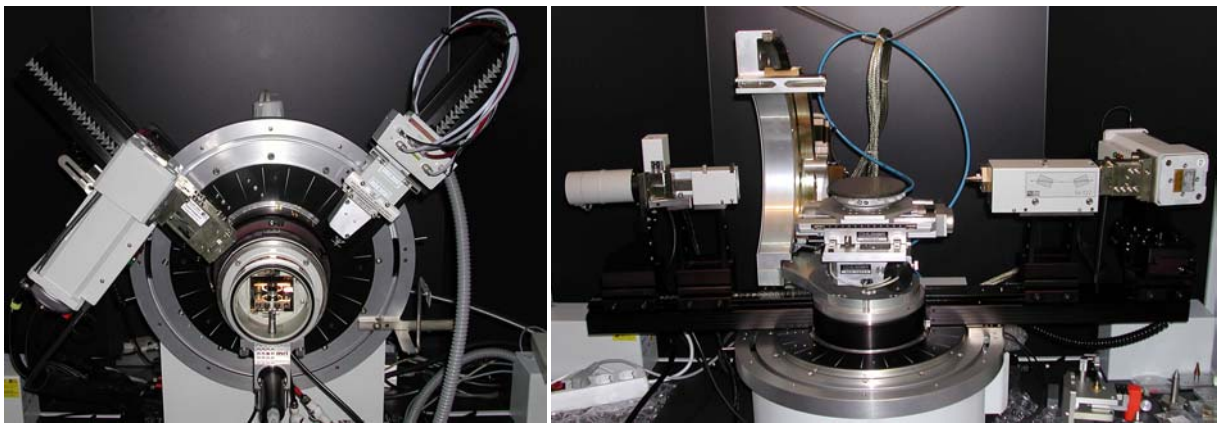

Figure 7: Left: High temperature sample holder of the D8 Advance system. Right: Four-circle high resolution X-ray diffractometer Bruker D8 Discover.

Figure 8: Quantum Design SQUID magnetometer.

The SQUID-magnetometer

For the analysis of the magnetic properties of materials, a Quantum Design SQUID magnetometer system as shown in Fig. 8 is used at the WMI. The SQUID magnetometer allows for measurements in the temperature regime from 1.5 to 400 K and provides excellent sensitivity particularly in the low field regime. Due to the excellent sensitivity of the system, thin film samples with a very small sample volume can be analyzed. In a special inset, samples can be measured up to temperatures well above room temperature (up to 700°C). For this option the sample volume has to be reduced. The SQUID magnetometer is equipped with a superconducting solenoid allowing for a maximum field of 7 T. At present, the magnetometer is used for the characterization of magnetic materials (both in bulk and thin film form). Examples are the doped manganites, magnetite, the double perovskites or magnetic semiconductors.

The High Field Laboratory

Transport and thermodynamic properties of samples are often studied as a function of applied magnetic field. For such measurements several superconducting magnets are available at the WMI. Two of them (8/10 and 15/17 Tesla magnet system) are located in the high magnetic field laboratory in the basement of the WMI. The magnet systems are lowered below the ground level to facilitate the access to the top flange and the change of the sample sticks. The magnet systems are decoupled from the building to avoid noise due to mechanical vibrations. A variety of sample holders can be mounted allowing for e.g. sample rotation during the measurement. For standard sample holders the accessible temperature regime is $1.5\,\mathrm{K} < T < 300\,\mathrm{K}$. However, also ^{3}He/^{4}He dilution refrigerator inserts ($T > 20\,\mathrm{mK}$) or high temperature units ($T < 700\,\mathrm{K}$) can be mounted. All measurements are fully computer controlled (by the use of the LabView software tool) allowing for remote control and almost continuous measurements.

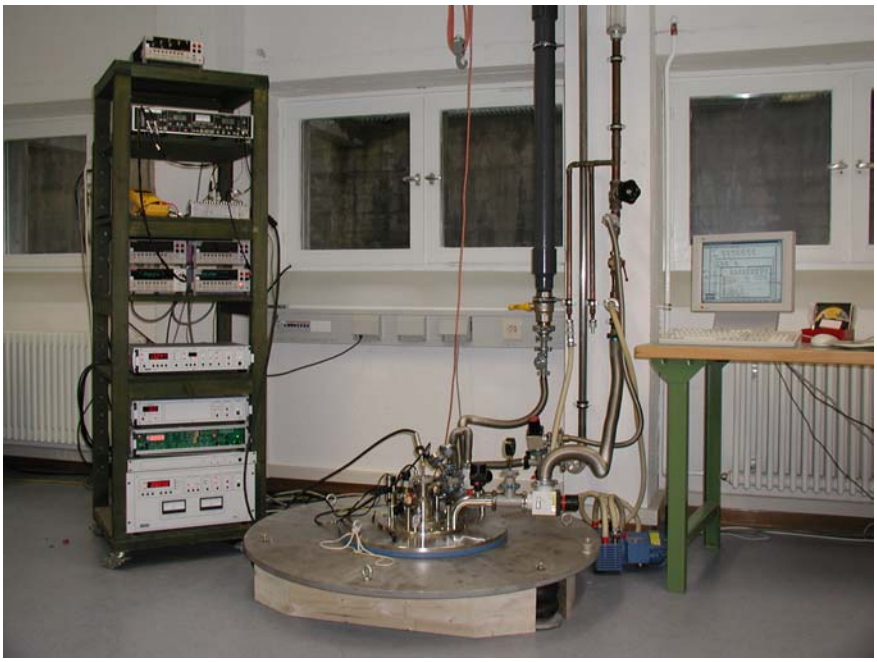

Figure 9: High field laboratory with Oxford 17 T magnet system.

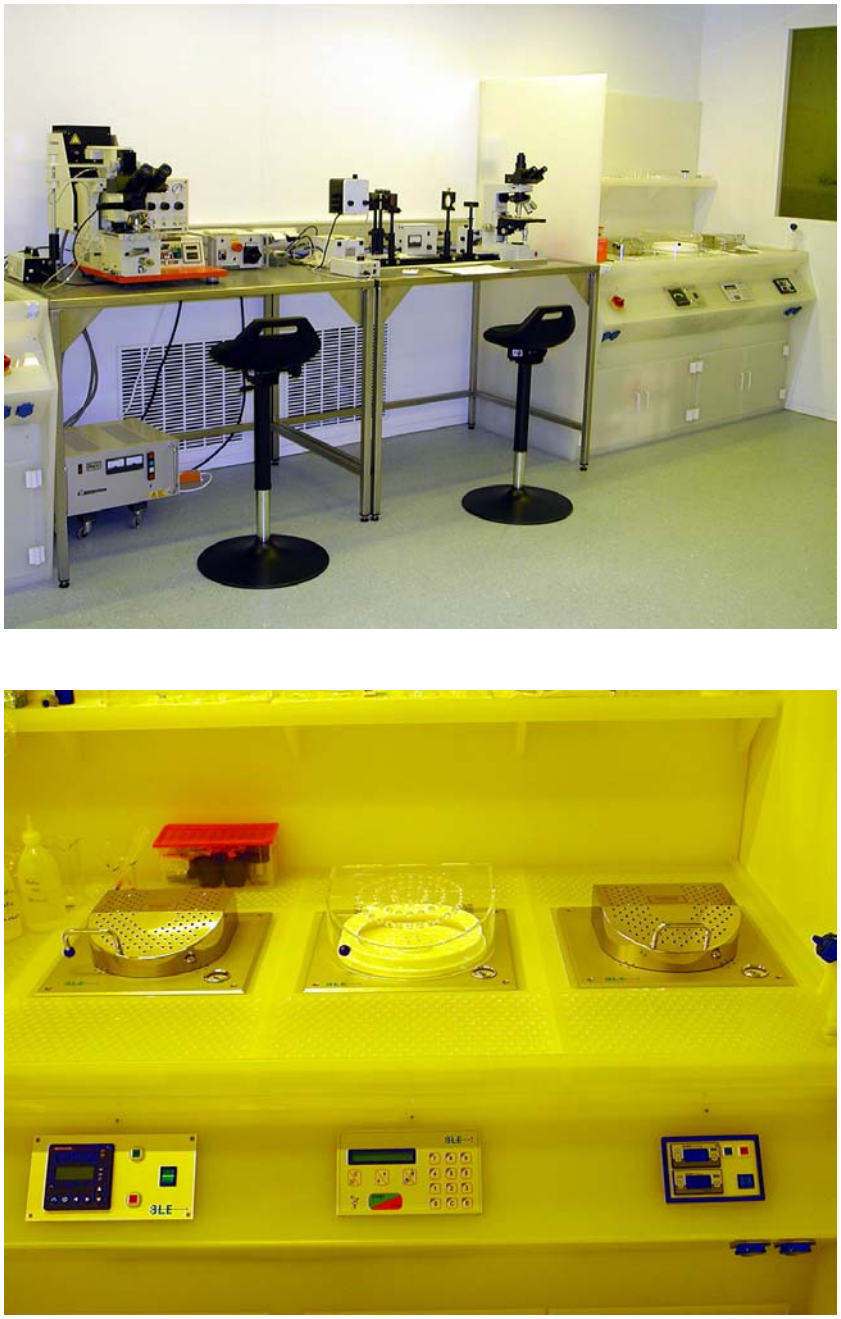

Figure 10: Top: Part of the clean room facility with optical lithography equipment and clean room benches. Bottom: Resist coater and hot plates.

The Clean Room Facility

For the fabrication of nanostructures and superconducting as well as spintronic devices the WMI operates a class 1000 clean room facility with an area of about $50\,m^2$. This clean room facility has been put into operation at the WMI within the year 2001. The clean room is subdivided into two parts for optical lithography and electron beam lithography, respectively. The clean room facility is equipped with the standard tools for optical lithography such as resist coaters, hot plates, wet benches, a Karl Süss MJB3 mask aligner and an optical projection lithography system. The technical infrastructure for the clean room is located in the basement of the WMI directly below the clean room area.

Electron Beam Lithography

The Electron Beam Lithography System is installed in one part of the clean room facility. It consists of a Philips XL 30 SFEG scanning electron microscope (SEM) with a Raith Elphy Plus electron beam lithography system and a laser stage. The SEM is equipped with a hot field emitter and typically provides a beam diameter of less than 1.5 nm at $\geq$ 10 keV or about 2.5 nm at 1 keV. The lithography unit allows the fabrication of nanostructures down to about 10 nm. We have realized the controlled fabrication of metallic strip patterns with a strip width of about 20 nm. The electron beam lithography is used for the fabrication of nanostructures in metallic and oxide systems required for the study of quantum effects in mesoscopic samples.

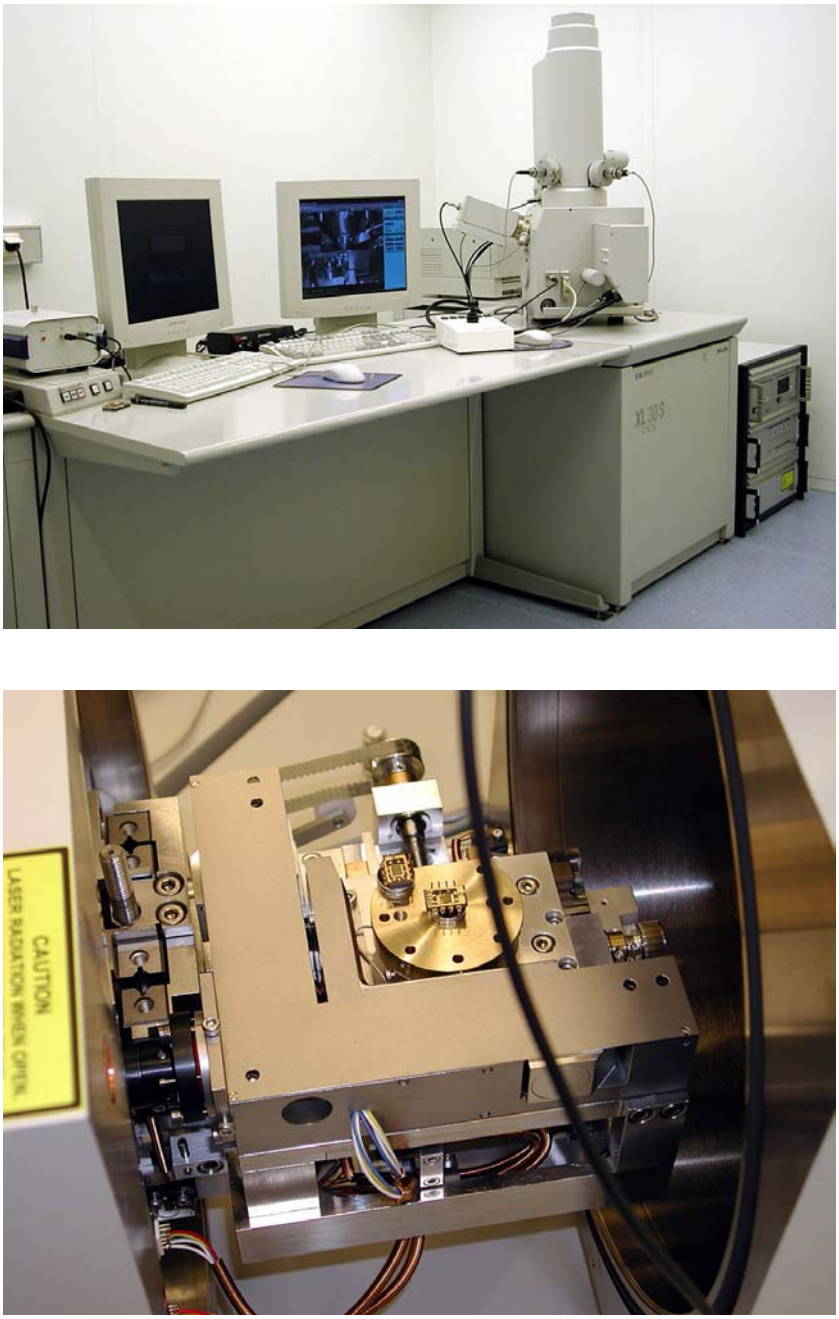

Figure 11: Top: Philips XL 30 SFEG Scanning Electron Microscope with Raith Elphy Plus Lithography System. Bottom: Raith Laser Stage.

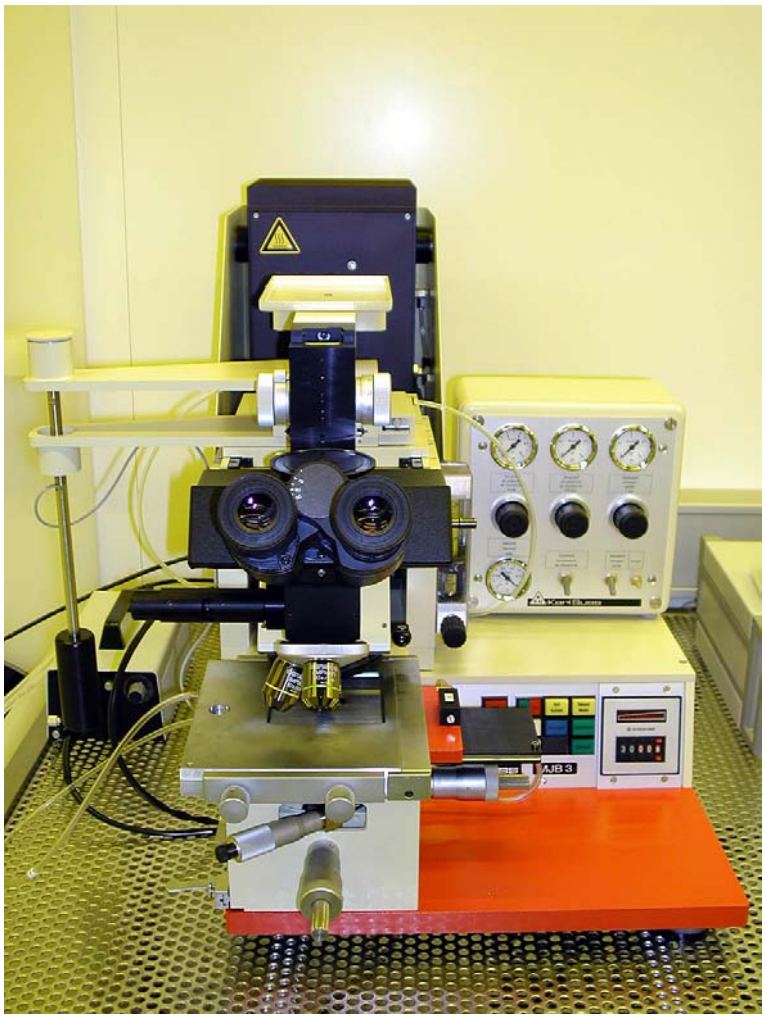

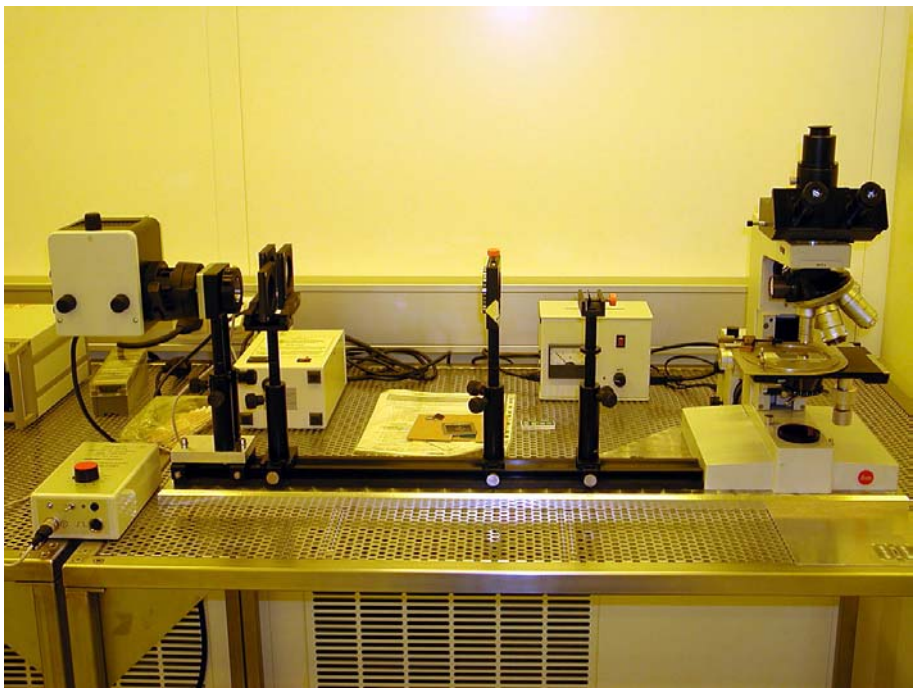

Figure 12: Top: Süss MJB 3 maskaligner for optical lithography. Bottom: Optical projection lithography based on an optical microscope.

Optical Lithography

For optical lithography a Karl Süss MJB 3 maskaligner or an optical microscope based projection system are used. The maskaligner is operating in the 1 : 1 soft or hard contact mode and is using chromium metal masks. In the projection system the mask pattern is demagnified by a factor of 5 to 100. Therefore, cheap foil masks can be used. With both systems microstructures with a lateral dimension down to $1\,\mu$m can be fabricated.

Low and Ultra-low Temperature Facilities

The Walther-Meissner-Institute operates several low and ultra-low temperature facilities that have been developed and fabricated in-house.

The lowest temperature is achieved by the nuclear demagnetization cryostat "Bayerische Millimühle 2". This ultra-low temperature facility consists of an in-house built dilution refrigerator and originally of two nuclear demagnetization stages. The first of those is based on a hyperfine enhanced van Vleck paramagnet $PrNi_5$ (0.9 mole), the second, which has been removed a few years ago, was based on purified copper (0.2 mole). The lowest temperature reached with this system was slightly below 30 μK in the copper nuclear spin system. At the moment, the first stage can be cooled to below 400 μK and, due to the large heat capacity of $PrNi_5$, it stays below the mixing chamber temperature (5 mK) for nearly 3 weeks. In this cryostat three measuring sites are provided, two in a magnetic field compensated region and one in the center of an 8 T magnet. They are suitable for specific heat measurements, for capacitive torque- and SQUID magnetometry, as well as for transport measurements (electrical und thermal conductivity). The cryostat is also equipped with a pressure cell for liquid and solid ^{3}He, which at the moment is used for nuclear spin resonance measurements below 1 mK.

Figure 13: The dilution refrigerator and the nuclear demagnetization stage of the nuclear demagnetization cryostat "Bayerische Millimühle 2".

Figure 14: A “dry” millikelvin cooler: dilution refrigerator with pulse-tube pre-cooling.

Within the last years, the Walther-Meissner-Institute has developed a dilution refrigerator with pulse-tube pre-cooling. We denote such system as a “dry millikelvin cooler”, since it does no longer require liquid helium for precooling. In contrast, this ultra-low temperature system is pre-cooled using a pulse tube refrigerator. The system is under test at the moment and temperature below 10 mK have already been achieved at the mixing chamber.

We note that the pulse-tube refrigerator based precooling system also cannot only be used for providing the base temperature of a dilution refrigerator but also for various other cryogenic systems. The dry systems are highly attractive for locations where the supply with liquid helium is complicated and/or expensive. In future they even may displace standard liquid helium systems in low temperature laboratories.

Figure 15: Dilution refrigerator insert with the Joule-Thompson stage, the heat exchanger and the mixing chamber.

The Walther-Meissner-Institute also develops and fabricates dilution refrigerator inserts for temperatures down to about 20 mK. The inserts fit into all cryogenic systems (e.g. superconducting magnets) having a two inch bore. They allow fast sample change and rapid cool down cycles of less than five hours.

The dilution refrigerator inserts are engineered and fabricated in-house and are also provided to other low temperature laboratories for ultra low temperature experiments.

New Network Infrastructure

In 2002 a new era for electronic data transfer began at the Walther-Meissner-Institute. A new data network infrastructure started operation. It was planned and installed in close cooperation with the Leibniz-Rechenzentrum and is based on fiber optic cables. It replaces the old coaxial ring line (”yellow cable”) which was installed in the early days of computer network technology. From February 25th to April 26th, 270 double fiber optic lines with an average length of 50 m were installed in the WMI together with the corresponding number of data link sockets in all the labs and offices. In the basement of the institute, one room has been renovated, which is now hosting a new central fiber optic network switch (see Fig. 16). There, the fibers coming from all rooms in the WMI meet together (Fig. 17, left). The switch provides the data link between the nodes within the WMI as well as from the WMI to the internet. The structured concept of the new network consisting of single node-to-node connections leads to higher reliability and efficiency for the data transfer as compared to the old coaxial ring lines (Fig. 17, right). With possible transfer rates up to 10 GBit/s per node the new WMI fiber optic network is prepared for the coming generations of hardware and software.

Figure 16: In the basement of the WMI a new stacked switch providing 68 fiber optic connectors was installed to switch data packets within the WMI as well as from the WMI to the internet and vice versa.

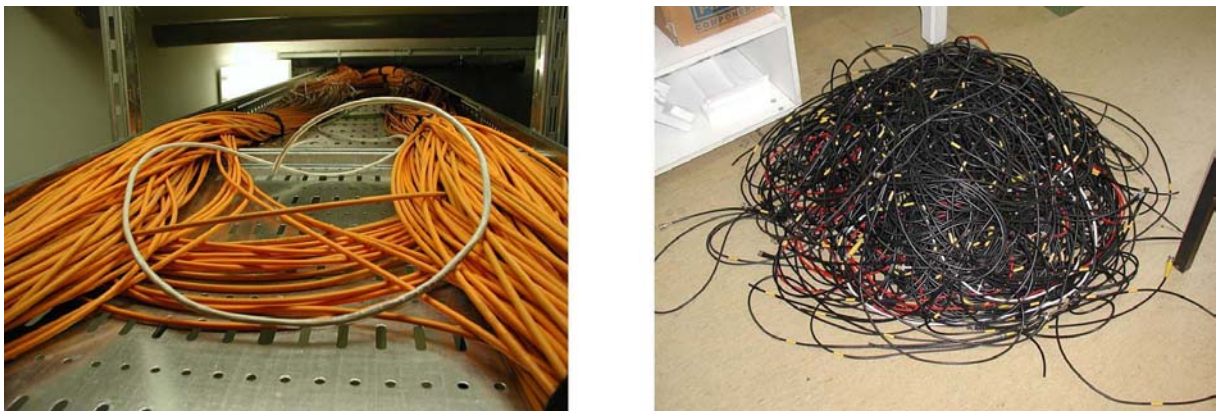

Figure 17: Left: 270 double optical fibers from all rooms of the WMI joining at the central switch. Right: The old coaxial cables after removal.

Publications

1. GRIGORIEV P.D., KARTSOVNIK M.V., BIBERACHER W., KUSHCH N.D., WYDER P.,
   Anomalous beating phase of the oscillating interlayer magnetoresistance in layered metals
   Phys. Rev. B **65**, 060403 (2002).
2. EINZEL D.,
   Universal Parameters in the Response of Unconventional Superconductors.
   J. of Low Temp. Phys. **126**, 867-879 (2002).
3. PHILIPP J.B., KLEIN J., RECHER C., ALFF L., GROSS R.,
   Growth and Magnetotransport Properties of Epitaxial Films of the Layered Perovskite $La_{2-2x}Sr_{1+2x}Mn_2O_7$.
   Phys. Stat. Sol. (a) **189**, 367-371 (2002).
4. KLEIN J., PHILIPP J.B., REISINGER D., ALFF L., GROSS R.,
   Structure of Coherently Strained Films of Doped Manganites.
   Phys. Stat. Sol. (a) **189**, 617-620 (2002).
5. UHLIG K.,
   Thermal shunt for quick cool-down of two-stage closed-cycle refrigerator.
   Cryogenics **42**, 67-69 (2002).
6. KARTSOVNIK M.V.,
   Interlayer magnetoresistance in layered organic conductors.
   in *Molecular Low Dimensional and Nanostructured Materials for Advanced Applications*, A. Graja et al. (eds.) pp. 159-168 (2002).
7. CAPKOVA P., POSPISIL M., LERF A.,
   Molecular simulations in structure analysis of tantalum sulfide intercalated with methylene blue.
   Solid State Sciences **4**, 671-676 (2002).
8. VENTURINI F., OPEL M., DEVEREAUX T.P., FREERICKS J.K., TÜTTÖ I., REVAZ B., WALKER E., BERGER H., FORRO L., HACKL R.,
   Observation of an Unconventional Metal-Insulator Transition in Overdoped CuO_2 Compounds.
   Phys. Rev. Lett. **89**, 107003 (2002).
9. VENTURINI F., ZHANG Q.-M., HACKL R., LUCARELLI A., LUPI S., ORTOLANI M., CALVANI P., KIKUGAWA N., FUJITA T.,
   Raman scattering versus infrared conductivity: Evidence for one-dimensional conduction in $La_{2-x}Sr_xCuO_4$.
   Phys. Rev. B **66**, 060502 (2002).
10. OPEL M., VENTURINI F.,
    Raman Scattering in Solids.
    European Pharmaceutical Rev. **3**, 76-82 (2002).
11. PESOTSKII S.I., LYUBOVSKII R.B., BIBERACHER W., KARTSOVNIK M.V., NIZHANKOVSKII V.I., KUSHCH N.D., KOBAYASHI H., KOBAYASHI A.,
    On the Possibility of a Radical Decrease in the Strength of Many-Body Interactions in the Organic Metal α-$(BETS)_2KHg(SCN)_4$.
    J. of Experimental and Theoretical Physics **94**, 431-433 (2002).
12. KARTSOVNIK M.V., GRIGORIEV P.D., BIBERACHER W., KUSHCH N.D., WYDER P.,
    Slow Oscillations of Magnetoresistance in Quasi-Two-Dimensional Metals.
    Phys. Rev. Lett. **89**, 126802 (2002).
13. DÓRA B., MAKI K., KORIN-HAMZIC B., BASLETIC M., VIROSZTEK A., KARTSOVNIK M.V., MÜLLER H.,
    The angular-dependent magnetoresistance in α-$(BEDT\text{-}TTF)_2KHg(SCN)_4$.
    Europhys. Lett. **60**, 737-742 (2002).
14. PESOTSKII S.I., LYUBOVSKII R.B., BIBERACHER W., KARTSOVNIK M.V., NIZHANKOVSKII V.I., KUSHCH N.D., KOBAYASHI H., KOBAYASHI A.,
    Quantum interference in quasi-two-dimensional organic metals κ-$(BETS)_2FeCl_4$ and κ-$(BETS)_2GaCl_4$.
    in *Molecular Low Dimensional and Nanostructured Materials for Advanced Applications*, A. Graja et al. (eds.), pp. 285-288 (2002).
15. KHASANOV S.S., ZORINA L.V., SHIBAEVA R.P., PESOTSKII S.I., KARTSOVNIK M.V., VEIROS L.F., CANADELL E.,

Molecular conductors based on radical cation hydrated halides: new crystal phase of the (BEDT-TTF)$_3$Br$_2 \cdot 2$H$_2$O organic metal.
Synthetic Metals **131**, 41-48 (2002).

16. UHLIG K.,
Neuer trockener Millikelvin-Kühler: Er funktioniert und erreicht minus 270°C.
Akademie Aktuell **01** (2002).
17. UHLIG K.,
^{3}He/^{4}He dilution refrigerator with pulse-tube refrigerator precooling.
Cryogenics **42**, 73-77 (2002).
18. KLEIN J., PHILIPP J.B., CARBONE G., VIGLIANTE A., ALFF L., GROSS R.,
Transport anisotropy in biaxially strained La$_{2/3}$Ca$_{1/3}$MnO$_3$ thin films.
Phys. Rev. B **66**, 052414 (2002).
19. PHILIPP J.B., KLEIN J., AFILAL S., RECHER C., WALTHER T., MADER W., SCHMID M., SURYANARAYANAN R., ALFF L., GROSS R.,
Microstructure and magnetoresistance in thin films of layered perovskite La$_{2-2x}$Sr$_{1+2x}$Mn$_2$O$_7$($x = 0.3, 0.4$).
Phys. Rev. B **65**, 184411 (2002).
20. GEGENWART P., CUSTERS J., GEIBEL C., NEUMAIER K., TAYAMA T., TENYA K., TROVARELLI O., STEGLICH F.,
Magnetic-field induced quantum critical point in YbRh$_2$Si$_2$.
Phys. Rev. Lett. **89**, 056402 (2002).
21. EINZEL D.,
Universal Parameters in the Response of Unconventional Superconductors
J. Low Temp. Phys. **126**, 867 (2002).
(Dedicated to Prof. Peter Wölfle on the occasion of his 60th birthday).
22. VENTURINI F., OPEL M., HACKL R., BERGER H., FORRO L., REVAZ B.,
Doping dependence on the electronic Raman spectra in cuprates.
J. of Physics and Chemistry of Solids **63**, pp. 2345-2348 (2002).
23. RAO M.S. Ramachandra, RAVINDRANATH V., LU Y, KLEIN J., GROSS R.,
Double-strain effect in doped La$_{0.7}$Ca$_{0.3}$MnO$_3$ PLD grown thin films and fabrication of high-resistance tunnel junctions using a novel nano-scale insulating tunnel barrier.
J. Phys. D: Appl. Phys. **35**, 287 (2002).
24. KLINGELER R., GECK J., GROSS R., PINSARD-GAUDART L., REVCOLEVSCHI A., UHLENBRUCK S., BÜCHNER B.,
Magnetism and charge order transition in lightly doped La$_{1-x}$Sr$_x$MnO$_3$.
Phys. Rev. B **65**, 174404 (2002).
25. HERBSTRITT F., KEMEN Th., MARX A., GROSS R.,
Ultra violet light assisted oxygenation process for sub-micron YBa$_2$Cu$_3$O$_{7-\delta}$ thin film devices.
J. Appl. Phys. **91**, 5411 (2002).
26. MICHELUCCI U., VENTURINI F., KAMPF A.P.,
Quantum interference phenomena between impurity states in d-wave superconductors.
Journal of Physics and Chemistry of Solids **63**, 2283-2286 (2002).
27. FIGUERAS J., PUIG T., OBRADORS X., ERB A., WALKER E.,
Anisotropy of the low-field critical point of the melting line in twinned YBCO single crystals.
Phys. Rev. B **65**, 092505 (2002).
28. FIGUERAS J., PUIG T., OBRADORS X., ERB A., WALKER E.,
Anisotropic behaviour of the melting line and the low critical field in YBCO.
Physica C **369**, 209-212 (2002).
29. WANG N.L., TIMUSK T., FRANCK J.P., SCHWEISS P., BRADEN M., ERB A.,
The oxygen isotope effect in the a-b-plane reflectance of underdoped YBa$_2$Cu$_3$O$_7$.
Phys. Rev. Lett. **89**, 087003 (2002).
30. KUSKO C., ZHAI Z., HAKIM N., MARKIEWICZ R.S., SRIDHAR S., COLSON D., VAILETUILLEN V., FORGET A., NEFYODOV Yu A., TRUNIN M.R., KOLESNIKOV N.N., MAIGNAN A., DAIGNERE A., ERB A.,
Anomalous microwave conductivity due to collective transport in the pseudogap state of cuprate superconductors.

Phys. Rev. B **65**, 132501 (2002).

31. UHLIG K.,
^{3}He/^{4}He dilution refrigerator precooled by Gifford-McMahon cooler II. Measurements of the vibrational heat leak.
Cryogenics, accepted for publication (2002).
32. PÉREZ-RODRIGUEZ J.L., PÉREZ-RODRIGUEZ L.A., POYATO J., LERF A.,
Layer charge modification by mechanical treatment of the Santa Olalla vermiculite.
Solid State Phenomena, accepted for publication (2002).
33. WELTER B., KROCKENBERGER Y., EINZEL D., NAITO M., ALFF L., GROSS R.,
Pseudogap and conservation of states in electron doped high-temperature superconductors.
Physica C, accepted for publication (2002).
34. PHILIPP J.B., ALFF L., MARX A., GROSS R.,
Low-frequency $1/f$ noise in doped manganite grain-boundary junctions.
Phys. Rev. B, accepted for publication (2002).
35. KLEIN J., PHILIPP J.B., REISINGER D., OPEL M., MARX A., ERB A., ALFF L., GROSS R.,
Orbital order and anisotropic transport in doped manganites induced by epitaxial coherency strain.
J. Appl. Phys., accepted for publication (2002).
36. STEGLICH F., SATO N.K., ASO N., GEGENWART P., CUSTERS J., NEUMAIER K., WILHELM H., GEIBEL C., TROVARELLI O.,
Recent trends in heavy-fermion physics.
Physica C, accepted for publication (2002).
37. EINZEL D.,
Interpolation of BCS response functions.
J. Low Temp. Phys., accepted for publication (2002).
38. EINZEL D.,
Analytic two-fluid description of unconventional superconductivity.
J. Low Temp. Phys., accepted for publication (2002).
39. RAO M.S. Ramachandra, RAVINDRANATH V., GROSS R.,
Evidence of reduction in spin disorder by Ho^{3+} doping in $La_{0.7}Ca_{0.3}MnO_3$. Phil. Mag. B, accepted for publication (2002).
40. KARTSOVNIK M.V., GRIGORIEV P., BIBERACHER W., GRÖGER A., ANDRES D., PESOTSKII S., KUSHCH N.,
Effects of low dimensionality on the classical and quantum parts of the magnetoresistance of layered metals with a coherent interlayer transport.
Synthetic Metals, accepted for publication (2002).
41. KOVALEV A.E., KARTSOVNIK M.V., ANDRES D., JANSEN A.G.M., KUSHCH N.D.,
Heat capacity on the $(ET)_2KHg(SCN)_4$ below the "kink" transition.
Synthetic Metals, accepted for publication (2002).
42. ANDRES D., KARTSOVNIK M.V., BIBERACHER W., NEUMAIER K., MÜLLER H.,
Direct evidence for superconductivity in the organic charge density-wave compound α-$(BEDT\text{-}TTF)_2KHg(SCN)_4$ under hydrostatic pressure.
J. Phys. IV, accepted for publication (2002).
43. PHILIPP J.B., REISINGER D., SCHONECKE M., OPEL M., MARX A., ERB A., ALFF L., GROSS R.,
Epitaxial growth and transport properties of Sr_2CrWO_6 thin films.
J. of Appl. Phys., submitted for publication (2002).
44. REISINGER D., BLASS B., KLEIN J., PHILIPP J.B., SCHONECKE M., ERB A., ALFF L., GROSS R.,
Sub-unit cell layer-by-layer growth of Fe_3O_4, MgO, and Sr_2RuO_4 thin films.
Appl. Phys. A, submitted for publication (2002).
45. CUSTERS J., GEGENWART P., NEUMAIER K., WILHELM H., OESCHLER N., ISHIDA K., KITAOKA Y., GEIBEL C., STEGLICH F.,
Quantum criticality in $YbRh_2Si_2$.
J. Phys. Condens. Matter, submitted for publication (2002).
46. ALFF L., WELTER B., KROCKENBERGER Y., GROSS R., MANSKE D., NAITO M.,
Hidden pseudogap regime under the dome of superconductivity in electron doped cuprate high-temperature superconductors.
Nature, submitted for publication (2002).

47. GÖNNENWEIN S.B.T., GRAF T., WASSNER T., BRANDT M.S., STUTZMANN M., PHILIPP J.B., GROSS R., KOEDER A., SCHOCH W., WAAG A.,
Spin wave resonance in $Ga_xMn_{1-x}As$.
Appl. Phys. Lett., submitted for publication (2002).
48. RAO M.S. Ramachandra, RAVINDRANATH V., YAFENG Lu, KLEIN J., KLINGELER R., UHLENBRUCK S., BÜCHNER B., GROSS R.,
Resistivity and Magnetization of Ho and Y Doped $La_{0.7}Ca_{0.3}MnO_3$.
Eur. Phys. J. B, submitted for publication (2002).
49. YAFENG Lu, KLEIN J., PHILIPP J.B., HERBSTRITT F., MARX A., GROSS R.,
Magnetotransport properties of manganite based magnetic tunnel junctions.
J. Appl. Phys., submitted for publication (2002).

Completed and ongoing Ph.D. and Diploma Theses

Ph.D. Theses

1. **Direktlithographische Herstellung und Charakterisierung von metallischen Nanostrukturen**
   Ben Samwer, Juni 2002.

2. **Rampenkontakte auf der Basis von supraleitenden und magnetischen Übergangsmetalloxiden**
   Mitja Schonecke, seit Dezember 1998

3. **Spinabhängiger Transport und Quanteninterferenzeffekte in mesoskopischen metallischen Systemen**
   Jürgen Schuler, seit Dezember 1998.

4. **Electronic Raman Scattering on High Temperature Superconductors**
   Francesca Venturini, seit Oktober 1998.

5. **Spinabhängiger Transport in Übergangsmetalloxiden**
   Jan Boris Philipp, seit April 2000.

6. **Symmetrie des Ordnungsparameters und Pseudogap-Verhalten in Hochtemperatur-Supraleitern**
   Bettina Welter, seit August 2000.

7. **Elektronische und magnetische Eigenschaften von organischen Metallen und Supraleitern**
   Dieter Andres, seit September 2000.

8. **Heteroepitaktische Schichtstrukturen aus oxidischen Materialien**
   Daniel Reisinger, seit Oktober 2000.

9. **Herstellung und Charakterisierung von supraleitenden Quantenbits**
   Frank Deppe, seit April 2002.

10. **Spininjektion in Halbleiter mit ferromagnetischen Oxiden**
    Petra Majewski, seit November 2002.

Diploma Theses

1. **Magnetisierung und thermodynamische Eigenschaften von festem ^{3}Helium**
   Frank Deppe, Februar 2002.

2. **Tunneldynamik von Quantenpunkten in externen Feldern**
   Jan Weber, Juli 2002.

3. **Epitaxie und Magnetismus dünner Schichten des Ferrimagneten Magnetit**
   Barbara Blass, September 2002.

4. **Pulsed NMR on Solid ^{3}He at Microkelvin Temperatures**
   Carmen Millán Chacartegui, September 2002

5. **Tunnelspektroskopie an elektronendotierten Kuprat-Supraleitern**
   Yoshiharu Krockenberger, September 2002.

6. **Herstellung und Charakterisierung von supraleitenden Quantenbits**
   Markus Tober, seit Juni 2002.

7. **Magnetische Eigenschaften von Mn dotiertem ZnO**
   Karl Nielsen, seit November 2002.

Research Projects and Cooperations

Many of our research projects have benefited from the collaboration with external groups via joint research projects, individual collaborations, exchange programs and visitors. Several collaborations are based on joint projects which are financially supported by different organizations (see list below). A large number of collaborations also exist with several universities and other research institutions without direct financial support. These are also listed below.

Funded Projects

Deutsche Forschungsgemeinschaft (DFG)

1. Elektronenmikroskopische Analyse von Defektstrukturen, lokalen strukturellen Eigenschaften und Ladungsordnungsphänomenen in dotierten Manganaten
   (R. Gross, Az. GR 1132/3-1)
   Partner: Universität Bonn

2. Untersuchung des niederfrequenten $1/f$ Rauschens in Josephson–Kontakten aus Hochtemperatur–Supraleitern zur Charakterisierung elementarer Rauschzentren und Klärung der Transportmechanismen
   (A. Marx und R. Gross, Az. Ma 1953/1-1+2)

3. Heteroepitaxie von Übergangsmetalloxiden
   (L. Alff und R. Gross, Az. Al 560/1-1+2)

4. Kristalline organische Metalle und Supraleiter: Synthese und elektronische Eigenschaften, gefördert von der DFG und der russischen Stiftung für Grundlagenforschung (RFFI)
   (W. Biberacher, WMI, und N. Kushch, Institut für Probleme der chemischen Physik, Cernogolovka, Az.: 436 RUS 113/592/0)

5. Untersuchung des Wechselwirkungspotentials in Kuprat–Supraleitern durch Vergleich verschiedener spektroskopischer Methoden
   (R. Hackl, Az. HA 2071/2-1+2)

Bundesminister für Bildung, Wissenschaft, Forschung und Technologie (BMBF)

1. Verbundprojekt: Ultra–schnelle und ultra–verlustarme Informationstechnik–Komponenten
   Teilvorhaben: Transport– und Rauscheigenschaften von Nano–SiGe–Bauelementen
   (R. Gross und A. Marx, Förderkennzeichen: 13N7902)
   Partner: DaimlerChrysler AG, AMO GmbH.

2. Wissenschaftlich–Technologische Zusammenarbeit mit Indien: Ferromagnetische Oxide mit hoher Spinpolarisation
   (R. Gross, Projektkennzeichen: IND 01/009)
   Partner: Prof. Dr. M. S. R. Rao, Indian Institute of Technology, Madras, India.

3. Verbundprojekt: Spinelektronik und Spinoptoelektronik in Halbleitern
   Teilprojekt: Ferromagnetische metallische Oxide mit hoher Spinpolarisation für die Spinelektronik
   (R. Gross, Förderkennzeichen: 13N8279)

Partners: Universities of Würzburg, Hamburg, Regensburg, Hannover and Marburg, Max–Planck–Institute Halle, Siemens AG, Infineon Technologies, Aixtron GmbH.

4. Wissenschaftlich–Technologische Zusammenarbeit mit Ungarn: Transporteigenschaften hochkorrelierter Schichtsysteme
(R. Hackl, Projektkennzeichen: HUN 01/008)
Partner: Ungarische Akademie der Wissenschaften, Institut für Festkörperphysik und Optik, Prof. Dr. Istvan Tüttö.

European Union

1. European Science Foundation Network *"Thin Films for Novel Oxide Devices: THIOX"*
(R. Gross; coordination: Prof. D. Blank, Univesity of Twente, The Netherlands)
partners: several European Universities and research facilities.

2. Research and Training of Young Researchers on the Magnetic Properties of ^{3}He by Means of Neutron Diffraction
(E. Schuberth; coordination: Dr. Konrad Siemensmeyer, Hahn–Meitner Institute Berlin GmbH)
European Community, Contract No.: HPRN-CT-2000-00166
Partners: Hahn–Meitner Institut, Berlin, Univ. of Florida, Royal Holloway College, London, Univ. Liverpool, CNRS, Grenoble and Univ. Paris, Saclay.

3. European Science Foundation Network *"Vortex Matter at Extreme Scales and Conditions"*
(R. Gross; coordination: Prof. Moshchalkov, Univ. Leuven)
Partners: several european Universities and research facilities.

4. High Field Infrastructure Cooperative Network
(W. Biberacher, coordination by CNRS Grenoble, contract No.: HPRI-CT-1999-40013)
Partners: in total 31 participants.

Deutscher Akademischer Austauschdienst (DAAD)

1. Projektbezogener Personenaustausch mit Spanien, Aciones Integradas Hispano–Alemanas
(A. Lerf)
Centro de Investigaciones Cientificas "Isla de Cartuja", Universidad de Sevilla, Prof. Dr. Jose Luis Perez Rodriguez

Collaborations

Other collaborations without direct project funding involve:

- Technion, Israel (Prof. G. Koren, Dr. E. Polturak)
- NTT, Japan (Prof. Dr. H. Takayanagi, Dr. M. Naito)
- Tokyo Institute of Technology, Japan (Prof. M. Kawasaki, Prof. K. Koinuma)
- Materials Physics Laboratory, Helsinki University of Technology (Dr. Tero Heikkilä)
- Department of Condensed Matter Physics, The Weizmann Institute of Science, Israel (Dr. Moshe Schechter)
- Chalmers University of Technology, Gothenburg, Sweden (Dr. Z. Ivanov, Prof. Dr. P. Delsing)
- University of Waterloo, Department of Physics, Ontario, Canada (Prof. Dr. T.P. Devereaux)
- Ludwig–Maximilians–University Munich, Germany (Prof. Kotthaus, Prof. von Delft, Dr. F. Wilhelm)
- University of Tübingen, Germany (Prof. R. Kleiner, Prof. D. Kölle)
- University of Würzburg, Germany (Prof. W. Hanke, Prof. L. Molenkamp)
- University of Augsburg, Germany (Prof. Dr. P. Hänggi)
- Max–Planck Institut für Metallforschung, Stuttgart (Dr. P. Wochner, Dr. A. Vigliante)
- Hungarian Academy of Sciences, Technische Universität Budapest, Budapest, Hungary (Prof. Dr. K. Kamaras, Dr. Attila Virosztek, Prof. Dr. A. Zawadowski)
- Eötvös Lorand University, Budapest, Hungary (Dr. I. Tüttö)
- Universitá di Roma ”La Sapienza”, Roma, Italy (Prof. Dr. Paolo Calvani)
- Institut für Experimentelle Physik, Slowakische Akademie der Wissenschaften, Kosice (Prof. K. Flachbart)
- Northwestern University Evanston, Illinois
- University of Florida
- Institute of Solid State Physics, Chernogolovka, Russia (Dr. R.P. Shibaeva, Prof. Dr. V. Ryazanov, Prof. Dr. Lev Vinnikov)
- Institute of Problems of Chemical Physics, Chernogolovka, Russia (Prof. Dr. O.A. Dyachenko)
- High–Magnetic–Field Laboratory, Grenoble, France (Dr. A.G.M. Jansen)
- National Pulsed–Magnetic–Field Facility, Toulouse, France (Dr. L. Brossard)
- B. Verkin Institute for Low Temperature Research and Engineering, Kharkov, Ukraine (Prof. V.G. Peschansky)
- Institute for Material Science, Barcelona, Spain (Prof. E. Canadell)
- Department of Chemistry, University of Cambridge, UK (Dr. Jacek Klinowski)
- Institut für Technologie Anorganischer Stoffe der TU Graz, Austria (Prof. Besenhard)
- University of Nantes, France (Prof. M. Danot)

Stays abroad

Extended visits of members of the Walther-Meissner-Institute at foreign research laboratories:

1. **Rudolf Hackl**
   Università di Roma La Sapienza, Istituto Nazionale di Fisica della Materia (Prof. Paolo Calvani) Rom, Italien
   28. 12. 2001 - 11. 01. 2002
2. **Rudolf Hackl**
   University of Waterloo, Department of Physics (Prof. Dr. T.P. Devereaux) Ontario, Canada
   12. 03. – 17. 03. 2002
3. **Rudolf Gross**
   Indian Institute of Technology (Prof. Dr. M. S. R. Rao), Madras, und Tata Institute of Fundamental Research (Prof. R. Pinto), Bombay, Indien
   16. 03. – 30. 03. 2002
4. **Rudolf Hackl**
   Technical University of Budapest and Research Institute for Solid State Physics (Profs. I. Tüttö, A. Virosztek, A. Zawadowski), Budapest, Ungarn
   23. 06. – 11. 08. 2002
5. **Rudolf Hackl**
   University of Waterloo, Department of Physics (Prof. Dr. T.P. Devereaux) Ontario, Canada
   27. 10. – 02. 11. 2002

Invited Conference Talks and Seminar Lectures

Lambert Alff

1. **Experiments with grain boundary junctions: What is the difference between electron and hole doped high-temperature superconductors?**
   04. 02. 2002
   13. Edgar Lüscher Seminar 2002, Serneus Schweiz

2. **Electron and hole doped high-temperature superconductors: What is the difference?**
   21. - 23. 04. 2002
   First International Workshop on the Symmetry in Macroscopic Quantum States- Quantitative Experiments and Theory, Augsburg

3. **Electron and hole doped high-temperature superconductors: What is the difference?**
   15. 04. 2002
   IFW, Dresden

4. **Order parameter and pseudogap in electron doped high-temperature superconductors**
   03. 09. 2002
   NTT-Seminar, Atsugi, Japan

5. **Korngrenzen in oxidischen Materialien: Von grundlegenden Experimenten mit unkonventionellen Supraleitern zu spinelektronischen Bauelementen aus Halbmetallen**
   16. - 18. 12. 2002
   Symposium “Grundlagenorientierte Materialforschung”, TU Braunschweig

Werner Biberacher

1. **Organization of a Round Table on Organic metals and superconductors in high magnetic fields**
   19. - 20. 09. 2002
   Third Annual Meeting of EU Network (HPRI-CT-1999-400013) on High Magnetic Fields, Grenoble, France

Dietrich Einzel

1. **Liquid ^{3}He in Aerogel: a dirty Fermi liquid**
   08. 01. 2002
   Seminar zur Theorie der kondensierten Materie, Universität Augsburg

2. **Response und Transport in unkonventionellen Supraleitern**
   24. 05. 2002
   Oberseminar über Festkörperphysik, Kirchhoff-Institut für Physik, Heidelberg

3. **The flow of liquid helium in restricted geometries**
   23. 10. 2002
   WE Heraeus-Seminar “Quantum transport through nano-wires, point contacts and near surfaces”, Physik-Zentrum der DPG, Bad Honnef

4. **Introduction to quantum information processing**
   26. 11. 2002
   Seminar zur Quanteninformationsverarbeitung am WMI, Garching

Andreas Erb

1. **MgB_2 a 39 K superconductor from the chemistry shelf**
   22. 02. 2002
   Max-Planck-Institut für Plasmaphysik, Garching

Rudolf Gross

1. **From Electronics to Spintronics**
   19. 03. 2002
   Department of Physics, Indian Institute of Technology, Madras, India
2. **Strain effects and anisotropic transport in doped manganites**
   20. 03. 2002
   Materials Science Research Center, Indian Institute of Technology, Madras, India
3. **High temperature superconductivity - order parameter symmetry, pseudo gap, and quantum critical points**
   21. 03. 2002
   Indian Physics Association, Madras Chapter, Chennai, India
4. **Electron doped high temperature superconductors - order parameter symmetry, pseudo gap, and quantum critical point**
   22. 03. 2002
   Indira Gandhi Center for Applied Research (IGCAR), Kalpakkam, India
5. **Metallic nanostructures - from physics to nanoelectronics**
   26. 03. 2002
   Materials Science Research Center, Indian Institute of Technology, Madras, India
6. **Spintronics based on ferromagnetic oxides**
   28. 03. 2002
   Tata Institute for Fundamental Research, Bombay, India.
7. **High temperature superconductivity: What can we learn from the electron doped materials ?**
   18. 06. 2002
   Colloquium of the Condensed Matter Department, University of Genova, Switzerland.
8. **Spin Electronics Based on Magnetic Oxide Thin Films and Heterostructure**
   24. 10. 2002
   MARTECH-Seminar, Florida State University, Tallahassee, Florida, USA.
9. **Als die Elektronen spinnen lernten - Spinelektronik mit ferromagnetischen Oxiden**
   25. 11. 2002
   Physikalisches Kolloquium, Universität Regensburg
10. **Orbital Order in Doped Manganites Induced by Epitaxial Coherency Strain**
    20. - 23. 10. 2002
    9th International Workshop on Oxide Electronics, St. Petersburg, Florida USA.
11. **Noise in magnetic oxides**
    08. - 10. 12. 2002
    Workshop on Noise and dynamic switching in magneto-electronic devices, Renvyle House, Connemara, Irland.

Rudolf Hackl

1. **Evidence for a metal-insulator transition in the cuprates from Raman scattering**
   21. 03. 2002
   APS March Meeting, Indianapolis, USA
2. **Raman-scattering evidence for a metal-insulator transition in strongly overdoped cuprates**
   13. - 18. 10. 2002
   Low Energy Electrodynamics in Solids 2002, Montauk, NY, USA

3. **A new piece in the puzzle: a metal-insulator transition in overdoped cuprates**
   14. 03. 2002
   University of Waterloo, Canada
4. **The puzzling phase diagram of copper-oxygen compounds: new Raman results**
   21. 10. 2002
   Washington University, St. Louis, USA
5. **One- and two-particle response in CuO_2 compounds: comparison of photoemission, transport and Raman results**
   23. 10. 2002
   University of Florida, Gainesville, USA
6. **The phase diagram of copper-oxygen compounds: new Raman results**
   31. 10. 2002
   Brock University, St. Catharines, Canada

Mark Kartsovnik

1. **Slow oscillations of magnetoresistance in layered organic metals**
   29. 06. - 05. 07. 2002
   International Conference on Science and Technology of Synthetic Metals, ICSM 2000, Shanghai, China
2. **High magnetic field induced transitions in the CDW state of α-(BEDT-TTF)$_2$KHg(SCN)$_4$: possible novel manifestation of the nesting vector quantization**
   19. 09. - 20. 09. 2002
   Third Annual Meeting of EU Network (HPRI-CT-1999-400013) on High Magnetic Fields, Grenoble, France
3. **Effects of low-dimensionality on the interlayer magnetotransport of layered (quasi-two-dimensional) organic metals**
   15. 01. 2002
   Seminar of Physical Institutes, University of Stuttgart

Anton Lerf

1. **Risiko Forschung? Über Wissenschaft, Technik und die Folgen**
   09. 01. 2002
   Seniorenstudium LMU, München (mit M. Schneider, Lehrst. f. Soziologie, TUM)
2. **Risiko Forschung? Über Wissenschaft, Technik und die Folgen**
   05. 03. 2002
   Garchinger Gespräche, Gemeindezentrum der evang. Pfarrgemeinde (mit M. Schneider, Lehrst. f. Soziologie, TUM)
3. **Electron transfer reactions in intercalation chemistry**
   07. - 12. 07. 2002
   Solid State Chemistry 2002, Bratislawa

Achim Marx

1. **Mesoscopic Normal-Conductor-Superconductor-Systems**
   04. 07. 2002
   Institut für Experimentelle und Angewandte Physik, Regensburg
2. **Mesoscopic Normal-Conductor-Superconductor-Systems**
   22. 10. 2002
   287. WE-Heraeus-Seminar: Quantum Transport through Nano-Wires, Point Contacts, and near Interfaces, Bad Honnef
3. **Tieftemperaturexperimente: Transport und Rauschen**
   26. 04. 2002
   Statustreffen des BMBF-Projekts Ultra^2, Daimler-Chrysler Forschung, Ulm

Karl Neumaier

1. **Tunneling experiments with the dilution insert**
   29. 11. 2002
   Symposium on Neutron Backscattering in honor of Toni Heidemann, Institute Laue-Langevin, Grenoble

Jan Boris Philipp

1. **Korngrenzeffekte in ferromagnetischen Oxiden**
   24. 05. 2002
   Seminar der Festkörperphysik an der Universität Tübingen

Erwin Schuberth

1. **Search for line splitting in the low field nuclear ordered phase of solid ^{3}He**
   22. - 29. 09. 2002
   2nd Summer School of the EU Project on Neutron Scattering from Solid ^{3}He and 1st European Cryogenic School Chichilliane, France
2. **Experimente bei ultratiefen Temperaturen**
   14. 02. 2002
   Lehrstuhl-Seminar, Prof. Weiss, Universität Regensburg
3. **Solid ^{3}He the simplest magnet?**
   06. 06. 2002
   Lehrstuhl-Seminar Prof. Paul, TU München
4. **Experimentelle Möglichkeiten mit einer $PrNi_5$ Kernstufe**
   25. 10. 2002
   Seminarvortrag, Universität Tübingen

Kurt Uhlig

1. **^{3}He/^{4}He-Mischkühler mit Pulsröhren-Refrigerator-Vorkühlung**
   22. 11. 2002
   Deutsche Kälte-Klima-Tagung 2002, Magdeburg

Francesca Venturini

1. **Evidence for a metal-insulator transition in Bi-2212: new Raman results**
   27. 02. 2002
   SFB-Seminar, Universität zu Köln
2. **Complete symmetry analysis of the Raman spectra in cuprates**
   21. 03. 2002
   APS March Meeting, Indianapolis, USA

Seminars, Courses, Lectures and other Scientific Activities

The WMI Seminars

The Friday Seminar — Walther-Meissner-Seminar on Current Topics in Low Temperature Physics

1. **Quantum dynamics of the phase in Josephson tunnel junctions at millikelvin temperatures**
   Dr. Andreas Wallraff, Phys. Institut III, Universität Erlangen-Nürnberg
   18. 01. 2002
2. **MBE growth of La_2CuO_{4+x} and $(LaSr)_2CuO_{4+x}$ thin films**
   Dr. Gennadi Logvenov, Oxxel GmbH, Technologiepark, Universität Bremen
   25. 01. 2002
3. **Pushing the resolution limits of the force microscope: from steps to atoms and atomic orbitals**
   Dr. Franz Giessibl, Universität Augsburg
   01. 02. 2002
4. **Elektronische Theorie für Cooper-Paarung in unkonventionellen Supraleitern: alte Fragen, neue Antworten?**
   Dr. Dirk Manske, Institut für Theoretische Physik, FU Berlin
   08. 02. 2002
5. **Bound states and d-density wave phases**
   Dr. Carsten Honerkamp, Massachusetts Institute of Technology
   15. 02. 2002
6. **Infrared observation of charge stripes in $La_{2-x}Sr_xCuO_4$**
   Prof. Dr. Paolo Calvani, Università di Roma La Sapienza, Italy
   01. 03. 2002
7. **The electronic structure of Bi-2212 superconductors from high resolution, angle-scanned photoemission**
   Dr. Sergey Borisenko, Institute for Solid State Research (IFF), IFW Dresden
   12. 04. 2002
8. **Bericht von APS March Meeting**
   Dr. Rudolf Hackl, Walther-Meissner-Institut, Garching
   16. 04. 2002
9. **SCUBA 2 - a wide field imager for the James Clerk Maxwell Telescope (Hawaii)**
   Dr. William D. Duncan, Royal Observatory, Edinburgh
   17. 04. 2002
10. **Single and multi-particle response in highly correlated systems**
    Dr. Istvan Tüttö, Research Institute for Solid State Physics and Optics, Hungarian Academie of Science
    19. 04. 2002
11. **Peculiarities of the excess resistance produced by spin-polarized electrons in Ta-Ni-Ta sandwiches**
    Prof. Dr. Valerij Ryazanov, Institute of Solid State Physics, Chernogolovka
    23. 04. 2002
12. **Supraleiter/Ferromagnet Schichtsysteme**
    Prof. Dr. Anatoli Sidorenko, Institute for Applied Physics, Kishinev, Moldava
    26. 04. 2002
13. **Thermal and transport properties of unconventional superconductors in a magnetic field**
    Dr. Ilya Vekhter, Theoretical Division, Los Alamos National Laboratory
    29. 04. 2002
14. **Transporteigenschaften von mesoskopischen Supraleiter-Normalleiter-Strukturen und Bericht vom First International Workshop on the Symmetry in Macroscopic Quantum States: Teil 1**
    Dr. Achim Marx und Dr. Lambert Alff, Walther-Meissner-Institut, Garching
    30 .04. 2002
15. **Lattice distortions charge-and orbital order in $La_{7/8}Sr_{1/8}MnO_3$: a new look at resonant x-ray scattering**
    Dr. Peter Wochner, MPI für Metallforschung, Stuttgart

03. 05. 2002

16. **Fluctuation phenomena in superconductors**
Prof. Dr. A.A. Varlamov, Instituto Nationale Fisica della Materia, Universita di Roma
13. 05. 2002
17. **Suche nach helikalen Spinanregungen und der Verletzung der Zeitumkehrinvarianz in Kupraten**
Dr. Rudolf Hackl, Walther-Meissner-Institut, Garching
17. 05. 2002
18. **Unconventional density waves in solids**
Prof. Dr. Attila Virosztek, Research Institute for Solid State Physics and Optics, Hungarian Academy of Sciences
24. 05. 2002
19. **Spin excitations in low-dimensional antiferromagnets**
Prof. Dr. T. Kopp, Universität Augsburg
03. 06. 2002
20. **Unconventional density waves in 1D and 2D electronic systems**
Prof. Kazumi Maki, University of Southern California
04. 06. 2002
21. **Low frequency electrodynamics in $La_{2-x}Ce_xCuO_4$**
Dr. A. Pronin, PD Dr. A. Pimenov, Experimentalphysik V, Universität Augsburg
07. 06. 2002
22. **Ferromagnetische Tunnelkontakte und ihre Anwendungen in magnetischen Datenspeichern**
H. Knoglinger, Technische Universität München
14. 06. 2002
23. **Magnetotransport properties of ferromagnetic oxides**
Prof. Dr. M.S. Ramachandra Rao, Indian Institute of Technology, Madras
17. 06. 2002
24. **Microanalyse mit Tieftemperatur-Calorimeter**
Dr. Matthias Bühler, VeryCold Technologies GmbH, Ismaning
18. 06. 2002
25. **Neue Wege in der Teilchendetektion - Kalorimetrie bei tiefen Temperaturen**
Dr. Christian Enss, Kirchhoff-Institut f. Physik, Universität Heidelberg
12. 07. 2002
26. **What high-pressure studies have taught us about high-temperature superconductivity**
Prof. Dr. James S. Schilling, Washington University, St. Louis
15. 07. 2002
27. **Optical studies of 1T-TaS_2**
Prof. Dr. Lev Gasprov, University of North Florida, Jacksonville
19. 07. 2002
28. **Brennstoffzellen aus keramischen Werkstoffen - Herstellung und Einsatzgebiete**
Dr. Sven Uhlenbruck, Forschungszentrum Jülich GmbH
02. 10. 2002
29. **Spintronik - vom Widerstandsmodell zum nichtlinearen Transport**
Dr. Georg Schmidt, Universität Würzburg
18. 10. 2002
30. **Transport properties and angular dependent mangetoresistance in UCDW systems**
Dr. Balázs Dóra, The Abdus Salam ICTP Trieste, Italy
28. 10. 2002
31. **Structural properties of the quasi-two-dimensional organic conductors α-(BEDT-TTF)$_2$MHg(SCN)$_4$ with M = K, Rb**
Dr. Pascale Foury-Leylekian, Université Paris Sud Orsay, France
15. 11. 2002
32. **Order parameter symmetry effects in Josephson structures combining high-T_c and low-T_c superconductors**
Prof. Dr. Hans Hilgenkamp, University of Twente
22. 11. 2002

33. **Eigenschaften und Anwendungen von Gold-Nanoteilchen: Physik am Übergang vom Cluster zum Festkörper**
    Prof. Dr. Paul Ziemann, Universität Ulm
    29. 11. 2002
34. **Hole localization and magnetic structure in lightly Ca doped $YBa_2Cu_3O_6$**
    Prof. András Jánossy, Technical and Economical University of Budapest
    04. 12. 2002
35. **Heusler alloys and double perovskites as half-metallic materials**
    Dr. Gerhard Jakob, Universität Mainz
    06. 12. 2002
36. **Competing orders and quantum phase transitions in the cuprates**
    Dr. Matthias Vojta, Universität Karlsruhe
    13. 12. 2002

The Tuesday Seminar – WS 2001/2002 and SS 2002

1. **Applications and limitations of Raman spectroscopy**
   Dr. Rudolf Hackl, Walther-Meissner-Institut, Garching
   15. 01. 2002
2. **Wie erkennt man ein Pseudogap?**
   Y. Krockenberger, Walther-Meissner-Institut, Garching
   22. 01. 2002
3. **Transporteigenschaften von $La_{2-2x}Sr_{1+2x}Mn_2O_7$**
   Boris Philipp, Walther-Meissner-Institut, Garching
   05. 02. 2002
4. **Magnetisierungsmessungen an festem ^{3}He bei ultratiefen Temperaturen**
   Frank Deppe, Walther-Meissner-Institut, Garching
   19. 02. 2002
5. **Anisotropic transport properties in biaxially strained films of doped manganites**
   Dr. Lambert Alff, Walther-Meissner-Institut, Garching
   26. 02. 2002
6. **Bericht über den Forschungsaufenthalt am Indian Institute of Technology, Madras, und am Tata Institute for Fundamental Research, Bombay, Indien**
   Prof. Dr. Rudolf Gross, Walther-Meissner-Institut, Garching
   09. 04. 2002
7. **Konferenzbericht: March Meeting of the American Physical Society**
   Rudi Hackl
   16. 04. 2002
8. **Transporteigenschaften von mesoskopischen Supraleiter-Normalleiter-Strukturen**
   Achim Marx
   30. 04. 2002
9. **Konferenzbericht: 1st Int. Workshop on the Symmetry in Macroscopic Quantum States**
   Lambert Alff
   30. 04. 2002
10. **Epitaxie von Magnetit auf keramischen und halbleitenden Substraten**
    Barbara Blass, Walther-Meissner-Institut, Garching
    07. 05. 2002
11. **Bericht vom First International Workshop on the Symmetry in Macroscopic Quantum States: Teil 2**
    Dr. Lambert Alff, Walther-Meissner-Institut, Garching
    14. 05. 2002
12. **Spectral measurement of the Hall angle response in normal state cuprate superconductors**
    Dr. Matthew Grayson, Walter-Schottky-Institut, Garching and University of Maryland
    11. 06. 2002
13. **Grundzustände organischer Metalle unter dem Einfluss von Magnetfeld und Druck**
    Dieter Andres, Walther-Meissner-Institut, Garching
    18. 06. 2002

14. **Transport Conducting Oxides (TCO) Thin films: Fundamentals to Frontiers**
    A. Subrahmanyam, Indian Institute of Technology
    25. 06. 2002
15. **Techniken zur Messung der spezifischen Wärme bei tiefen Temperaturen**
    Dr. Karl Neumaier, Walther-Meissner-Institut, Garching
    02. 07. 2002
16. **Bau und Betrieb eines Mischkühlers**
    Dr. Christian Probst, Walther-Meissner-Institut, Garching
    08. 10. 2002

Topical Seminar on Quantum Information Processing – WS 2002/2003

This topical seminar is held for students in the 7th and 8th semester. It is part of the special physics courses in magnetism and magnetoelectronics as well as in superconductivity and low temperature physics offered by the WMI.

1. **Einzelne Quantenbits — Präparation, Messung, Manipulation, Kontrolle**
   Dietrich Einzel
   26. 11. 2002
2. **Zwei-Qubit-Systeme — Verschränkung, EPR-Paradoxon, Bell-Ungleichungen**
   Dominik Bauer
   03. 12. 2002
3. **Quantenkryptographie und Teleportation**
   Stefan Ahlers
   10. 12. 2002
4. **Quantencomputing — Modelle, Gatter, Algorithmen**
   Sebastian Bauer
   17. 12. 2002
5. **Der Ionenfallen-Quantencomputer**
   M. Janoschek
   07. 01. 2003
6. **Der NMR-Quantencomputer**
   Martin Stadlbauer
   14. 01. 2003
7. **Qubits basierend auf Spins in Nanostrukturen**
   Dominik Heiss
   21. 01. 2003
8. **Supraleitende Qubits I: Ladungs-Qubits**
   Stefanie Wagner
   28. 01. 2003
9. **Supraleitende Qubits II: Fluss/Phasen-Qubits**
   Markus Tober
   04. 02. 2003

Lectures

Lambert Alff

WS 2001/2002	• Übungen zu Experimentalphysik III in Gruppen (Experimental Physics III, exercises) (with R. Gross)
SS 2002	• Magnetismus (Introduction to Magnetism) • Übungen zu Experimentalphysik IV in Gruppen (Experimental Physics IV, exercises) (with R.Gross)
WS 2002/2003	• Magnetismus (Introduction to Magnetism) • Übungen zu Experimentalphysik III in Gruppen (Experimental Physics IV, exercises) (with R.Gross)

Dietrich Einzel

WS 2001/2002	• Mathematische Methoden der Physik I (Mathematical Methods of Physics I) • Supraleitung und Suprafluidität: Theorie (Superconductivity and Superfluidity: Theory) • Übungen zu Mathematische Methoden der Physik I (Mathematical Methods of Physics I, Problem Sessions)
SS 2002	• Mathematische Methoden der Physik II (Mathematical Methods of Physics II) • Übungen zu Mathematische Methoden der Physik II (Mathematical Methods of Physics II, Problem Sessions) • Ausgewählte Kapitel aus der Tieftemperaturphysik
WS 2002/2003	• Mathematische Methoden der Physik I (Mathematical Methods of Physics I) • Übungen zu Mathematische Methoden der Physik I (Mathematical Methods of Physik I, Problem Sessions)

Rudolf Gross

WS 2001/2002	• Experimentalphysik III (Experimental Physics III) • Übungen zu Experimentalphysik III in Gruppen (Experimental Physics III, exercises) • WMI-Seminar über aktuelle Fragen der Tieftemperatur-Festkörperphysik (WMI Seminar on Current Topics of Low Temperature Solid State Physics) (with L. Alff, D. Einzel, E. Schuberth)
SS 2002	• Magnetoelektronik I (Magnetoelectronics I) • Experimentalphysik IV (Experimental Physics IV) • Übungen zu Experimentalphysik IV in Gruppen (Experimental Physics IV, exercises) • WMI-Seminar über aktuelle Fragen der Tieftemperatur-Festkörperphysik (WMI Seminar on Current Topics of Low Temperature Solid State Physics) (with L. Alff, D. Einzel, E. Schuberth)
WS 2002/2003	• Experimentalphysik III (Experimental Physics III) • Übungen zu Experimentalphysik III in Gruppen (Experimental Physics III, exercises) • Magnetoelektronik II (Magnetoelectronics II) • WMI-Seminar über aktuelle Fragen der Tieftemperatur-Festkörperphysik (WMI Seminar on Current Topics of Low Temperature Solid State Physics) (with L. Alff, D. Einzel, E. Schuberth) • Seminar über Quanteninformationsverarbeitung (Seminar on Quantum Information Processing)

Anton Lerf

WS 2001/2002	• Angewandte Chemie II (Festkörperchemie) für Lehramt Gymnasium
	• Nanostrukturierte Materie (Nanostructured Materials)
	• Festkörperchemie (mit Prof. Köhler), (Solid State Chemistry)
SS 2002	• Nanostrukturierte Materie (Nanostructured Materials)
WS 2002/2003	• Festkörperchemie (mit Prof. Köhler), (Solid State Chemistry)
	• Nanostrukturierte Materie (Nanostructured Materials)

Erwin Schuberth

WS 2001/2002	• Experimentalphysik II für Lehrberufe (Experimental Physics Part II for Teachers)
	• Übungen zu Experimentalphysik II für Lehrberufe (Experimental Physics Part II, Problem Sessions)
SS 2002	• Experimente bei tiefsten Temperaturen (Experiments at very Low Temperatures)
WS 2002/2003	• Experimente bei tiefsten Temperaturen (Experiments at very Low Temperatures)

Staff of the Walther-Meissner-Institute

Director
Prof. Dr. Rudolf Gross

Technical Director
Dr. Karl Neumaier

Administration/Secretary's Office
Jutta Laaser
Emel Dönertas

Scientific Staff
Dr. habil. Lambert Alff
Dr. Werner Biberacher
Dr. habil. Dietrich Einzel
Dr. habil. Andreas Erb
Dr. habil. Rudi Hackl
Dr. Mark Kartsovnik
Dr. habil. Anton Lerf
Dr. Achim Marx
Dr. Matthias Opel
Dr. Christian Probst
Dr. habil. Erwin Schuberth
Dr. Kurt Uhlig
Dipl.-Phys. Dieter Andres
Dipl.-Phys. Boris Philipp
Dipl.-Phys. Daniel Reisinger
Dipl.-Phys. Mitja Schonecke
Dipl.-Phys. Jürgen Schuler
Dipl.-Phys. Francesca Venturini
Dipl.-Phys. Bettina Welter
Dipl.-Phys. Carmen Millan-Chacartegui
Dipl.-Phys. Petra Majewski

Technical Staff
Thomas Brenninger
Joachim Geismann
Gabrielle Görblich
Ulrich Guggenberger
Dieter Guratzsch
Wolfgang Hehn
Josef Höss
Julius Klaus
Robert Müller
Jan Naundorf
Georg Nitschke
Walter Nitschke
Christian Reichlmeier
Harald Schwaiger
Helmut Thies
Siegfried Wanninger

Assistants
Sybilla Plöderl
Gülcay Kursat

Permanent Guests
Prof. Dr. B. S. Chandrasekhar
Dr. Robert Doll
Prof. Dr. Schöllhorn

Guest Researchers

1. Prof. Dr. B.S. Chandrasekhar
   permanent guest
2. Dr. Robert Doll
   permanent guest
3. Prof. Dr. Schöllhorn
   permanent guest
4. Dr. Dirk Manske, Institut für Theoretische Physik, Freie Universität Berlin
   06. 02. – 10. 02. 2002
5. Prof. Dr. Jeevak M. Parpia, Cornell University, Ithaka, USA
   07. 03. – 14. 03. 2002
6. Dr. Pavel Grigoriev, Hochgeld-Magnetlabor, Grenoble
   11. 03. – 05. 04. 2002, 23. 09. – 05. 11. 2002
7. Prof. Dr. Valeriy Ryazanov, Institute of Solid State Physics, Chernogolovka, Russia
   10. 04. – 24. 04. 2002
8. Dr. Istvan Tüttö, SZFKI, Ungarische Akademie d. Wissenschaften, Budapest, Hungary
   10. 04. – 24. 04. 2002, 05. 12. – 11. 12. 2002
9. Prof. Dr. A. Zawadowski, Technische Universität Budapest, Hungary
   01. 05. – 31. 05. 2002
10. Dr. Sergei Pesotskii, Institute of Problems of Chemical Physics RAS, Chernogolovka, Russia
    14. 05. – 12. 06. 2002
11. Prof. Dr. M.S. Ramachandra Rao, Materials Science Research Centre, Indian Institute of Technology, Madras, India
    17. 05. – 14. 07. 2002
12. Dr. Attila Virosztek, Central Research Institute for Solid State Physics and Optics, Hungarian Academy of Sciences, Technische Universität Budapest, Budapest, Hungary
    21. 05. – 29. 05. 2002, 07. 11. – 19. 11. 2002
13. Dr. Luis Perez Maqueda, Instituto de Ciencia de Materiales de Sevilla, Sevilla, Spanien
    17. 06. – 05. 07. 2002
14. Prof. Dr. Juan Poyato Ferrera, Instituto de Ciencia de Materiales de Sevilla, Sevilla, Spanien
    15. 07. – 21. 07. 2002 – 27. 07. 2002
15. Prof. Dr. Jose Luis Perez Rodriquez und Prof. Dr. Juan Poyato Ferrera, Instituto de Ciencia de Materiales de Sevilla, Sevilla, Spanien
    15. 07. – 19. 07. 2002
16. Prof. Dr. Lev Gasparov, University of North Florida, Jacksonville, USA
    18. 07. – 21. 07. 2002
17. Ferenc Borondics, Central Research Institute for Solid State Physics and Optics, Budapest, Hungary
    21. 08. – 04. 09. 2002
18. Dr. Natalya Kushch, Institute of Problems of Chemical Physics, Chernogolovka Russia
    09. 09. – 01. 11. 2002
19. Dr. Balazs Dora, The Abdus Salam ICPT Trieste, Italy
    27. 10. – 30. 10. 2002
20. Prof. Dr. A. Janossy, Technische Universität Budapest, Budapest, Hungary
    02. 12. – 08. 12. 2002

21. Prof. Dr. K. Kamaras, Central Research Institute for Solid State Physics and Optics, Hungarian Academy of Sciences, Technische Universität Budapest, Budapest, Hungary
    02. 12. – 08. 12. 2002
22. Chiara Coppi, Universität Florenz, Italy
    13. 12. – 20. 12. 2002
23. Leonardo Tassini, Universität Florenz, Italy
    13. 12. – 20. 12. 2002

Commission for Low Temperature Physics

Members of the Commission for Low Temperature Physics of the Bavarian Academy of Sciences:

Kaiser, Wolfgang, Leiter (Technische Universität München)
Brenig, Wilhelm, stellv. Leiter (Technische Universität München)
Landwehr, Gottfried (Universität Würzburg)
Hänsch, Theodor (Max-Planck Institut für Quantenoptik, Garching)
Koch, Frederick (Technische Universität München)
Kotthaus, Jörg Peter (Ludwig-Maximilians-Universität München)
Rainer, Dierk (Universität Bayreuth)
Renk, Karl Friedrich (Universität Regensburg)
Schwoerer, Markus (Universität Bayreuth)